VOLUME 34 OCTOBER 1956 NUMBER 10

Canadian Journal of Physics

Editor: G. M. VOLKOFF

Associate Editors:

L. G. ELLIOTT, *Atomic Energy of Canada, Ltd., Chalk River*
J. S. FOSTER, *McGill University*
G. HERZBERG, *National Research Council of Canada*
L. LEPRINCE-RINGUET, *Ecole Polytechnique, Paris*
R. W. PRINGLE, *University of Manitoba*
B. W. SARGENT, *Queen's University*
Sir FRANCIS SIMON, *Clarendon Laboratory, University of Oxford*
W. H. WATSON, *University of Toronto*

Published by THE NATIONAL RESEARCH COUNCIL
OTTAWA CANADA

CANADIAN JOURNAL OF PHYSICS

(Formerly Section A, Canadian Journal of Research)

Under the authority of the Chairman of the Committee of the Privy Council on Scientific and Industrial Research, the National Research Council issues THE CANADIAN JOURNAL OF PHYSICS and six other journals devoted to the publication, in English or French, of the results of original scientific research. Matters of general policy concerning these journals are the responsibility of a joint Editorial Board consisting of: members representing the National Research Council of Canada; the Editors of the Journals; and members representing the Royal Society of Canada and four other scientific societies.

EDITORIAL BOARD

Representatives of the National Research Council

A. N. Campbell, *University of Manitoba*
G. E. Hall, *University of Western Ontario*
H. G. Thode, *McMaster University*
D. L. Thomson, *McGill University*
W. H. Watson (Chairman), *University of Toronto*

Editors of the Journals

D. L. Bailey, *University of Toronto*
T. W. M. Cameron, *Macdonald College*
J. B. Collip, *University of Western Ontario*
G. A. Ledingham, *National Research Council*
Léo Marion, *National Research Council*
R. G. E. Murray, *University of Western Ontario*
G. M. Volkoff, *University of British Columbia*

Representatives of Societies

D. L. Bailey, *University of Toronto*
Royal Society of Canada
T. W. M. Cameron, *Macdonald College*
Royal Society of Canada
J. B. Collip, *University of Western Ontario*
Canadian Physiological Society
R. G. E. Murray, *University of Western Ontario*
Canadian Society of Microbiologists
H. G. Thode, *McMaster University*
Chemical Institute of Canada
T. Thorvaldson, *University of Saskatchewan*
Royal Society of Canada
G. M. Volkoff, *University of British Columbia*
Royal Society of Canada; Canadian Association of Physicists

Ex officio

Léo Marion (Editor-in-Chief), *National Research Council*
F. T. Rosser, Director, Division of Administration, *National Research Council*

Manuscripts for publication should be submitted to Dr. Léo Marion, Editor-in-Chief, Canadian Journal of Physics, National Research Council, Ottawa 2, Canada.
(For instructions on preparation of copy, see **Notes to Contributors** (inside back cover).)

Proof, correspondence concerning proof, and orders for reprints should be sent to the Manager, Editorial Office (Research Journals), Division of Administration, National Research Council, Ottawa 2, Canada.

Subscriptions, renewals, requests for single or back numbers, and all remittances should be sent to Division of Administration, National Research Council, Ottawa 2, Canada. Remittances should be made payable to the Receiver General of Canada, credit National Research Council.

The journals published, frequency of publication, and prices are:

Canadian Journal of Biochemistry and Physiology	Bimonthly	$3.00 a year
Canadian Journal of Botany	Bimonthly	$4.00 a year
Canadian Journal of Chemistry	Monthly	$5.00 a year
Canadian Journal of Microbiology	Bimonthly	$3.00 a year
Canadian Journal of Physics	Monthly	$4.00 a year
Canadian Journal of Technology	Bimonthly	$3.00 a year
Canadian Journal of Zoology	Bimonthly	$3.00 a year

The price of single numbers of all journals is 75 cents.

Canadian Journal of Physics

Issued by THE NATIONAL RESEARCH COUNCIL OF CANADA

VOLUME 34 OCTOBER 1956 NUMBER 10

THE NUMBER DENSITY OF METEOR TRAILS OBSERVABLE BY THE FORWARD-SCATTERING OF RADIO WAVES[1]

BY ROBERT E. PUGH[2]

ABSTRACT

The number of meteor trails which can be detected by the forward-scattering of radio waves varies with the region of the sky under observation. The number density is determined theoretically, as a function of position relative to the transmitter and receiver.

I. INTRODUCTION

Meteor trails can be detected by the forward-scattering of radio waves. At a receiver, the signal scattered from an individual trail appears as a short pulse. A convenient way to measure the relative number of trails thus detected under different conditions is to count the number of pulses which have an amplitude greater than a certain given amplitude. In this paper, trails which cause such pulses are called 'observable'. Observable trails are not uniformly distributed over the sky, because of certain observational factors which vary with position. These factors are synthesized in the present paper, and a distribution function for observable trails is found.

In the development undertaken here, an isotropic distribution of meteor radiants is assumed. That is, the number of meteors incident from an element of solid angle on the celestial sphere is assumed to be independent of the direction of the element concerned. This assumption is not justified on an hour to hour basis, but since there is a considerable smoothing of the incidence pattern of meteors when averaged over a whole day, the assumption is reasonable when mean measurements are considered. Accordingly, this paper takes account of observational factors only insofar as they affect mean measurements. A similar development has been published by Eshleman and Manning (1954), but with different approximations and a somewhat different purpose. It is contrasted with the present work in a companion paper (Hines and Pugh 1956).

II. FORMULATION

Since specular scattering of radio waves from underdense meteor trails is essentially a process of Fresnel diffraction (Eshleman 1952), almost all of the

[1]Manuscript received June 5, 1956.
Contribution from the Radio Physics Laboratory, Defence Research Board, Ottawa, Ontario. The work was performed under project PCC No. D48–95–11–01.
[2]Present address: Department of Physics, University of California, Berkeley 4, California.

scattered radiation can be attributed to the principal Fresnel zone. For this reason, the following working hypothesis (Hines 1955) is adopted: those trails which contain the center points P of the associated principal Fresnel zones within their lengths are 'potentially observable', and those that do not are not. The points P are those at which the meteor trails become tangent to one or other of a family of ellipsoids of revolution having the transmitter–receiver axis TR as axis of revolution, and the points T and R as foci.

A cartesian coordinate system, (x, y, z), will be employed, having its origin at the center V of the TR axis, its positive x direction along VR, and its positive z axis in the direction of the zenith over V (see Fig. 1). It is convenient

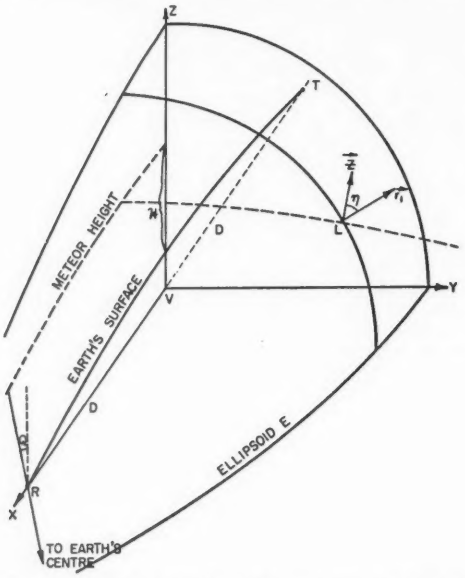

FIG. 1. Geometry of potentially observable trails: the center of the principal Fresnel zone of a trail is that point at which the trail is tangent to some ellipsoid of revolution, E, with foci at T and R.

to introduce the position vector $\mathbf{r} = (x, y, z)$ and the subsidiary vector $\mathbf{r}_1 \equiv (x/a^2, y/(a^2-D^2), z/(a^2-D^2)) \equiv (x_1, y_1, z_1)$. Here, D is half the distance between T and R, and a is the semimajor axis of the relevant ellipsoid, E, passing through (x, y, z); a may be determined from the equation of E, $\mathbf{r}.\mathbf{r}_1 = 1$, for any given point (x, y, z).

In the first instance, meteor trails may be thought of as extending between heights $\mathfrak{H}$ and $\mathfrak{H}+\delta$ (with $\delta \ll \mathfrak{H}$) above the earth's surface. In fact, of course, they occur with varying ionization content over a range of heights, so their effects would actually be determined by a weighted integral over a δ varying between some lower and upper limits. However, neither the weighting factor nor the limits vary appreciably as a function of orientation according to the

present theory of trail formation (Herlofson 1946–47). Moreover, the effects to be considered are free from any marked variation with height. It appears, then, that the integrated effect would have essentially the same variation with x and y as the integrand itself, and so the simple picture of trail extension would lead to a reasonably valid result. This simple picture will therefore be adopted.

The vertical height δ corresponds to a slant height

$$\delta' = \delta/\cos\eta \tag{1}$$

measured along the normal to the ellipsoid at the point (x, y, z), where η is the zenith angle of the normal (see Fig. 1). The direction of the zenith at (x, y, z) is given by

$$\mathbf{Z} = (x/(R'+z), y/(R'+z), 1) \tag{2}$$

where R' is the distance of V from the earth's center. This distance is never less than about 6300 km., in practice, and the relevant values of x and y are normally less than 500 km.; accordingly, $\mathbf{Z}$ is nearly a unit vector. (These restrictions are introduced by horizon effects, since the trail must lie within the region of the sky common to both the transmitter and the receiver, if it is to be detected.) Cos η may be calculated with the aid of (2):

$$\cos\eta = \mathbf{r}_1.\mathbf{Z}/r_1 Z. \tag{3}$$

At any point L, with coordinates (x, y, z), all potentially observable trails must lie in the plane tangent to the ellipsoid E at L. The number of potentially observable trails which can be attributed to an area element $dx\,dy$ between x and $x+dx$, y and $y+dy$, at height $\mathfrak{H}$, will now be calculated. The point L is assumed to lie on a sphere with center at the earth's center and with

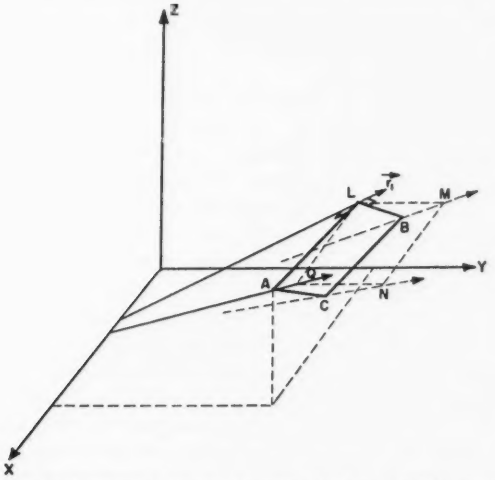

FIG. 2. The normal projection of the area element, $dx\,dy = LMNQ$, onto the plane tangent to the ellipsoid through L.

radius $R+\mathfrak{H}$, R being the radius of the earth. The corner points of the area element are denoted by L, M, N, Q, respectively, in the sense indicated in Fig. 2. These points can be projected along the normals to the corresponding ellipsoids, onto the points L, B, C, A, respectively, lying in the plane through L tangent to the ellipsoid E. The various normals differ in direction only by differential angles, so the projection may also be thought of as a normal projection onto the tangent plane.

The positions of the points A, B, and C are given by the position vectors:

$$\begin{cases} \mathbf{r}_A = \mathbf{r}+\Delta\mathbf{r}, \\ \mathbf{r}_B = \mathbf{r}+\Delta'\mathbf{r}, \\ \mathbf{r}_C = \mathbf{r}+\Delta\mathbf{r}+\Delta'\mathbf{r}, \end{cases} \tag{4}$$

respectively. The components of $\Delta\mathbf{r}$ satisfy the equations

$$\begin{cases} \mathbf{r}_1.\Delta\mathbf{r} = 0, \\ (\Delta x-dx)/x_1 = \Delta y/y_1 = \Delta z/z_1. \end{cases} \tag{5}$$

Here, as throughout the development, differentials of higher order than those necessary are omitted. These equations lead to the following expression for $\Delta\mathbf{r}$:

$$\Delta\mathbf{r} = (y_1^2+z_1^2,\ -x_1y_1,\ -x_1z_1)r_1^{-2}\,dx. \tag{6}$$

The components of $\Delta'\mathbf{r}$ satisfy equations similar to (5). They yield the expression

$$\Delta'\mathbf{r} = (-x_1y_1,\ x_1^2+z_1^2,\ -y_1z_1)r_1^{-2}\,dy. \tag{7}$$

The angle between AL and LB is denoted by ξ (see Fig. 3). Cos ξ may be found from the relation

$$\cos\xi = \frac{\Delta\mathbf{r}\cdot\Delta'\mathbf{r}}{|\Delta\mathbf{r}|\,|\Delta\mathbf{r}|} = \frac{-x_1y_1}{\sqrt{(x_1^2+z_1^2)(y_1^2+z_1^2)}}. \tag{8}$$

The following formulation will be adopted: those trails which pass through the rectangular element of area defined by the two sides LA and $\delta'\mathbf{r}_1/r_1$, and which have associated P points lying between this element and a parallel plane through M, will be attributed to the element $dx\,dy$. This formulation provides one method of taking into account all potentially observable trails, and of assigning them to area elements near their respective P points. It erroneously includes some trails whose P points would be just below the $\mathfrak{H}$ level, but it automatically compensates for this by ignoring a like number whose P points lie just below the $\mathfrak{H}+\delta$ level.

Attention may first be confined to a trail which passes through L. It will intersect the plane $BMNC$ at some point Y', whose projection onto $LBCA$ lies at Y, a point on BC (produced, if necessary). If the trail is to be attributed to the element $dx\,dy$, then its P point must lie between L and Y'. This will occur if the angle YLY' is less than the differential angle, $d\chi$, between the ellipsoid normal at L and that at Y or Y'. This differential angle depends on the position of Y along BC, and so on the angle β between YL and LA. This β, incidentally, is essentially the same as that introduced by Eshleman (1952), and employed by Eshleman and Manning (1954), in specifying trail orientation.

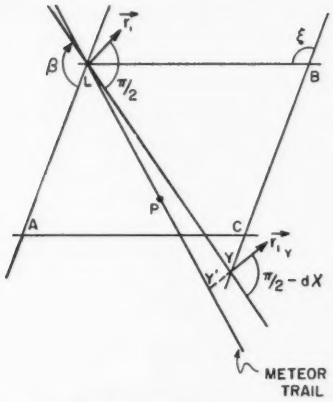

FIG. 3. A trail through L is considered potentially observable, and attributable to the area element $dx\,dy$, if its P point lies between L and Y'. This implies that the angle between such a trail and the normal at L lies in the range $\pi/2$ to $\pi/2+d\chi$.

Using (6), (7), and (8), it is not difficult to show that the coordinates of Y are

$$\mathbf{r}_Y = \mathbf{r}+\mathbf{r}_{LY}dy. \tag{9}$$

Here, $\mathbf{r}_{LY}$ is a vector lying in the LY direction given by

$$\mathbf{r}_{LY} = \frac{z_1}{r_1}\left(-\cot\beta, \frac{x_1y_1\cot\beta + r_1z_1}{y_1^2+z_1^2}, \frac{x_1z_1\cot\beta - r_1y_1}{y_1^2+z_1^2}\right). \tag{10}$$

Since Y lies in the plane which is tangent at L, it follows that the semimajor axis of the ellipsoid through Y differs from the semimajor axis of the ellipsoid through L only by a second order differential. The normal at Y then has the direction:

$$\mathbf{r}_{1_Y} = \mathbf{r}_1+\mathbf{r}_{1_{LY}}\,dy \tag{11}$$

where $\mathbf{r}_{1_Y}$ and $\mathbf{r}_{1_{LY}}$ are found from $\mathbf{r}_Y$ and $\mathbf{r}_{LY}$ in the same way as $\mathbf{r}_1$ is found from $\mathbf{r}$. (Divide the x component by a^2, and the y and z components by a^2-D^2.) The angle $d\chi$ may now be calculated from (10) and (11):

$$d\chi = \cos(\tfrac{1}{2}\pi - d\chi) = \frac{\mathbf{r}_{LY}\cdot\mathbf{r}_{1_Y}}{r_{LY}r_{1_Y}} = \frac{\mathbf{r}_{LY}\cdot\mathbf{r}_{1_{LY}}}{r_{LY}r_{1_{LY}}}\,dy \tag{12}$$

$$= \frac{z_1\sin\beta(a^2r_1^2+\cot^2\beta)}{r_1^3a^2(a^2-D^2)\sqrt{y_1^2+z_1^2}}\,dy.$$

As derived, $d\chi$ applies only to trails which pass through L. However, a similar development for trails passing through any other point of the rectangle, $LA.\delta'\mathbf{r}_1/r_1$, would have led to an angle differing from $d\chi$ by higher order differentials only. Accordingly (12) is applicable to all β-oriented meteor trails attributable to $dx\,dy$.

The area perpendicular to those trails with orientation β is the normal projection of the element defined by LA and $\delta'\mathbf{r}_1/r_1$ onto the plane normal to the trail axis. This area is

$$da_\perp = |\Delta\mathbf{r}|\delta'|\sin\beta| = \frac{\delta'\sqrt{y_1^2+z_1^2}}{r_1}|\sin\beta|dx. \tag{13}$$

It is now evident that those potentially observable trails with orientations in the range β to $\beta+d\beta$, which are to be attributed to the element $dx\,dy$, must come from an element of solid angle $d\chi\,d\beta$ and must pass through an element of area $da_\perp$ in a plane normal to their path. Then, with the assumption of an isotropic distribution of meteor radiants, the number fulfilling these conditions will have the functional form of $d\chi\,d\beta\,da_\perp$.

III. NUMBER DENSITY OF OBSERVABLE TRAILS

In order that a scattered signal be considered observable at the receiver, its amplitude must exceed a certain minimum amplitude, A_c, say. Following the method of Hines (1955), the fraction of potentially observable trails which scatter a signal to the receiver, of amplitude greater than A_c, is proportional to $G(x, y)f_0(x, y, \beta)/A_c$, where $G(x, y)$ is the geometric mean of the transmitter and receiver antenna gains, and

$$f_0 = \frac{\cos\zeta|\cos\gamma|}{\sqrt{d_1d_2(d_1+d_2)}\sqrt{1-\cos^2\beta\sin^2\phi}} \tag{14}$$

is an amplitude factor derived from Eshleman's formula for forward-scattered power. This is the Eshleman amplitude factor as modified by Hines to take into account the variation of ionization density with orientation of the trail, for the case in which the transmitting antenna propagates, and the receiving antenna accepts, only particularly polarized components of the electric vector. These will be taken to be the horizontally polarized components here. In (14), ζ is the zenith angle of the trail and γ is the angle between the electric vector of the wave incident on the trail and that component accepted by the receiving antenna; d_1 and d_2 are the respective distances from L to T and to R, and 2ϕ is the forward-scattering angle TLR. The zenith angle ζ is calculated with the aid of equations (2) and (10) from the relation

$$\cos\zeta = \pm\mathbf{r}_{LY}.\mathbf{Z}/r_{LY}Z \qquad \text{according as } \beta \gtrless \pi. \tag{15}$$

The zenith at T has the direction

$$\mathbf{Z}_T = (-\sin Q, O, \cos Q) \tag{16}$$

where Q is the angle subtended at the earth's center by the line VT (see Fig. 1). The line TL has the direction

$$\mathbf{r}_{TL} = (x+D, y, z)\,. \tag{17}$$

The condition for horizontal polarization implies that, if (λ, μ, ν) are the direction cosines of the electric vector incident on the trail at P, then

$$-\lambda\sin Q+\nu\cos Q = 0. \tag{18}$$

The condition for a transverse wave implies

$$(x+D)\lambda+\mu y+\nu z = 0. \tag{19}$$

Equations (18) and (19), together with the implicit condition $\lambda^2+\mu^2+\nu^2 = 1$, yield expressions for λ, μ, and ν. Similar equations may be obtained for the direction cosines (λ', μ', ν') of the component accepted by the receiving antenna, merely by replacing D and Q by $-D$ and $-Q$. Combining these results, $|\cos\ \gamma|$ is found to be

$$|\cos\gamma| = |\lambda\lambda'+\mu\mu'+\nu\nu'| \tag{20}$$

$$= \frac{|y^2(1-\tan^2 Q)+x^2-(D+z\tan Q)^2|}{(y^2\sec^2 Q+[D+x+z\tan Q]^2)^{\frac{1}{2}}(y^2\sec^2 Q+[D-x+z\tan Q]^2)^{\frac{1}{2}}}.$$

Combining equations (12) and (13) with the expression given above for the fraction of potentially observable trails which are, in fact, observable, the number of observable trails with orientation between β and $\beta+d\beta$ is proportional to

$$n(x, y, \beta)\, dx\, dy\, d\beta \tag{21}$$

$$= \frac{G(x, y)f_0(x, y, \beta)\ \delta' z_1 \sin^2\beta(a^2 R_1{}^2+\cot^2\beta)\, dx\, dy\, d\beta}{r_1{}^4 a^2(a^2-D^2)}.$$

Integrating over all possible orientations, the mean number of observable trails which are attributable to $dx\, dy$ is proportional to

$$n(x, y)\, dx\, dy = \int_{\beta_{\min}}^{\beta_{\max}} n(x, y, \beta)\, dx\, dy\, d\beta. \tag{22}$$

The limits of integration are chosen such that the zenith angle ζ is $\frac{1}{2}\pi$ at the limits, with a minimum in between. Since $\cos\zeta$, as given by equation (15), is of the form

$$\cos\zeta = b(x, y)\cos\beta+c(x, y)\sin\beta, \tag{15a}$$

it follows that

$$\beta_{\min} = \beta_{\max}-\pi \tag{23}$$

and that $\pi \leqslant \beta_{\max} \leqslant 3\pi/2$ because of the signs of $b(x, y)$ and $c(x, y)$.

The integration indicated in (22) can be carried out by standard methods. The result is:

$$n(x, y)\, dx\, dy = G(x, y)U(x, y)I(x, y)\, dx\, dy \tag{24}$$

where

$$U(x, y) = \frac{|\cos\gamma|\delta' z_1}{r_1{}^4\sqrt{d_1 d_2(d_1+d_2)}\, a^2(a^2-D^2)} \tag{25}$$

and

$$I(x, y) = \left\{\left(1-\frac{z}{R'+z}\right)\frac{y_1}{\sqrt{y_1{}^2+z_1{}^2}}\right\} \tag{26}$$

$$\times\left\{\frac{a^2 r_1{}^2}{\sin\phi}\sin^{-1}(\sin\phi\cos\beta_{\min})+\frac{\cos\beta_{\min}}{a^2 r_1{}^2}\sqrt{1-\cos^2\beta_{\min}\sin^2\phi}\right\}$$

$$+\left\{\left(1-\frac{z}{R'+z}\right)\frac{x_1z_1}{r_1\sqrt{y_1^2+z_1^2}}-\frac{D^2x_1\sqrt{y_1^2+z_1^2}}{r_1(R'+z)}\right\}$$
$$\times\left\{\frac{1}{2\sin\phi}\ln\frac{\sqrt{1-\cos^2\beta_{\min}\sin^2\phi}+\sin\beta_{\min}\sin\phi}{\sqrt{1-\cos^2\beta_{\min}\sin^2\phi}-\sin\beta_{\min}\sin\phi}\right.$$
$$\left.+\frac{\sin\beta_{\min}}{a^2r_1^2}\sqrt{1-\cos^2\beta_{\min}\sin^2\phi}\right\}.$$

Normally, in evaluating (26), it is sufficient to adopt the approximations

$$(27)\quad \sin\beta_{\min}=\frac{x_1z_1}{\sqrt{(x_1^2+y_1^2)(y_1^2+z_1^2)}},\ \cos\beta_{\min}=\frac{y_1r_1}{\sqrt{(x_1^2+y_1^2)(y_1^2+z_1^2)}}.$$

These reduce $\cos\zeta$ to a value of the order x/R or y/R, rather than to zero as required for the exact integration limit, but this should suffice in practice; for $x, y \leqslant 500$ km., the limiting ζ's are within 3° of the required 90°. The error is negligible since the number density of observable trails is proportional to $\cos\zeta$, so the number of trails omitted at one limit of integration or added at the other will be extremely small compared with the total.

The geometric relation

$$(28)\quad \sec\phi = ar_1$$

may be used to determine ϕ in (26) as a function of x, y, and z. It has, in fact, been employed already in reducing the various factors there. In conjunction with the approximations (27), it further simplifies (26) to the form

$$(29)\quad I(x,y)=\frac{P}{a^3r_1^3}\left\{1-\frac{z_1P^2}{(R'+z)(x_1^2+y_1^2)}\right\}$$
$$+\left\{1-\frac{z}{R'+z}\right\}\left\{\frac{a^3r_1^3y_1}{D(y_1^2+z_1^2)}\sin^{-1}\left(\frac{D\,y_1}{a\sqrt{x_1^2+y_1^2}}\right)\right\}$$
$$+\left\{\frac{a\,x_1}{2D(y_1^2+z_1^2)}\right\}\left\{z_1-\frac{D^2y_1^2+a^2z_1^2}{R'+z}\right\}\left\{\ln\frac{r_1P+D\,x_1z_1}{r_1P-D\,x_1z_1}\right\}$$

where $P=\sqrt{x\,x_1+y\,y_1}=\sqrt{1-z\,z_1}$.

Except for $G(x, y)$, which depends on the particular antenna patterns employed, all factors entering $n(x, y)$ can be calculated once a specific D and $\mathfrak{H}$ are adopted. The product $U(x, y)I(x, y)$ for D = 500 km., $\mathfrak{H}$ = 100 km., is presented in the form of a contour chart in the following paper (Hines and Pugh 1956).

ACKNOWLEDGMENT

The author would like to express his thanks to Dr. C. O. Hines, who proposed and supervised this problem, for the many helpful discussions held throughout the performance of the work.

REFERENCES

ESHLEMAN, V. R. 1952. Tech. Rept. No. 49. Electronics Research Laboratory, Stanford University, Stanford, California. July 15.
ESHLEMAN, V. R. and MANNING, L. A. 1954. Proc. I.R.E. **42**: 530.
HERLOFSON, N. 1946–47. Repts. Progr. Phys. **11**: 444.
HINES, C. O. 1955. Can. J. Phys. **33**: 493.
HINES, C. O. and PUGH, R. E. 1956. Can. J. Phys. **34**: 1005.

THE SPATIAL DISTRIBUTION OF SIGNAL SOURCES IN METEORIC FORWARD-SCATTERING[1]

By C. O. Hines and R. E. Pugh[2]

ABSTRACT

The spatial distribution of observable meteor trails is determined, with the aid of the 'cylindrical approximation' appropriate to forward-scattering observations. Contour charts of the distribution are presented, and found to compare favorably with those obtained from a more exact analysis, presented in a companion paper. Typical effects of the signal durations are also examined. The whole is compared with an earlier development by Eshleman and Manning (1954), which treats closely related aspects of meteoric forward-scattering.

I. INTRODUCTION

When meteor trails are detected by the forward-scattering of radio waves, they do not appear to be distributed uniformly over the sky. Instead, the method of observation itself leads to a selective enhancement of certain regions at the expense of others. In a companion paper (Pugh 1956), which will be designated henceforth as I, the basic effects were considered and a theoretical distribution function was derived. The development was complicated, since the simplifying assumptions were purposely kept to a minimum. In particular, the ellipsoidal geometry associated with specular forward-scattering was retained.

In an earlier analysis (Hines 1955), which will be designated as II, a different aspect of the same problem was treated. There, it was found convenient to replace the relevant ellipsoids by a family of cylinders having the transmitter–receiver line T–R as common axis. This cylindrical approximation greatly simplifies the conception of meteoric scattering problems, and greatly reduces the analytical and computational labor involved. It is inherently accurate when regions equidistant from T and R are considered, and such regions are often of greatest importance in practice as a result of antenna illumination.

In the present development, the problem treated in I is reconsidered with the aid of the cylindrical development in II. The resulting formulae are naturally simpler, and so are more readily employed. The principal purpose of the analysis, however, is to obtain some indication of the validity of the cylindrical approximation itself. This is accomplished by displaying, on a single contour chart, the distribution of observable trails as computed by the two methods separately.

It is found that the two sets of curves are in close agreement over most of the region of practical importance. A similar agreement is to be expected whenever the transmitter–receiver separation exceeds that used in the computations, which is 1000 km. For such path lengths, then, the further use of the cylindrical approximation seems to be justified.

[1]Manuscript received June 5, 1956.
Contribution from the Radio Physics Laboratory, Defence Research Board, Ottawa, Ontario. The work was performed under project PCC No. D48-95-11-01.
[2]Present address: Department of Physics, University of California, Berkeley 4, California.

Some effects of signal durations are considered in a later section, and illustrated by contour charts. Finally, the whole analysis is contrasted with that given previously by Eshleman and Manning (1954).

II. OBSERVABILITY AS A FUNCTION OF ORIENTATION

The development presented in II is summarized and extended in this section, to provide a framework for the subsequent analysis. Reference may be made to the original work for details.

The cartesian space coordinates to be used are those defined in I, rather than those in II. The transmitter and receiver are located on the x axis, at $x = -D$ and $x = +D$ respectively. The z axis is directed upwards from the point midway between them. The y coordinate then measures distance to either side of the T–R axis.

Two parameters, β and ψ, specify the orientation of a meteor trail. These are such that the direction cosines of the trail axis are given by [cos β, $-\sin\beta \times\sin\psi$, sin β cos ψ]. Thus β measures the angle between the trail axis and the T–R axis, while ψ measures the angle between the vertical x, z plane and the inclined plane in which β is measured (see Fig. 1). These definitions are equiva-

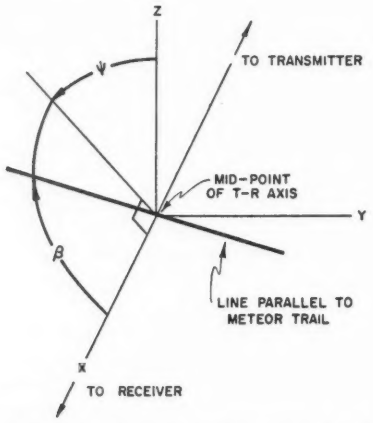

FIG. 1. Definition of meteor trail orientation parameters, β and ψ, relative to cartesian coordinate system.

lent to those given in II, where β and ψ were initially introduced to locate the meteor radiant on the celestial sphere. The definition of β is also equivalent to that given in the companion paper when the trail is located near the y, z plane. This is often the region of greatest interest, since it is often the region most strongly illuminated by the antenna systems.

A meteor trail is considered to be 'potentially observable' only if it can support specular scattering between T and R. Specular scattering occurs if the trail is tangent to one of a family of prolate spheroids about T and R as common foci. Near the y, z plane, these spheroids approximate to cylinders,

and the analysis is greatly simplified if the condition for exact specular scattering is replaced by one for tangency to a cylinder.

With the use of the cylindrical approximation, it can be shown that trails with β, ψ orientation are potentially observable if and only if they cross the plane

$$z = y \tan \psi. \tag{1}$$

Trails are confined to a narrow range of heights, located about some representative level at height $\mathfrak{H}$ above the earth's surface. Near the y, z plane again, this level is cut by the observation plane (1) at $z = z(\psi)$ given by

$$z^2 \csc^2\psi + 2zR \cos Q = D^2 + 2R\mathfrak{H} + \mathfrak{H}^2 \tag{2}$$

where R is the earth's radius and $\sin Q = D/R$. The corresponding $y = y(\psi)$ can be obtained by inserting (1) in (2).

Within the approximations, then, meteor trails with a specific orientation are potentially observable only if they lie near a specific line. This line extends in the x direction, and lies at a distance $y(\psi)$ to the side of the TR axis and at distance $z(\psi)$ above it. Potentially observable trails are formed in an element dx of this line, at some rate proportional to the total incidence rate from the β, ψ radiant position, and proportional to a factor $s_1(\beta, \psi)dx$ which takes into account the cross section of the region of potential observation.

The peak amplitude of the signal received via one of these trails depends on $\beta, \psi, x, y(\psi)$, and $z(\psi)$, and it may be taken also as proportional to m, the mass of the parent meteor. The form

$$A_p = ms_2(\beta, \psi, x) \tag{3}$$

will be adopted for this peak amplitude.

One of the most simply interpreted observables in meteor-scattering studies is the occurrence rate of peak amplitudes which exceed some arbitrary counting level A_c. From (3), such signals are received from trails whose parent meteors had masses exceeding

$$m_c \equiv A_c/s_2(\beta, \psi, x)\,. \tag{4}$$

It will be assumed that an inverse square law holds for the mass distribution, so the incidence rate of sufficiently massive meteors is proportional to

$$\int_{m_c}^{\infty} m^{-2} dm = m_c^{-1} = s_2(\beta, \psi, x)/A_c. \tag{5}$$

Finally, since these scattered signals come only from potentially observable trails, the desired occurrence rate of signals exceeding A_c is found to be proportional to

$$s_1(\beta, \psi)s_2(\beta, \psi, x)dx/A_c$$

and to the total incidence rate from the β, ψ direction. The trails which provide these signals are termed 'observable.'

The full analysis results in the following 'differential observability factor' for the product s_1s_2dx:

$$dF \simeq \frac{G(x, \psi)\sin^2\beta \cot \psi |\cos \gamma| dx}{[r_T r_R (r_T + r_R)(1 - \cos^2\beta \sin^2\phi)]^{\frac{1}{2}}[1 + z/(R+\mathfrak{H}) \sin^2\psi]}. \tag{6}$$

Here $G(x, \psi)$ is the geometric mean of the transmitting and receiving antenna gains in the direction of x, $y(\psi)$, $z(\psi)$; r_T and r_R are the corresponding distances; 2ϕ is the 'forward-scattering angle' subtended by T–R at the trail; and γ is the angle between the polarization vector incident on the wave and that component which is accepted by the receiving antenna. It will be assumed in this work that the transmitting antenna propagates, and the receiving antenna accepts, only a horizontal component of the electric vector.

A finite observability factor, applicable to the β, ψ orientation without reference to x, can be found by integrating dF along the line $y = y(\psi), z = z(\psi)$. In practice, with common antenna systems and large transmitter–receiver separations, it is often found that $G(x, \psi)$ provides the dominant variation of the integrand in this process. Indeed, it is only on the assumption that G falls rapidly to zero as $|x|$ increases that the earlier approximations may be justified. Accordingly, it may be equally valid to calculate the remaining factors of the integrand for $x = 0$ alone, and so reduce the integration to the evaluation of $\int G dx$. The observability factor $F_0{}^*$ derived in II would then result, except for an irrelevant $\sqrt{2}$ factor. The relations for $x = 0$ are

$$r_T = r_R = r \equiv (D^2 + y^2 \sec^2\psi)^{\frac{1}{2}}, \tag{7}$$

$$\sin \phi = D/r,$$

$$|\cos \gamma| \simeq |D^2 - y^2|/(D^2 + y^2).$$

With regard to the total incidence rate from the β, ψ direction, which must multiply $F_0{}^*$, two cases are to be distinguished. The first is that of shower meteors, which are incident from a single β, ψ radiant position at any time. If the strength of the shower remains constant as the radiant moves across the sky, then the time variation of the observation rate will be given directly by the time variation of $F_0{}^*(\beta, \psi)$, where $\beta = \beta(t)$, $\psi = \psi(t)$. Results for typical showers have been given and compared with the corresponding observations elsewhere (Forsyth, Hines, and Vogan 1955).

When random meteors are to be considered, incident from all β, ψ radiant positions, the interpretation is slightly more involved. A distribution function $s_0(\beta, \psi)$ must then be introduced, such that the incidence rate of meteors from radiant positions within an element of solid angle $d\sigma$ about the β, ψ position has the form $s_0(\beta, \psi) d\sigma$. This distribution differential should then be multiplied by $F_0{}^*(\beta, \psi)$ and integrated over the visible celestial hemisphere ($0 \leqslant \beta \leqslant \pi$; $-\pi/2 \leqslant \psi \leqslant \pi/2$) to obtain the net observation rate. In practice, $s_0(\beta, \psi)$ is not uniform over the celestial sphere, and it changes in the course of the day. The diurnal variation of the integral then gives the diurnal variation of the observation rate for random meteors. Typical results from this sort of analysis are presented elsewhere (Hines 1956).

III. OBSERVABILITY AS A FUNCTION OF POSITION

It is a primary purpose of this paper to indicate the spatial distribution of observable trails. As has been seen, the location of such trails depends on their orientation, and so the new problem is linked directly to the old. The transformation from the one to the other is presented in this section.

The two coordinates x and y are sufficient for the purpose, since $z = z(x, y)$

by virtue of the restriction to the $\mathfrak{H}$ level. The x variation of the distribution is already contained in dF, and it only remains to obtain the y variation explicitly. This is accomplished by rewriting $y = y(\psi)$ as $\psi = \psi(y)$, $z = z(\psi)$ as $z = z(y)$, and the observation rate $s_0\, dF\, d\sigma$ as $s_0\, dF \sin\beta\, d\beta (d\psi/dy) dy$. This quantity gives the rate at which meteors are observed, by means of received signals exceeding the counting level, in the region above the element $dx\, dy$, for radiant positions in the range β to $\beta + d\beta$. The condition on β is removed by integration, to provide the total rate applicable to the element $dx\, dy$.

For simplicity, and for comparison with the companion paper, it will be assumed that s_0 is constant; it can therefore be ignored as an irrelevant normalizing factor (unless absolute rates are required). The β variation is confined to a factor $\sin^3\beta(1-\cos^2\beta \sin^2\phi)^{-\frac{1}{2}}$, and an elementary quadrature yields

$$\Phi(\phi) \equiv \int_0^{\pi} \frac{\sin^3\beta d\beta}{(1-\cos^2\beta \sin^2\phi)^{\frac{1}{2}}} = \frac{\cos\phi}{\sin^2\phi} + \frac{2\sin^2\phi - 1}{\sin^3\phi}\,\phi. \tag{8}$$

Direct calculation reveals that this integral varies by only a few per cent over the whole region of interest ($|x|, |y| \lesssim 500$ km., $35° \lesssim \phi \lesssim 75°$, for $2D = 1000$ km., $\mathfrak{H} = 100$ km.). The value of its further retention is therefore doubtful, and it may be totally ignored in any rough computation. From (1) and (2), the relation

$$d\psi/dy = -(z^2+y^2+zR\cos Q)/(z+R\cos Q)(z^2+y^2) \tag{9}$$

can be derived without difficulty. Except at large $|y|$'s, near the extreme limits of the region of interest, both (6) and (9) can be reduced by taking the mathematical limit as $R \to \infty$.

To summarize the foregoing transformation explicitly, the distribution function

$$n(x, y) = \frac{G(x, y)\cot\psi|\cos\gamma|\Phi}{[r_T r_R(r_T+r_R)]^{\frac{1}{2}}[1+z/(R+\mathfrak{H})\sin^2\psi]} \cdot \frac{d\psi}{dy} \tag{10}$$

may be introduced. This gives a measure of the number of signals which will be observed, above a given amplitude level, after scattering from meteor trails traversing a unit area of the $\mathfrak{H}$ level at x, y. In it, the forms $z = z(y)$, $\psi = \psi(y)$ are assumed to be derived from (1) and (2). The approximations (7) may be employed without serious error when $|x|$ is small, although more accurate relations are easily derived.

IV. CONTOUR CHARTS FOR THE SPATIAL DISTRIBUTION OF OBSERVABLE TRAILS

In Fig. 2 are presented contour charts representing the distribution function $n(x, y)/G(x, y)$, as derived from the formulae of I (solid curves) and as derived here with the aid of the cylindrical approximation (broken curves). In each case, the distribution is normalized to a value of 100 at the saddle point ($x = 0$, $y \simeq 100$ km.). The figure represents only one quadrant of the $\mathfrak{H}$ level, with origin above the mid-point of the T–R axis and the $x = 500$ km., $y = 0$ point above the receiver; the remaining quadrants can be pictured by symmetry. The parameters $2D = 1000$ km., $R = 6370$ km., $\mathfrak{H} = 100$ km., were employed.

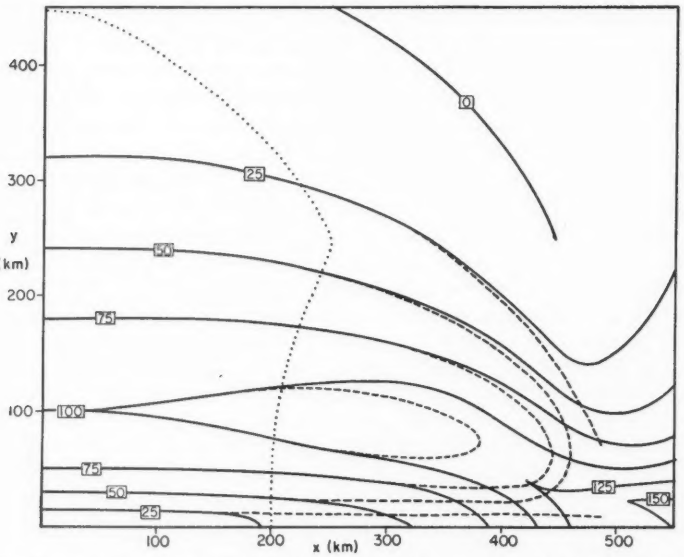

FIG. 2. Contours of observable meteor distribution (number density of meteors giving received signals above a counting level). Solid curves computed from formulae of the companion paper; broken curves from the cylindrical approximation. Dotted curve is representative of normal boundary of effective antenna illumination. The receiver is at $x = 500$ km., $y = 0$; the path mid-point is at the origin; other quadrants by symmetry. Isotropic incidence is assumed.

The calculations for the companion paper, I, were derived directly from the product $U(x, y)I(x, y)$ presented there. The testing of the cylindrical approximation was rendered more significant by ignoring the relations in (7), computing r_T, r_R, and

$$\phi = (\tfrac{1}{2}) \text{ arc } \sin(2Dz/r_T r_R \sin\psi) \tag{11}$$

as functions not only of y but also of x. In these calculations, z was still considered to be a function of y alone, as given by (1) and (2), since this approximation is inherent in some of the formulae derived here. For convenience, however, $|\cos\gamma|$ was taken to be the same function of x and y as that computed for the more exact curves, even though this assumes $z = z(x, y)$. The distinction becomes relevant only in the region where the cylindrical approximation breaks down in any case.

It is to be noted that the quotient $n(x, y)/G(x, y)$ is illustrated, rather than $n(x, y)$ alone. This is because the gain factor $G(x, y)$ may be quite different for different experimental arrangements, whereas the quotient n/G is typical for all cases in which $2D \simeq 1000$ km. In practice, then, the true distribution of observable trails can be found from the contour chart only after the computation of the appropriate $G(x, y)$, and its subsequent superposition on the figure. Conversely, the figure can be employed to suggest the most efficient antenna arrangements for experimental use.

The dotted curve in the figure represents a contour of constant gain, as derived for typical broad-beamed (50°) antennas at the transmitter and receiver, directed at the 100 km. level over the mid-point. (See II for more detailed specifications.) The contour shown is that on which $G(x, y)$ has fallen to one tenth of the maximum value, $G(0, 0)$. Accordingly, by far the greater part of the received energy must come from within the region outlined by the dots.

This region has been introduced as illustrative of the broadest area in the $\mathfrak{H}$ level that will normally be illuminated by the antennas on a propagation path of length $\gtrsim$1000 km. It is apparent that, within this region, the cylindrical approximation leads to an extremely good agreement with the more accurate results. Except when unusual antenna configurations are employed, with appreciable illumination outside the region shown, it would seem that the further application of the cylindrical approximation is justified.

It may be noted that, if the approximations (7) had been employed, the broken lines would have been parallel to the x axis, maintaining essentially the same y values as those computed here for $x = 0$. It is evident that the resulting errors would have been a few per cent at most, in the region of greatest interest, and that these errors are of a self-compensating nature when integrated results are considered. Because of the basic physical uncertainties, and the inherent statistical variations in any observations, such errors should be quite acceptable.

Just as $F_0^*(\beta, \psi)$ is of use when different incidence patterns $s_0(\beta, \psi)$ are to be treated, so the quotient $n(x, y)/G(x, y)$ is of use when different illumination patterns $G(x, y)$ are considered. Typical results obtained from Fig. 2, with varying illuminations, are presented elsewhere (Hines, Forsyth, Vogan, and Pugh 1955).

V. EFFECTS OF SIGNAL DURATIONS

The foregoing analysis has been concerned with numbers of signals, and with peak amplitudes. But many aspects of meteor scattering are concerned, as well, with the durations of the scattered signals. Two such aspects of the problem are treated in this section.

Once again, it is assumed that the peak amplitude A_p is given by $ms_2(\beta, \psi, x)$, as in (3). This form is applicable to the so-called underdense trails, and it will be assumed that all trails are of this nature. The signal from these trails will be considered to rise instantaneously from zero amplitude to the peak value A_p, at time $t = 0$, and then to decay exponentially according to the law

$$A(t) = A_p \exp(-t/\tau), \qquad t \geqslant 0. \tag{12}$$

The decay constant τ may vary from trail to trail, but its variation is presumed to be expressible as a function of β, ψ, and x.

The first effect to be considered is that on the mean signal level, or, more precisely, on the mean detected power level. Because of the variation in durations, the regions which contribute most to this level are not necessarily the regions where the greatest number of observable trails occur. The effective

distribution of mean signal sources can, however, be determined formally without difficulty.

For this purpose, and to obtain results in finite form, it is necessary to introduce a saturation amplitude, A_s. A saturation would arise in practice from equipment parameters, or else, in effect, from the changed radiation characteristics of densely ionized trails. The assumption to be made is that received signals with amplitude $A(t)$ would be detected as signals with amplitude $A(t)$, except if $A(t) > A_s$, when they would be detected as signals with amplitude A_s.

The calculation of the mean signal level now proceeds in two parts, the first of which takes into account signals having $A_p > A_s$. For these, the detected power is A_s^2 (by suitable choice of units) until the time

$$t = t_s \equiv \tau \ln(A_p/A_s). \tag{13}$$

The detected energy is then given by $A_s^2\tau \ln(A_p/A_s)$ for this time interval. Subsequently, the detected power is $A_p^2 \exp(-2t/\tau)$ and the detected energy is

$$\int_{t_s}^{\infty} A_p^2 \exp(-2t/\tau)dt = (A_p^2\tau/2) \exp(-2t_s/\tau) = A_s^2\tau/2. \tag{14}$$

The net detected energy is then

$$A_s^2\,\tau(\ln A_p/A_s + \tfrac{1}{2}) = A_s^2\,\tau(\ln ms_2 + \tfrac{1}{2} - \ln A_s) \tag{15}$$

where (3) has been employed. This result applies to all signals with $A_p > A_s$, so to all potentially observable meteors with mass $m > m_s \equiv A_s/s_2$. The detected energy from all meteors in this category (in the range $d\sigma\,dx$) is then of the form

$$s_0 s_1\,d\sigma\,dx \int_{m_s}^{\infty} A_s^2\tau(\ln ms_2 + \tfrac{1}{2} - \ln A_s)\, m^{-2}dm = (\tfrac{3}{2})\, s_0 s_1 s_2 \tau\, A_s\, d\sigma\, dx. \tag{16}$$

The second part of the calculation is concerned with the remaining signals, those with $A_p \leqslant A_s$. The energy obtained from any one of them is derived as in (14), but with t_s replaced by 0; it is then given by $A_p^2\tau/2$. This result applies to all potentially observable meteors with mass $m \leqslant m_s$, and so leads to a net detected energy of the form

$$s_0 s_1\,d\sigma\,dx \int_0^{m_s} (m^2 s_2^2\tau/2)\, m^{-2}dm = (\tfrac{1}{2}) s_0 s_1 s_2 \tau\, A_s\, d\sigma\, dx. \tag{17}$$

By adding (16) and (17), it is seen that the net contribution to the mean signal level from all potentially observable trails in the range $ds\,dx$ has the form

$$2s_0 s_1 s_2 \tau A_s\, d\sigma\, dx$$

where, for present purposes, the constant factor $2A_s$ is irrelevant and the incidence pattern s_0 may be ignored. The factor $s_1 s_2$ gives the functional form of the observable trail distribution, in the sense previously defined, whereas the factor τ provides the modification necessary for converting that distribution to a distribution of the mean signal source. This illustrates one effect of signal durations on meteor scattering observations.

Signal durations will naturally have an effect upon the length of time the signal level exists above any arbitrary counting level, and this is the second effect to be considered here. It will be assumed that the counting level A_c is sufficiently high that there is no appreciable overlap of individual signals. The correction for overlapping signals is fairly routine, once the fraction of time spent above the counting level is determined. The actual fraction depends on absolute incidence rates, which are not under consideration here.

The analysis is once again concerned with observable signals alone, and so with $A_p > A_c$ and $m > m_c \equiv A_c/s_2$. The time spent by a particular signal above A_c is

$$\tau \ln(A_p/A_c) = \tau \ln(ms_2/A_c) , \tag{18}$$

and the distribution of time spent above A_c by all observable signals has the form

$$s_1 \int_{m_c}^{\infty} \tau \ln(ms_2/A_c)\, m^{-2} dm = s_1 s_2 \tau / A_c. \tag{19}$$

It is apparent that the same functional dependence is obtained in this problem as in that of the mean signal.

In calculating duration effects, it will be assumed that the decay constant τ has the form

$$\tau = \tau_0 \sec^2 \phi \tag{20}$$

with τ_0 constant, as given by Eshleman and Manning (1954). The transformation from a β, ψ description to an x, y description would proceed as

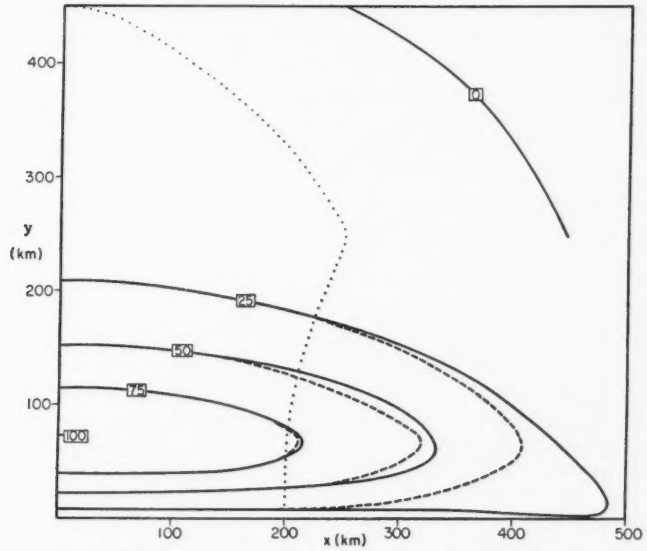

FIG. 3. As in Fig. 2, but contours illustrate distribution of sources of mean signal level, or sources of signal duration above a counting level.

before, the extra factor τ being carried through. Accordingly, the spatial distribution corresponding to $s_1 s_2 \tau$ can be derived from the earlier calculations simply by a multiplication by $\sec^2\phi$. The resultant contour charts (renormalized to a maximum of 100) are presented in Fig. 3, where the solid curves and broken curves have the same significance as before. It may be noted that the $\sec^2\phi$ factor is strongly dependent on x, and so the approximation given for ϕ in (7) cannot normally be applied to duration effects, without introducing appreciable errors.

VI. COMPARISON WITH THE WORK OF ESHLEMAN AND MANNING

Eshleman and Manning (1954) derived contour charts similar to those in Figs. 2 and 3, in one of the first theoretical discussions of meteoric forward-scattering. Their analysis differed somewhat in principle, as well as in detail, from that presented here, but a comparison of the two methods of attack is of interest.

With regard to the principles, comparison may first be made between their Fig. 4 and the present Fig. 2 (solid lines). Although very similar in appearance, these two figures display essentially different quantities. Theirs, on the one hand, displays the distribution of what have here been termed potentially observable trails. The present contours, on the other hand, take the scattered signal strength into account as well, and require that it be above a given counting level.

Their Fig. 5, like the present Fig. 3, is intended to display the distribution of mean signal sources. It does this, however, by modifying the potentially observable distribution by a power factor. The appearance of s_2 in (16) and (17), rather than s_2^2, indicates that an amplitude correction is in fact in order, even though it is the received power that is being considered. The distinction is important in practice, when the use of high gain antennas is contemplated; their effect is not nearly as great as might previously have been supposed. (This is a direct result of the assumed inverse square distribution of meteor masses, and of the assumed linear dependence of signal amplitude on mass.) The effect of the exponential decay on mean signal was taken as proportional to τ by Eshleman and Manning, a choice which has been justified in the preceding section under a suitable definition of 'mean signal'.

In addition to the differences of principle between the two analyses, there are some differences of detail. Eshleman and Manning, for example, considered a plane meteoric region 100 km. above the T–R axis, whereas a curved layer has been adopted here and in I, 100 km. above the earth's surface. This introduces a difference of some 20 km., which is the depth of the mid-point of the 1000 km. T–R axis below the curved surface of the earth. Again, they assumed the polarization factor to be close to unity, whereas here the factor is that appropriate to horizontally polarized transmission and reception. It is this factor that introduces the truncated 'zero' contour in Figs. 2 and 3, and provides a related warping of the other contours.

Eshleman and Manning adopted meteor trails of constant length, and neglected the variation of ionization density with orientation. Here, the variation of ionization density with height was taken to be independent of

orientation, while the actual density at a specific height was taken to vary as the cosine of the zenith angle ζ. These conditions introduce an extra sec ζ factor in s_1 and a cos ζ factor in s_2. The inverse square law of mass distribution leads to a direct product of these two factors, $s_1 s_2$, and so the net result is no different on this account.

Finally, Eshleman and Manning attributed potentially observable trails to the region in which the center of the trail lay. Here, trails were attributed to the $\mathfrak{H}$ level at the points where the latter was intersected by the inclined plane of observation—or, in the more exact description of I, at the points where it was cut by the normals to the appropriate ellipsoids. In effect, each analysis contains some error inherent in reducing the three-dimensional array of observation points to a two-dimensional description, and the errors are somewhat different in the two cases.

VII. SUMMARY

The trails which contribute to meteoric forward-scattering are not distributed uniformly over the sky. Their effective distribution can be derived from Fig. 2, for a 1000 km. path, by calculating the gain pattern $G(x, y)$ appropriate to the 100 km. level, and combining it with the contours shown there. In this case, the distribution refers to the number of trails which provide signals exceeding some arbitrary level. The solid curves should be used for accurate work; the broken curves result from the cylindrical approximation. The incidence pattern of meteors is assumed to be isotropic.

Similarly, the contours in Fig. 3 can be combined with the gain pattern to give the distribution of mean signal sources, or the distribution of sources for length of time of signal above a counting level.

The cylindrical approximation provides accurate results with much less labor than the full analysis, for illumination patterns which are largely confined to a region within 100 or 200 km. of the y, z plane at meteor heights. The continued use of this approximation therefore seems to be justified. The approximations implied by (7) are useful also, except for calculating ϕ when duration effects are involved.

Although different in principle and in detail, the analysis of Eshleman and Manning led to contour charts which are quite similar to those presented here. Extensions of that analysis, as to the case of anisotropic incidence patterns (Villard, Eshleman, Manning, and Peterson 1955), should yield results which would be comparable to corresponding extensions of the present development.

ACKNOWLEDGMENT

The authors would like to acknowledge the help of Mr. D. A. Trumpler, who very kindly assisted in the computation of the contour charts.

REFERENCES

ESHLEMAN, V. R. and MANNING, L. A. 1954. Proc. I.R.E. **42**: 530.
FORSYTH, P. A., HINES, C. O., and VOGAN, E. L. 1955. Can. J. Phys. **33**: 600.
HINES, C. O. 1955. Can. J. Phys. **33**: 493.
——— 1956. J. Atm. and Terrest. Phys. In press.
HINES, C. O., FORSYTH, P. A., VOGAN, E. L., and PUGH, R. E. 1955. Can. J. Phys. **33**: 609.
PUGH, R. E. 1956. Can. J. Phys. **34**: 997.
VILLARD, O. G., ESHLEMAN, V. R., MANNING, L. A., and PETERSON, A. M. 1955. Proc. I.R.E. **43**: 1473.

HIGH RESOLUTION RAMAN SPECTROSCOPY OF GASES

VII. ROTATIONAL SPECTRA OF *s*-TRIAZINE AND *s*-TRIAZINE-d_3[1]

By J. E. Lancaster[2] and B. P. Stoicheff[3]

ABSTRACT

The pure rotational Raman spectra of *s*-triazine ($C_3H_3N_3$) and *s*-triazine-d_3 ($C_3D_3N_3$) vapor were photographed in the second order of a 21-ft. grating spectrograph. The rotational constants were found to be $B_0(C_3H_3N_3) = 0.2146_6 \pm 0.00008$ cm^{-1} and $B_0(C_3D_3N_3) = 0.1935_8 \pm 0.0001_5$ cm^{-1}. These values, together with the assumption that the molecule is planar and has a CH bond length of 1.084 Å, give the following values for the structural parameters: $r_0(CN) = 1.338 \pm 0.001$ Å, $\angle NCN = 127°$, and $\angle CNC = 113°$.

A. INTRODUCTION

The molecular symmetry and structural parameters of symmetrical triazine in the solid state have recently been determined by X-ray diffraction. Siegel and Williams (1954) have found that the molecule is planar and has the symmetry D_{3h} as represented in Fig. 1. Wheatley (1955) confirmed these results and also determined the structural parameters; he obtained $r(CN) = 1.319 \pm 0.005$ Å, $r(CH) = 1.00$ Å, $\angle NCN = 126.8 \pm 0.4°$, and $\angle CNC = 113.2 \pm 0.4°$.

The purpose of photographing the pure rotational Raman spectrum of *s*-triazine vapor was to provide an independent check of the molecular dimensions, particularly since recent investigations of the benzene molecule, to which the triazine molecule is similar both in geometrical structure and in

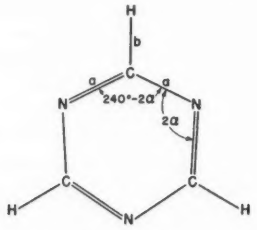

FIG. 1. Structure and structural parameters of the *s*-triazine molecule, drawn to scale.

number of electrons, seemed to show a difference between the C—C distances in the vapor and solid phases. The value obtained spectroscopically for benzene vapor (Stoicheff 1954*b*) was 0.02 Å larger than that given initially for the solid by X-ray diffraction (Cox and Smith 1954). Cox, Cruickshank, and Smith (1955) have shown that this difference is only apparent, and is due

[1]Manuscript received July 13, 1956.
Contribution from the Stamford Research Laboratories, American Cyanamid Company, Stamford, Connecticut, and the Division of Pure Physics, National Research Council, Ottawa, Canada. Issued as N.R.C. No. 4067.
[2]Stamford Research Laboratories, American Cyanamid Company, Stamford, Connecticut.
[3]Division of Pure Physics, National Research Council, Ottawa, Canada.

to the effects of anisotropic thermal oscillations of the benzene molecule in the crystal lattice. Further, these authors state, "the possibility of systematic errors in atomic positions due to angular oscillations of the molecules (or parts of them) arises in nearly all crystal structure analyses". The results of the present spectroscopic investigation of *s*-triazine vapor give further evidence to support this view; a value of 1.338 Å was obtained for the C—N distance, which is to be compared with the value of 1.319 Å found in the crystal.

B. EXPERIMENTAL

The apparatus described in paper I (Stoicheff 1954*a*) was modified recently to include four lamps in place of the two original lamps, resulting in a twofold gain in intensity. Also, a tenfold reduction in exposure time was obtained by placing a cylindrical lens in front of the photographic plate of the spectrograph.

The samples of *s*-triazine and *s*-triazine-d_3 were prepared at the Stamford Research Laboratories of the American Cyanamid Company, Stamford, Conn., in connection with a study of the vibrational spectra (Lancaster and Stamm 1956). The preparation of *s*-triazine has been outlined by Grundmann and Kreutzberger (1954). The deuterated sample was obtained by using DCN and DCl in place of HCN and HCl as reactants. Mass analysis of the deuterated triazine indicated an isotopic purity of better than 95%. Both triazines were repeatedly sublimed over P_2O_5 before using. In both experiments small samples in the crystalline form were sealed in the Raman tube and the temperature of the Raman tube was then raised to about 75°C. with the coldest part kept at 70±2°C. According to the relation between vapor pressure (P in mm. Hg) and temperature (T in °K.), $\log_{10}P = -2672.7/T + 9.954$, the vapor pressure at 70°C. is about 140 mm. Hg. This pressure was maintained during the experiments with *s*-triazine, but the pressure of *s*-triazine-d_3 was probably not higher than 100 mm. Hg owing to the small quantity available for these experiments.

Several plates of the rotational Raman spectra were obtained in the second order of a 21-ft. grating spectrograph, at a linear dispersion of 1.2 Å/mm. One photograph of the *s*-triazine rotational spectrum was taken without the cylindrical lens in an exposure time of 30 hr., another with the cylindrical lens in three hours. Two spectra of the deuterated *s*-triazine were photographed with the cylindrical lens in 9 and 10 hr. Second- and third-order iron lines were used for wavelength calibration, the source being an iron hollow cathode similar to that described by Crosswhite, Dieke, and Legagneur (1955). Unfortunately, in the region of λ 4358 Å only a few lines excited with this source have been measured interferometrically, and therefore the values of the wavelengths listed in the M.I.T. Tables were used. For the few intense lines which have been measured interferometrically (Stanley and Dieke 1955), a comparison with the values in the M.I.T. Tables shows a small and almost constant wavelength shift. However, this shift does not affect the absolute accuracy of the Raman displacements since, as is usually the case for rotational lines, the displacements are the averages of the Stokes and anti-Stokes lines.

C. OBSERVED SPECTRA AND ROTATIONAL ANALYSIS

Photographs of the Stokes rotational lines of *s*-triazine and *s*-triazine-d_3 are shown in Fig. 2. Each spectrum consists of a series of finely spaced lines extending to about 50 cm^{-1} from the exciting line. These are the *S* branches ($\Delta J = 2$) with spacings of approximately 0.86 cm^{-1} and 0.77 cm^{-1} for *s*-triazine and *s*-triazine-d_3, respectively. Although the region close to the exciting line is overlapped by many grating ghosts, a few lines of the *R* branches ($\Delta J = 1$) can be seen in both spectra. For the *R* branches, the line spacing is half that of the *S* branches. The line spacing of 0.39 cm^{-1} for *s*-triazine-d_3 is the closest structure that has been resolved with the present apparatus.

The wave number displacements of the rotational lines of each molecule were measured on two plates and the average values are listed in Table I. Agreement for unblended lines was within ± 0.02 cm^{-1}. The measurements for *s*-triazine are considered to be slightly more accurate than those for *s*-triazine-d_3 since the plates of the latter spectrum are somewhat inferior.

As mentioned in Section A, the X-ray diffraction investigations have shown that *s*-triazine is planar and has the symmetric top configuration of point group D_{3h}. The observed rotational Raman spectra of both isotopic molecules

TABLE I

OBSERVED WAVE NUMBER SHIFTS OF THE ROTATIONAL RAMAN LINES OF *s*-TRIAZINE AND *s*-TRIAZINE-d_3

J	$\lvert\Delta\nu\rvert$,[a] cm^{-1}		J	$\lvert\Delta\nu\rvert$,[a] cm^{-1}	
	s-Triazine	*s*-Triazine-d_3		*s*-Triazine	*s*-Triazine-d_3
23	21.01_8	—	45	39.91_0	35.99_2
24	21.89_4	—	46	40.76_0	36.76_6
25	22.76_0	—	47	41.62_2	37.59_6*
26	23.60_6	21.25_9	48	42.49_1	— *
27	24.47_8	22.02_1	49	43.35_0	39.08_1
28	25.31_3	22.82_4			
29	26.17_9	23.61_8*	50	44.19_7	39.86_6
			51	45.03_8	40.64_4
30	27.03_1	24.43_0	52	45.92_3	41.40_3
31	27.90_9*	25.16_7	53	46.79_2	42.16_9
32	28.72_1*	25.94_8	54	47.62_3*	42.95_2
33	29.58_9	26.75_4	55	48.45_4	43.68_2
34	30.46_3	27.48_1[b]*	56	49.31_0	44.45_8
35	31.32_2	28.20_1[b]*	57	50.19_6	45.18_7
36	32.18_6	29.03_2*	58	51.05_6	46.00_7
37	33.03_9	29.79_6	59	51.92_5	46.85_9*
38	33.90_1	30.53_1			
39	34.75_4	31.30_0	60	52.80_2[b]	— *
			61	53.63_5[b]	48.34_3*
40	35.62_0	32.10_3	62	54.47_4[b]	49.06_5
41	36.48_4	32.90_3*	63	55.35_3[b]	49.86_9
42	37.34_1	33.70_6	64	56.22_2[b]	50.66_7
43	38.26_3*	34.45_2	65	—	51.45_0
44	39.05_4	35.19_9	66	—	52.19_0
			67	—	52.96_2
			68	—	53.78_7
			69	—	54.54_4

[a]All values are averages of the Stokes and anti-Stokes lines measured on two plates, except the values marked [b].

[b]Stokes lines measured on one plate only.

*Lines blended with grating ghosts.

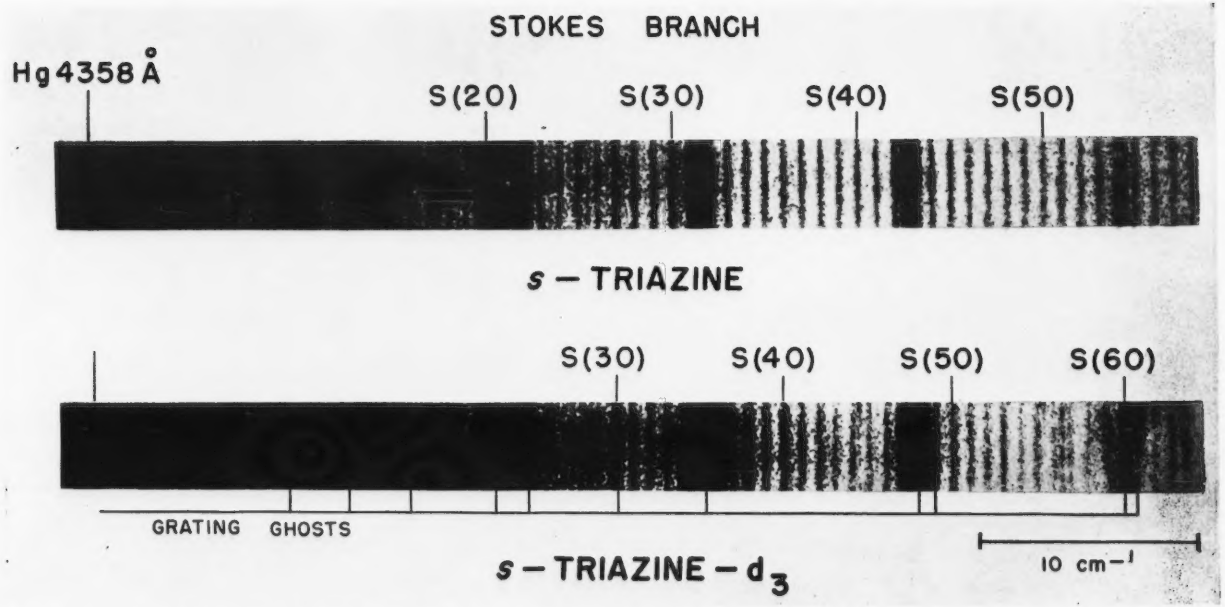

FIG. 2. Rotational Raman spectra (Stokes branches) of *s*-triazine and *s*-triazine-d_3 photographed with a 21-ft. grating. Gas pressures of about 15 cm. Hg were used.

are consistent with such a structure. For a detailed analysis of the rotational Raman spectra of symmetric top molecules, the reader is referred to earlier papers in this series on benzene and allene (Stoicheff 1954*b*, 1955).

The present analysis is based on the lines of the S branches. Their wave number displacements are given (to a very good approximation) by

$$|\Delta\nu| = 4B_0(J+3/2)-8D_J(J+3/2)^3.$$

According to this equation, the rotational constants B_0 and D_J can be obtained from a graph of $|\Delta\nu|/(J+3/2)$ plotted against $(J+3/2)^2$. Such graphs are shown in Fig. 3 for both molecules. The constants obtained in this way are:

s-triazine: $B_0 = 0.2146_0 \pm 0.00008$ cm^{-1} and $D_J \approx 1.3\times10^{-8}$ cm^{-1},

s-triazine-d_3: $B_0 = 0.1935_8 \pm 0.0001_5$ cm^{-1} and $D_J \approx 2.5\times10^{-8}$ cm^{-1}.

As a check these values were used to calculate back the positions of the rotational lines, and the agreement with the measurements was within ± 0.02 cm^{-1}.

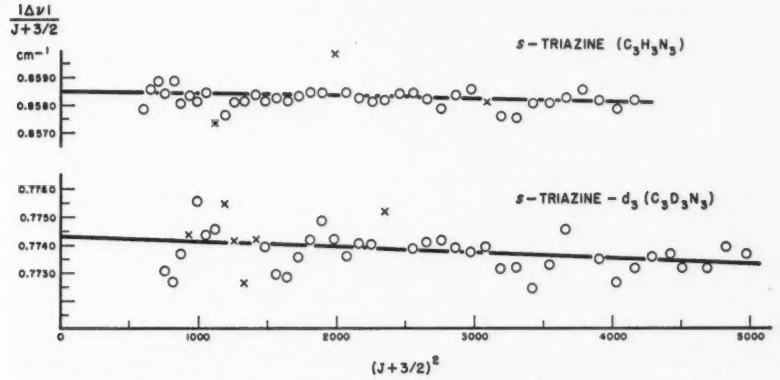

FIG. 3. $|\Delta\nu|/(J+3/2)$ graph for the ground states of s-triazine and s-triazine-d_3. (× lines blended with grating ghosts.)

D. MOLECULAR STRUCTURE OF s-TRIAZINE

Although the observed rotational Raman spectra are consistent with a symmetric top structure for s-triazine, they do not provide direct evidence of planarity or of deviation of the molecule from a regular hexagon.[4] Both results were obtained from the X-ray data and are used below to determine the molecular dimensions from the Raman data.

The moment of inertia about any axis in the plane of the molecule passing through the figure axis is

$$I_B{}^0 = 2\{m_C a^2\sin^2\alpha + m_N a^2\sin^2(120-\alpha) + m_H(\tfrac{1}{2}\sqrt{3}\, b + a\sin\alpha)^2\}$$

where $a = r_0(\mathrm{CN})$, $b = r_0(\mathrm{CH})$, $2\alpha = \angle\mathrm{CNC}$, and $2(120-\alpha) = \angle\mathrm{NCN}$

[4]This result may be inferred indirectly by assuming the regular hexagonal structure and calculating the C–N and C–H distances from the Raman data above. The values so obtained are $r_0(\mathrm{CN}) = 1.256$ and $r_0(\mathrm{CH}) = 1.116$ Å; the C–N distance is far different from the X-ray value and the C–H distance is larger than that found in similar ring molecules.

(see Fig. 1). A similar equation is obtained for *s*-triazine-d_3 with m_H replaced by m_D. Thus, if it is assumed that $r_0(CH) = r_0(CD)$ these two equations are functions of the three unknowns, a, b, and α.

The numerical values of the moments of inertia obtained from the values of B_0 given above and the atomic constants of Cohen, DuMond, Layton, and Rollett (1955) are

$$I_B^0(s\text{-triazine}) = (130.42_4 \pm 0.04_9) \times 10^{-40} \text{ gm. cm.}^2,$$
$$I_B^0(s\text{-triazine-}d_3) = (144.58_6 \pm 0.11_2) \times 10^{-40} \text{ gm. cm.}^2$$

Since the two values are insufficient for the determination of the three unknown parameters, several values of the CH distance (from 1.05 to 1.09 Å) were assumed, and the remaining parameters were evaluated. The values of the structural parameters, compatible with the observed moments of inertia, are given in Table II. Since the CH bonds in benzene and *s*-triazine have a

TABLE II

STRUCTURAL PARAMETERS OF *s*-TRIAZINE DETERMINED FROM THE ROTATIONAL RAMAN SPECTRA OF *s*-TRIAZINE AND *s*-TRIAZINE-d_3

r_0(CH) (assumed), Å	r_0(CN), Å	∠CNC	∠NCN
1.050	1.339_0	117.9°	122.1°
1.070	1.338_2	115.2°	124.8°
1.084	1.338_1	113.2°	126.8°
1.090	1.338_0	112.5°	127.5°

similar bond environment, the bond lengths are expected to be nearly equal. Thus, included in Table II are the values of the parameters assuming $r_0(CH) = 1.084$ Å, the value found in benzene. Estimates of the accuracy of the parameters were obtained from the probable errors of the B_0 values: these yield probable errors of ±0.001 Å in the CN bond length and ±1.5° in the angles.

The CN bond length is almost independent of the C—H distance and has the value 1.338±0.001 Å. In marked contrast, the angles are strongly affected by the value assumed for the C—H distance.

E. DISCUSSION

The value of the CN bond length, 1.338 Å, determined from the present Raman data of *s*-triazine vapor is 0.019 Å larger than that found by Wheatley (1955) for the solid. This difference is well outside the experimental error of both investigations. As mentioned earlier (Section A), this result is analogous to the original discrepancy of 0.02 Å found between the C—C distances of benzene in the vapor and solid phases. In benzene, this difference was accounted for when the full anisotropy of the thermal motions was evaluated. Most likely the present difference between the C—N distances in the vapor and solid phases of *s*-triazine is also not real and arises from similar rigid-body oscillations in the crystal lattice, the effects of which have not been included in the X-ray analysis (Wheatley 1956).

A comparison of the values of the angles found here for $r_0(CH) = 1.084$ Å and in the X-ray investigation shows good agreement (although the errors in the present values appear to be larger than in the X-ray study). Moreover, the correction for thermal motion discussed above is expected to change the X-ray values of the angles only very slightly, if at all. As a result, it is believed that the above values of the angles and the assumed value of 1.084 Å for the C—H distance are fairly reliable. Thus, the combined X-ray and spectroscopic data give the following dimensions for *s*-triazine:

$$r_0(CN) = 1.338_1 \pm 0.001 \text{ Å}, \quad r_0(CH) = 1.084 \pm 0.009 \text{ Å},$$
$$\angle NCN = 126.8 \pm 0.4°, \text{ and } \angle CNC = 113.2 \pm 0.4°.$$

It is of interest to note that the C—N distance in *s*-triazine is the same as that found in pyridine and in melamine. A value of 1.340±0.005 Å was obtained for the C—N distance in pyridine from the microwave spectrum (Bak, Hansen, and Rastrup-Andersen 1954) and a value of 1.345±0.01 Å was obtained for the C—N distance in the ring of melamine from the X-ray diffraction data of the crystal which included the corrections for thermal motions (Hughes 1941). This similarity of the CN bond length in *s*-triazine, pyridine, and melamine suggests that the length of CN bonds in all such ring structures is in the range 1.338 to 1.345 Å.

REFERENCES

BAK, B., HANSEN, L., and RASTRUP-ANDERSEN, J. 1954. J. Chem. Phys. **22**: 2013.
COHEN, E. R., DUMOND, J. W. M., LAYTON, T. W., and ROLLETT, J. S. 1955. Revs. Mod. Phys. **27**: 363.
COX, E. G., CRUICKSHANK, D. W. J., and SMITH, J. A. S. 1955. Nature, **175**: 766.
COX, E. G. and SMITH, J. A. S. 1954. Nature, **173**: 75.
CROSSWHITE, H. M., DIEKE, G. H., and LEGAGNEUR, C. S. 1955. J. Opt. Soc. Amer. **45**: 270.
GRUNDMANN, C. and KREUTZBERGER, A. 1954. J. Am. Chem. Soc. **76**: 632.
HUGHES, E. W. 1941. J. Am. Chem. Soc. **63**: 1737.
LANCASTER, J. E. and STAMM, R. F. 1956. To be published.
SIEGEL, L. A. and WILLIAMS, E. F. 1954. J. Chem. Phys. **22**: 1147.
STANLEY, R. W. and DIEKE, G. H. 1955. J. Opt. Soc. Amer. **45**: 280.
STOICHEFF, B. P. 1954*a*. Can. J. Phys. **32**: 330.
——— 1954*b*. Can. J. Phys. **32**: 339.
——— 1955. Can. J. Phys. **33**: 811.
WHEATLEY, P. J. 1955. Acta Cryst. **8**: 224.
——— 1956. Private communication.

THE PHOTOPROTONS EMITTED FROM OXYGEN-16 NUCLEI[1]

By D. L. Livesey[2]

ABSTRACT

The photographic plate method has been used to study photoprotons emitted from oxygen gas exposed to bremsstrahlung of maximum energies 30, 35, and 70 Mev. The proton energy distributions above 5 Mev. show maxima corresponding to peaks in the (γ, p) excitation function at 20.7, 21.9, and 24.0 Mev. The proton angular distributions are anisotropic, in general agreement with a $\sin^2\theta$ function, but the high-energy protons exhibit a degree of asymmetry about the 90° angle which may be due to a small electric-quadrupole interference effect.

I. INTRODUCTION

Since beams of high-energy bremsstrahlung produced by electron-accelerators have become available, many experiments have been designed to study the nuclear particles emitted in photodisintegration. The greatest interest attaches to the emission of single nucleons, and the work of Byerly and Stephens (1951) and Dixon (1955) on photoneutrons from copper and lead has revealed the main features of their energy and angular distributions. These phenomena at moderate energies can largely be accounted for by theories assuming that a compound nucleus is formed, with the residual nucleus left in one of many accessible excited states. The emission of photoprotons from medium and heavy elements is more difficult to deal with in theory because the "Coulomb-barrier" effect restricts the yield of charged particles and alters the energy distributions considerably. Nevertheless, experiments by Byerly and Stephens (1951), Toms and Stephens (1951), Diven and Almy (1950), Dawson (1955), and others have demonstrated that the compound-nucleus theory can explain the main features of photoproton emission from medium elements between magnesium and copper. It is also clear that the photoprotons emitted from heavy nuclei show anisotropy in angular distributions which may be explained by assuming a direct electric-dipole interaction, as suggested by Courant (1951), together with a certain amount of electric-quadrupole interference in some cases.

More recently, attention has been paid to the emission of photoprotons from light nuclei, where the Coulomb barrier is usually negligible and specific effects due to known excited states of the residual nuclei may be expected. A reaction of particular interest is the disintegration of oxygen-16:

$$O^{16}+h\nu = H^1+N^{15}-12.1 \text{ Mev.}$$

Here the residual nucleus has no level between the ground state and states more than 5 Mev. above it, so that for photon energies up to 5 Mev. above the threshold proton emission must leave the N^{15} nucleus in its ground state. The energy distribution of the protons then reproduces the main features of

[1]Manuscript received June 12, 1956,
Contribution from the Department of Physics, Queen's University, Kingston, Ontario.
[2]Formerly National Research Council Postdoctorate Fellow. Present address: Oundle School, Oundle, Northants, England.

the excitation function for the reaction. Spicer (1955) has shown that investigation of the oxygen photoprotons reveals at least one peak in the excitation function near 15 Mev., while at slightly higher energies the existence of various minor peaks has been deduced by Johansson and Forkman (1955). Stephens, Mann, Patton, and Winhold (1955) extended the measurements into the region of the main electric-dipole or "giant" resonance near 22 Mev. They showed that the energy distribution of protons with energies exceeding 6 Mev. exhibits a pronounced peak due to the main resonance, with some indications of subsidiary peaks as well, but the energy region above the resonance could not be explored.

In order to study the dipole resonance in more detail, it is desirable to use a method giving adequate resolution of proton energies and to extend the measurements to photon energies well above 22 Mev. It is of particular importance to locate the positions of narrow peaks within the main resonance in view of experiments by Katz and others (1954) and by Penfold (1955) on the "breaks" in the activation curves for the $O^{16}(\gamma, n)$ reaction in this energy region. One expects each "break" to correspond with a separate sharp level in the O^{16} nucleus, but this has not been checked, and there are difficulties in the way of accurate energy calibrations in the betatron experiments. Another reason for prosecuting the work on oxygen photoprotons is the possibility of establishing angular distributions of the emitted particles and so throwing light on the process of photodisintegration in the main resonance region.

This paper describes the results obtained in a detailed investigation of photoprotons emitted from oxygen exposed to bremsstrahlung produced by the 70 Mev. synchrotron at Queen's University. The machine was operated at three different energies, namely 30, 35, and 70 Mev., and the protons were recorded in photographic plates distributed around the gas column exposed to the beam. Energy distributions of protons above 5 Mev. were found, also the angular distributions of various energy groups over the angular range of 35° to 145° with respect to the incident photons. The same apparatus has been used in experiments on photodisintegration processes in other elements available in gaseous form.

II. APPARATUS AND EXPERIMENTAL METHOD

The plate exposures were carried out in a camera designed specially for work on particles emitted from gases at high pressure and shown diagrammatically in Fig. 1. The X-ray beam was collimated by lead blocks, 14 in. thick, before it reached the camera, and the beam diameter could be adjusted to either 1.5 cm. or 0.6 cm. at the center of the plate-holder, which was at a distance of 130 cm. from the synchrotron target. The beam passed into the apparatus through an aluminum-alloy plate machined locally to a thickness of 1/10 in. and it left the chamber through a similar plate. The body of the camera was of steel tubing, and the end-plates were held together by six steel rods. Before the experiments were started the apparatus was tested successfully at a pressure of 600 lb./sq. in. The control of gas pressure over a wide range up to

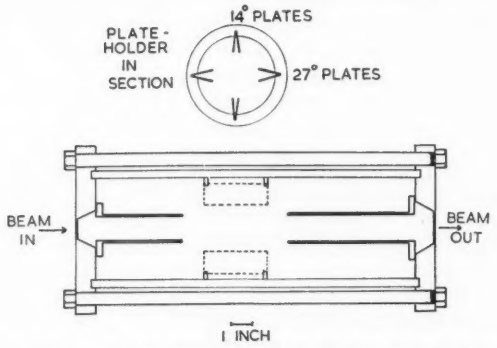

FIG. 1. Diagram of gas camera in section, with a transverse section of the plate-holder to show the arrangement of plates around the X-ray beam.

high values was an extremely useful feature of the method, enabling one to suppress low-energy tracks where necessary and providing a sufficient yield of particles from gases of low atomic mass. In this experiment the pressure was measured with an Ashcroft Duragauge reading from −30 in. of mercury to +75 lb./sq. in. with a retarded scale up to 150 lb./sq. in. The available accuracy of about 1% was considered sufficient in view of the possible impurities in gases obtained directly from cylinders, and the filling system used a pair of needle-valves which performed to the same degree of accuracy.

In order to prevent charged particles ejected from the aluminum reaching the plates in the center of the camera, the beam was surrounded by cylindrical brass shields fixed to the end-plates. The free space of 5 in. between the shields formed a column of gas around which four photographic plates were exposed in pairs. With the geometry adopted, particles emitted from the gas column and entering the near edge of each plate made angles between 25° and 155° to the beam direction. In practice tracks at the extreme angles were recorded but the data were not relied on and the useful range of angles was from 35° to 145°. The plates, which measured 3 in. by 1 in., were fitted in a plexiglass holder in the dark room before being loaded into the camera. In section across the apparatus the short side of each plate was tangential to a circular aperture slightly larger than the actual X-ray beam in use, the pairs of plates being at 27° with the 1.5 cm. beam and at 14° with the narrow beam. The maximum angle of dip recorded for tracks entering the near edge of a plate was 35° with the larger beam and 20° with the narrow beam. Reduced angles of dip could be selected by measuring tracks at the further edge of a plate.

Before each set of exposures the central line of the camera and collimator was aligned in the direction of the maximum X-ray intensity by the use of X-ray films exposed in several positions along the axis. During a run on the synchrotron, which might last several hours, the pressure and temperature of the oxygen were checked periodically. The energy of the electron beam was fixed by controlling the r-f. pulse length, and the beam intensity was monitored continuously by an ion chamber coupled via a d-c. amplifier to a recording

meter. The calibration of the monitor in roentgens was carried out with the 70 Mev. beam by experiments on the activity induced in standard copper foils near the target, but the correct calibration at 30 and 35 Mev. was not known at the time of these experiments.

The plates were of the Ilford C.2 and E.1 types, coated with 200 μ and 400 μ emulsion layers. It was found that the usual procedure for processing these plates, described by Dawson and Livesey (1956), did not yield satisfactory tracks, apparently because the long exposures in high-pressure oxygen bombarded by X-rays led to some inhibition of the latent image. The procedure finally adopted involved the use of D.19 developer, which caused a certain amount of surface marking but gave strong proton tracks of full range. Some plates were allowed to "fade" for a few days before being processed but these gave only faint indications of the initial parts of proton tracks in the surface of the emulsion. Most of the plates were placed shortly after exposure in distilled water, then in a cold solution consisting of D.19 developer diluted with 20 parts of water, and they were kept so overnight in a refrigerator at 4°C. The developer was allowed to warm slowly to room temperature, spending 30 min. between 15°C. and 20°C. The plates were again washed in distilled water before they were put in an acid stop-bath, which was placed in the refrigerator for 30 min. The fixing solution was also kept cold during the first 30 min. of the plates' immersion, after which fixation was completed at room temperature. After being washed the plates were soaked in a 30% solution of glycerine before being dried, and this treatment was effective in keeping the net shrinkage factor close to unity.

Two observers measured the tracks seen in microscope traverses across the plates, and for each track the range and angle were recorded; different magnifications were employed and frequent cross-checkings of similar data were carried out. In this experiment all tracks were assumed to be protons, except a few dense tracks which were possibly alpha-particles and which were omitted in analysis. The observed proton range in the emulsion was corrected by the addition of a range equivalent to the gas traversed between the center of the beam and the point of entry into the emulsion, and the proton energy was found from the range–energy relation of Gibson, Prowse, and Rotblat (1954). The width of the beam introduced a spread into the energies calculated, but this did not amount to more than ± 0.1 Mev. in the wide beam exposures and was quite negligible in the case of the narrow beam.

The observers also recorded all tracks which went right through the emulsion, and these were used in the compilation of angular distributions at high proton energies. Otherwise these angular distributions would be modified considerably by the escape effect, because tracks at right angles to the beam are much more likely to enter the emulsion at steep angles than those making small angles to the beam. The observed energy distributions are necessarily affected by escape, which causes losses from 8.5 Mev. upwards in 200 μ plates exposed with the wide X-ray beam. In 400 μ plates losses occur above 11.5 Mev., while the use of the narrow beam with 200 μ plates makes the escape correction unnecessary below 12 Mev. The upper energy limit for detection depended on

the particular plate in use, and on the degree of fogging, but in the least favorable cases tracks up to 15 Mev. were seen clearly and in one of the 70 Mev. plates a proton of energy 29 Mev. was recorded.

The geometry of the plates relative to the cylindrical beam was such that the number of tracks recorded in a small unit area at distance R from the center of the beam should be given by the expression:

$$F \,.\, N \,.\, y/R^2 \,.\, s(\theta) \sin\theta \,.\, d\theta,$$

where F = net photon flux in the beam,

N = number of target nuclei per unit volume in the gas,

y = perpendicular distance of the beam axis from the plane of the plate,

θ = angle between protons and incident photons,

and $s(\theta)$ = differential cross-section per unit solid angle at angle θ.

A small correction for the finite size of the beam was calculated, and in estimating the flux F a Schiff type of spectrum was used. The data were grouped to form energy distributions and angular distributions in which the numbers per 10° interval in θ were divided by $\sin\theta$ to obtain ordinates proportional to the yield per unit solid angle.

At all stages in these experiments efforts were made to detect spurious proton tracks produced by photons and neutrons outside the defined X-ray beam. Background runs were undertaken with the camera evacuated, a separate experiment on the fast neutron flux inside and outside the beam was carried out, and various spurious effects were investigated theoretically. All tracks which did not come within the correct angle limits in dip and azimuth were rigidly excluded. These did not number more than a few per cent of the total abundance, and it is believed that background effects are negligible in the following results.

III. RESULTS AT 30 MEV. AND 35 MEV.

Previous experiments on the (γ, p) reaction in oxygen have shown that, with the maximum bremsstrahlung energy not exceeding 25 Mev., the energy distribution of protons above 5 Mev. is due to those processes leaving N^{15} in its ground state. If the measurements are extended to higher energies there is the possibility that excited states of N^{15} will affect the distribution, but this is less likely if, as is expected, the excitation function drops sharply beyond the dipole resonance at 22 Mev. If, on the other hand, the function shows peaks in this region, there will be corresponding peaks at lower energies in the proton energy distributions where the excited states of N^{15} are brought into play. It is important, therefore, to investigate the higher proton energies first before discussing the distribution at lower energies. As will be seen from the present results, the main features of the dipole resonance are reproduced in the proton energy distributions obtained with 30 Mev. and 35 Mev. bremsstrahlung. At 30 Mev. all tracks recorded are likely to be protons from the (γ, p) reaction because the thresholds for multiple reactions of the (γ, pn) and $(\gamma, 2p)$ types and for deuteron emission are too high to allow particles of

sufficient range to be produced. The 35 Mev. results are less easy to interpret at the lower proton energies but they extend the useful range for study of the (γ, p) reaction to photon energies well above the resonance. Throughout this work possible reactions in the rare isotopes of oxygen have been ignored.

The first results were obtained from a 200 μ and a 400 μ plate exposed at 30 Mev. and the energy distribution of 724 tracks above 7 Mev. is shown in Fig. 2A. The main feature of the histogram is a pronounced peak at 9.2 ± 0.1 Mev. and this is believed to be due to the dipole resonance which is therefore

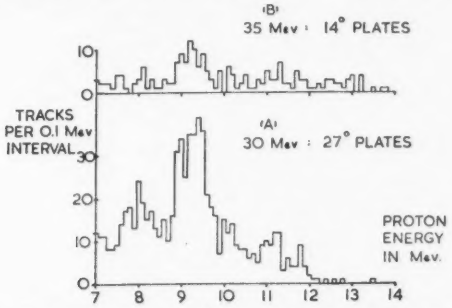

FIG. 2. A. Lower. Energy distribution of 724 proton tracks in plates exposed at 30 Mev. with full beam.
B. Upper. Energy distribution for 205 tracks in a 200 μ plate exposed at 35 Mev. with narrow beam.

located at 21.9 ± 0.1 Mev. photon energy. The quoted error may be doubled when we take into account similar peaks observed in other energy distributions and possible errors in the range–energy relations used. The first results also yielded evidence of subsidiary peaks near 8 Mev. and 11 Mev. proton energies, but the high-energy side of the resonance could not well be investigated owing to the low abundance of photons above 25 Mev. in the bremsstrahlung spectrum. In the series of plates exposed at 35 Mev., 768 tracks were measured in one 200 μ plate and two 400 μ plates, with results shown in Fig. 3A. Difficulty

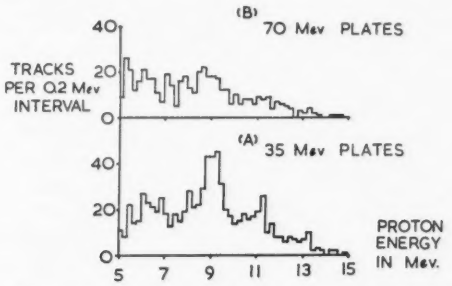

FIG. 3. A. Lower. Energy distribution of 768 proton tracks in plates exposed at 35 Mev. with full beam.
B. Upper. Energy distribution of 487 proton tracks in plates exposed at 70 Mev. with full beam.

was experienced in processing these plates and the final energy resolution was inferior to that obtained previously, but the same general features were found in the distribution. In order to check the details, a set of plates was exposed at the 14° position with the narrow beam passing through the camera. The yield of tracks was very low, but the energy distribution of 205 protons, shown in Fig. 2B, agrees closely with that in Fig. 2A.

Finally, to test the significance of possible peaks in the foregoing distributions, all data referring to 30 Mev. and 35 Mev. plates were collected in one

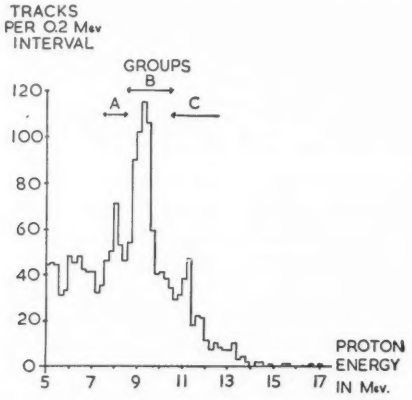

FIG. 4. Combined energy distribution of all proton tracks in 30 and 35 Mev. plates.

histogram, shown as Fig. 4. This confirms the existence of at least three main energy groups marked A, B, and C in the diagram:

Group	Energy range (Mev.)	Peak photon energy (Mev.)
A	7.5–8.5	20.7±0.2
B	8.6–10.4	21.9±0.2
C	10.5 upwards	24.0±0.2

There is also a possible peak near 13 Mev., corresponding to a photon energy of 26 Mev. Some of the protons with energies below 7.5 Mev. may have left the residual N^{15} in an excited state, but tests based on the abundance of tracks in Groups A and C showed that Group A could not have been caused in this way and must be due to a genuine minor peak within the main resonance. At the same time one cannot rule out the possibility that some of the tracks in Group A among the 35 Mev. results are due to excited states of N^{15}.

The positions of peaks A and B agree very closely with those of "breaks" in the (γ, n) activation curve for oxygen as determined in early work at Saskatoon (Katz *et al.* 1954). On the other hand, betatron experiments at higher resolution have shown that there are in fact many more "breaks" in this region, and recent work by Penfold (1955) revealed sharp levels congregating in two broader groups around 21.2 Mev. and 22.6 Mev., i.e. at least

0.5 Mev. higher than the present figures. Until the calibration of the betatron energies is rendered more certain it is difficult to decide the correct result, but the present experiment does confirm the existence of level structure within the main resonance.

The nature of the resonance may be studied by means of the angular distributions of protons emitted at various energies. Fig. 5 includes results for

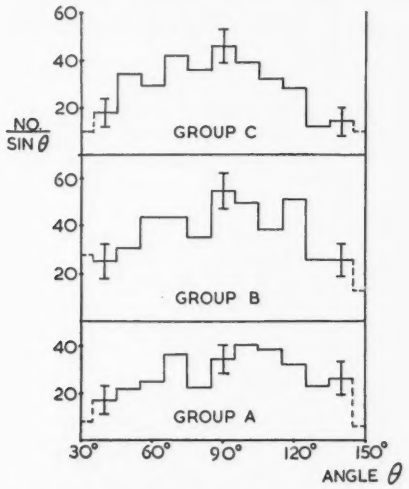

FIG. 5. Angular distributions of protons in energy groups A, B, and C, the ordinates being proportional to yield per unit solid angle of collection.

Groups A, B, and C in all the plates exposed at 30 Mev. and 35 Mev. These histograms show significant maxima near 90°, but the high-energy protons have the peak forward, near 80°, while that in the Group A results is probably above 90°, near 110°. This asymmetry about a line perpendicular to the beam may also be judged by comparing the actual numbers of tracks recorded in the angular ranges 35° to 85° ("forward") and 95° to 135° ("backward"):

Group	Forward	Backward
A	105±10	136±12
B	230±15	235±15
C	210±15	147±12

The statistics do not warrant detailed conclusions but it is probable that there is a change in the form of the angular distribution of protons as the photon energy varies through the resonance region. The results at 30 Mev. and 35 Mev. were very similar to each other, so it is not likely that the excited states of N^{15} influence these results appreciably.

The form of the distribution was studied analytically after asymmetrical effects had been cancelled out by averaging the values for supplementary

angles. These average ordinates were plotted against $\sin^2\theta$, as shown in Fig. 6. The straight line obtained passes close to the origin and is in agreement with a distribution of the form:

$$f(\theta) = A + B \sin^2\theta,$$

where

$$A/B = 0.1 \pm 0.05.$$

The ratio A/B may be too low because of some systematic error as yet undetected, but all the observed distributions agreed with the above result.

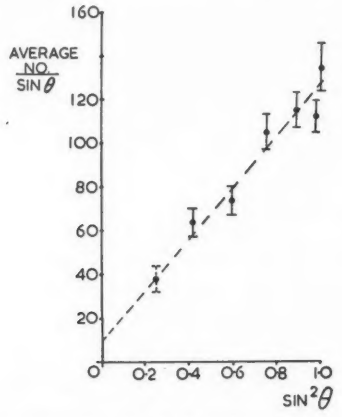

FIG. 6. Yields of protons in energy groups A, B, and C averaged over supplementary angles and plotted against $\sin^2\theta$.

IV. RESULTS AT 70 MEV.

The foregoing results show that the excitation function for the (γ, p) reaction in oxygen has a considerable "tail" above the main resonance, extending to at least 26 Mev. An attempt was made to obtain further evidence by exposing plates with the synchrotron running at 70 Mev. The resulting data cannot be interpreted unambiguously because the tracks recorded may have originated in many reactions besides the (γ, p) process. About 500 tracks were measured in one 200 μ plate and one 400 μ plate, and the proton energy distribution is shown in Fig. 3B, where it may be compared with results obtained under similar conditions at 35 Mev. The resolution of groups is poor and the main resonance peak near 9 Mev. is not prominent. Many long tracks were found to traverse the entire emulsion even in the 400 μ plate, so there must be a large number of tracks with proton energies above 12 Mev. For this reason it is difficult to ascertain the exact shape of the spectrum above this limit, and no new groups were detected.

The highest proton energy recorded was 21.8 Mev., corresponding to a photon energy of 35.4 Mev., and there were two tracks at 18.5 Mev., photon energy 31.8 Mev. These figures agree, perhaps fortuitously, with peaks in the excitation function of the alternative reaction $O^{16}(\gamma, 4\alpha)$, as reported by

Dawson and Livesey (1956). The angular distributions of various energy groups at 70 Mev. were not markedly different from those in Fig. 5, but it is clear from the energy distribution that the low-energy protons must differ in properties from those observed at 30 Mev. and 35 Mev. The greatest interest attaches to the angular distribution of high-energy protons, and Fig. 7 shows this for all protons observed with energies above 10.5 Mev. The dashed curve represents the function:

$$f(\theta) = A + B(\sin\theta + p\sin\theta\cos\theta)^2$$

with $A/B = 0.2$ and $p = 0.2$.

The errors in the parameters quoted may be large, but the small quadrupole term in the expression may be sufficient to explain the asymmetry of the observed angular distribution.

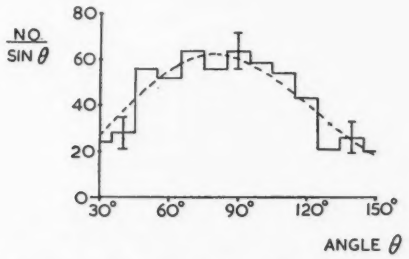

FIG. 7. Angular distribution of all proton tracks observed with energies greater than 10.5 Mev. The dashed curve represents the function:

$$f(\theta) = A + B(\sin\theta + p\sin\theta\cos\theta)^2$$

with $A/B = 0.2$ and $p = 0.2$.

Calculations were also made on the partial cross-sections of the (γ, p) reaction for transitions to the ground state of N^{15}, but these depend on rather unreliable estimates of the photon flux. The average of all data gives a partial cross-section rising to a peak of 10 mb. at 22 Mev., with a subsidiary peak of 5 mb. at 24 Mev., and an integrated cross-section between 20 and 25 Mev. of 20 Mev-mb.

V. CONCLUSIONS

This experiment leads to the following deductions concerning the (γ, p) reaction in oxygen-16:

(*a*) the cross-section exhibits a sharp maximum at 21.9±0.2 Mev. with subsidiary peaks at 20.7 and 24.0 Mev.,

(*b*) the integrated partial cross-section for transitions to the ground state of N^{15} is approximately 20 Mev-mb. between 20 Mev. and 25 Mev.,

(*c*) the angular distributions of protons are anisotropic, the particles being preferentially emitted at right angles to the incident photons,

(*d*) when averaged over supplementary angles, the numbers of protons per unit solid angle are closely proportional to $\sin^2\theta$ at all energies above 7.5 Mev., and

(*e*) the protons with energies exceeding 10.5 Mev. show a forward peak in their angular distribution.

ACKNOWLEDGMENTS

The author is deeply indebted to Professor B. W. Sargent for help and advice, and to the National Research Council for financial assistance. Mr. R. D. Bradfield contributed to the design of the gas camera and constructed it. Mr. H. Janzen ran the synchrotron, and Mrs. E. MacPhail measured a large proportion of the tracks. Thanks are due to Drs. L. Katz, D. H. Wilkinson, L. E. H. Trainor, and B. M. Spicer for discussions and correspondence. The experiment was part of the synchrotron program at Queen's University supported financially by the Atomic Energy Control Board.

REFERENCES

Byerly, P. R., Jr. and Stephens, W. E. 1951. Phys. Rev. **83**: 54.
Courant, E. D. 1951. Phys. Rev. **82**: 703.
Dawson, W. K. 1955. Bull. Am. Phys. Soc. **30** (4): Abstr. Q1.
Dawson, W. K. and Livesey, D. L. 1956. Can. J. Phys. **34**: 241.
Diven, B. C. and Almy, G. M. 1950. Phys. Rev. **80**: 407.
Dixon, W. R. 1955. Can. J. Phys. **33**: 785.
Gibson, W. M., Prowse, D. J., and Rotblat, J. 1954. Nature, **173**: 1180.
Johansson, S. A. E. and Forkman, B. 1955. Phys. Rev. **99**: 1031.
Katz, L., Haslam, R. N. H., Horsley, R. J., Cameron, A. G. W., and Montalbetti, R. 1954. Phys. Rev. **95**: 464.
Penfold, A. S. 1955. Proceedings of the Photonuclear Conference at Case Institute of Technology, Cleveland, Ohio, U.S.A.
Spicer, B. M. 1955. Phys. Rev. **99**: 33.
Stephens, W. E., Mann, A. K., Patton, B. J., and Winhold, E. J. 1955. Phys. Rev. **98**: 839.
Toms, M. E. and Stephens, W. E. 1951. Phys. Rev. **82**: 709.

THE LIFETIME OF POSITRONS ANNIHILATING IN ALUMINUM[1]

By G. Jones[2] and J. B. Warren

ABSTRACT

The absolute lifetimes of positrons decaying in aluminum and mica have been found to be $1.7 \pm 0.4 \times 10^{-10}$ sec. and $2.4 \pm 0.4 \times 10^{-10}$ sec., in accord with the determination by Bell and Graham using a different technique.

INTRODUCTION

At the present time there is no satisfactory explanation for both the absolute values of lifetimes and the variation in lifetime of positrons annihilating in condensed materials, the experimental data for which have been mainly given by Bell and Graham (1953) and by de Benedetti *et al.* (1952). The lifetimes in all the metals so far examined appear to be quite similar, centering about a value of $1.5(\pm 0.5) \times 10^{-10}$ sec. with some tendency for slightly shorter values in high Z metals. This is close to the value of 1.25×10^{-10} sec. expected theoretically for para-positronium, which is in accord with Deutsch's measurements on the magnetic quenching of three-quantum annihilation in a gas (Deutsch 1953). If it is assumed that this more or less constant lifetime in a metal arises from the formation of positronium atoms, presumably both the long-lived (1.4×10^{-7} sec.) ortho- and para-positronium are formed, and a rapid conversion by electron exchange occurs between these two states of the atom. In this way the probability of a positronium atom annihilating while in the triplet, ortho, state is very small but, unfortunately, since the ortho–para conversion can occur both ways, as Garwin (1953) pointed out the positronium atom would exist in the ortho state for three-quarters of its life and for only one-quarter in the para-state. Consequently a positron lifetime of $4 \times 1.25 \times 10^{-10}$ sec. would be expected, not the 1.5×10^{-10} sec., as found experimentally.

Minton (1954), using a rather different technique to Bell and Graham, found values of 2.9×10^{-10} sec. for the annihilation in aluminum and 3.5×10^{-10} sec. in lead. In view of this discrepancy it seemed worth while to try to make a further independent measurement of the absolute lifetime in aluminum.

TECHNIQUE

In measurements of lifetimes by the delayed coincidence technique, in cases where the lifetime to be determined is short compared to the resolution time of the apparatus, a prompt resolution curve is needed to complete the analysis. Since the time of occurrence of the pulse from a scintillation counter is a function of the energy dissipated in the phosphor it is highly desirable, though not usually possible, to use as "prompt source" an isotope emitting gamma rays of nearly the same energy as those being measured.

[1]Manuscript received July 13, 1956.
Contribution from the Department of Physics, University of British Columbia, Vancouver, Canada.

[2]Present address: Chalk River Laboratories, Atomic Energy of Canada Ltd., Chalk River, Ontario.

Bell and Graham used a Na^{22} source of positrons mounted in a fast phosphor, so that the emergence of the positron provided the zero time for the coincidence circuit. The positrons were then energy selected and focused onto a second phosphor to produce the prompt curve, or focused onto an absorber in front of the second phosphor to produce the delayed curve. The symmetry of the arrangement is thus not quite the same for the two curves; in the prompt measurement the second counter detects positrons of one energy stopping in a region close to the front face of the crystal, while in the delayed measurement the second counter is responding to the Compton electrons of various energies arising from the interaction of 0.51 Mev. gammas throughout the phosphor.

Minton (1954) used the 1.28 Mev. gamma ray from the Na^{22} source to fix the zero time and obtained the prompt curve by using the cascade gamma rays from Co^{60}, selecting suitable parts of the Compton electron spectrum with side channel discrimination. With narrow side channel energy discrimination to ensure good equality of pulse amplitudes with these two sources, it is difficult to get an adequate coincidence rate.

In this measurement essentially the same technique as used by Minton was followed, except that As^{76} was chosen as prompt source rather than Co^{60}. At the time this work was done it seemed that the decay scheme of As^{76}, summarized in Nuclear Data (1950), included two cascade gamma rays of 1.20 Mev. and 0.55 Mev. The similarity of these energies to those from Na^{22}, 1.28 Mev. and 0.51 Mev., would thus practically eliminate any chance of a spurious lifetime effect due to inequalities between the energies of test source and prompt source. Recently, however, Kurbatov *et al.* (1955) confirmed, on the basis of γ–γ and β–γ coincidence measurements, the decay scheme shown in Fig. 1, first proposed by Kraushaar and Goldhaber (1953). If this

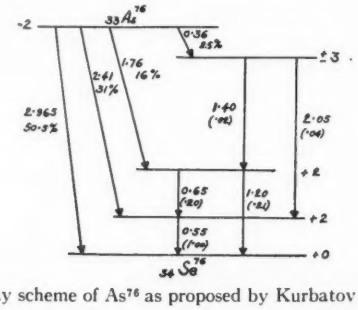

FIG. 1. Decay scheme of As^{76} as proposed by Kurbatov *et al.* (1955).

scheme is correct, then the coincidences recorded would correspond to those between the 0.55 Mev. and 2.05 Mev. cascade gamma rays, with a smaller contribution from the 0.65 and 1.40 Mev. cascade radiations. Since the positron emission from As^{76} is less than 1/10% of the negatron (Havens *et al.* 1948), the annihilation radiation from this source is negligible. In both cascades the lower energy component is close in energy to 0.51 Mev., so that there should be little, if any, effect of shifting the coincidence resolution curve due to pulse shape variations.

APPARATUS

The delayed coincidence apparatus is described elsewhere (Jones and Warren, to be published). Basically it consisted of a fast coincidence scheme as developed by Bell, Graham, and Petch (1952) but the time separation of associated events was converted to pulse height and sorted with a conventional kicksorter, so enabling the whole coincidence resolution curve to be obtained at one time and avoiding any correction for source decay.

The Na^{22} positron source consisted of a deposit of about 0.01 mc. of $Na^{22}Cl$ on the inside of an aluminum tube of $\frac{1}{4}$ in. outside diameter. The wall thickness was 1/16 in., twice that needed to stop the 540 kev. positrons. As the sodium chloride was of high specific activity, a negligible number of positrons was stopped in the NaCl itself. A source of about 0.001 mc. of As^{76}, 26.8 hr. half-life, was prepared by placing some 99.95% pure $As_2^{75}O_3$ in an aluminum tube, similar to that used for the positron source, and irradiating with a flux of thermal neutrons.

The general layout of the apparatus is shown in Fig. 2. The source–counter distance was 2 cm. for the positron emitter and about 3 mm. for the As^{76}

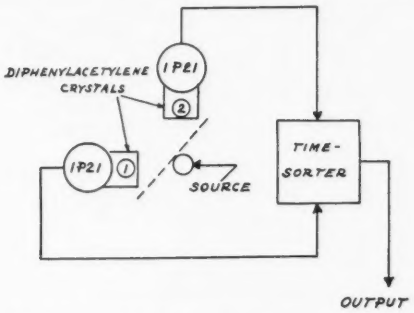

FIG. 2. Apparatus layout for coincidence measurements.

so as to keep the coincidence counting rates approximately the same. It was necessary to widen the side channel windows for the As^{76} source after about 10 hr. running to raise the counting rate. The two sources were alternated to determine whether any slow gain shifts were occurring.

RESULTS

Typical coincidence resolution curves, including a comparative one taken with the positrons annihilating in mica, are shown in Fig. 3. The curves were analyzed by the centroid shift method (Newton 1950). Checks made on the time-sorter pulse height dependence on coincidence counting rate, by altering the counter–source distance, showed that there was an effect. Due allowance was made for this, since the counting rates with the As^{76} source were lower than with the Na^{22}. The time calibration of the apparatus was obtained by measuring the centroid shift due both to inserted delay in one side and to varying the gamma ray flight time to one of the counters. The measurements

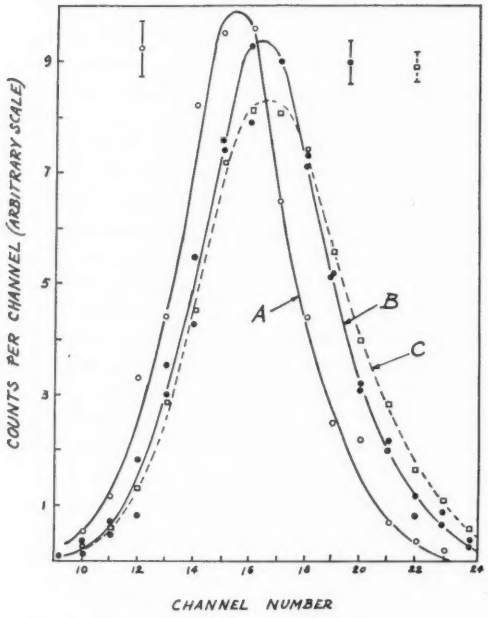

FIG. 3. Delayed coincidence resolution curves:
A. Prompt curve obtained with As^{76} source.
B. Curve from positrons decaying in aluminum.
C. Curve from positrons decaying in mica.

were repeated under slightly different conditions a month later to ensure that the reproducibility was good.

The centroid shift between the prompt coincidence resolution curve and that from positrons annihilating in aluminum was found to correspond to a time delay of 1.6×10^{-10} sec. The lifetime of the 550 kev. state of Se^{76} is about 1.5×10^{-11} sec. (Temmer and Heydenburg 1955). The lifetime of the second 2+ state involved in the 1.40–0.65 Mev. cascading gamma rays would not be expected to be any longer. Both the 0.65 Mev. mixed magnetic dipole – electric quadrupole radiation (Kraushaar and Goldhaber 1953) from the 2+ state to 2+ state transition and the 0.55 Mev. electric quadrupole radiation from the 2+ state to 0+ state transition are favored one-phonon jumps, and the collective nature of the excitation gives rise to fast transitions (Scharff-Goldhaber and Weneser 1955).

Consequently the lifetime of positrons decaying in aluminum according to our measurements is 1.7×10^{-10} sec. The experimental error to be attached to this result is considered to be $\pm0.4\times10^{-10}$ sec.

The shift of the centroid on changing from aluminum to mica amounts to $(0.7\pm0.4)10^{-10}$ sec. in accord with the result of Bell and Graham (1953).

These results are in good accord with those of Bell and Graham and would confirm the fact that the lifetime in metals is probably a little longer than that of free para-positronium but certainly not by a factor of four.

ACKNOWLEDGMENTS

We are much indebted to Professor W. Burcham and the University of Birmingham cyclotron group who made the Na^{22} for us. We wish to thank Dr. K. Erdman for preparing the As^{76} source with the U.B.C. Van de Graaff generator and for many helpful discussions. One of us (G.J.) gratefully acknowledges the award of an N.R.C. bursary held during the time this work was carried out.

REFERENCES

BELL, R. E. and GRAHAM, R. L. 1953. Phys. Rev. **90**: 644.
BELL, R. E., GRAHAM, R. L., and PETCH, H. E. 1952. Can. J. Phys. **30**: 35.
DE BENEDETTI, S. and RICHINGS, H. J. 1952. Phys. Rev. **85**: 377.
DEUTSCH, M. 1953. *In* Progress in nuclear physics. Vol. 3. *Edited by* O. R. Firsch. Academic Press, Inc., New York. p. 131.
GARWIN, R. L. 1953. Phys. Rev. **91**: 1571.
HAVENS, W. W., RAINWATER, L. J., and WU, C. S. 1948. Phys. Rev. **74**: 1248.
JONES, G. and WARREN, J. B. To be published.
KRAUSHAAR, J. J. and GOLDHABER, M. 1953. Phys. Rev. **89**: 1081.
KURBATOV, J. D., MURRAY, B. B., and SAKAI, M. 1955. Phys. Rev. **98**: 674.
MINTON, G. H. 1954. Phys. Rev. **94**: 758.
NEWTON, T. D. 1950. Phys. Rev. **78**: 490.
"Nuclear Data". 1950. Natl. Bur. Standards, Circ. No. 449.
SCHARFF-GOLDHABER, G. and WENESER, J. 1955. Phys. Rev. **98**: 212.
TEMMER, G. M. and HEYDENBURG, N. P. 1955. Phys. Rev. **100**: 961.

THE ABSORPTION OF ULTRAVIOLET IONIZING RADIATION IN GASES[1]

By G. R. Bainbridge[2] and W. A. Prowse

ABSTRACT

The sparking probability of a test gap, to which short-duration direct high voltage pulses are applied, is shown to depend on the distance of the gap from a source of short wavelength, ultraviolet radiation. The radiation is restricted to a small volume of gas midway between the electrodes. The sparking probability can therefore be used as a parameter in examining the absorption of the radiation responsible for triggering a discharge in the gas. Absorption of ultraviolet radiation by the gases argon, air, nitrogen, and oxygen has been studied.

I. INTRODUCTION

Photoionization of gas atoms is of importance in studies of many forms of electrical discharge in gases. Cravath (1935) suggested two forms of radiation active in corona discharges, one of which was five times more heavily absorbed by the gas than the other and so was considered to be the radiation active in ionizing the gas. Further studies of corona have been made by many workers (Kip 1939; Trichel 1939; and many papers by Loeb and his colleagues). In the upper atmosphere, at heights greater than 20 km., the ionization produced by short wavelength photons from the sun is of great interest (Appleton 1935*a*, *b*; Massey 1938; and Sayers 1943). Photoionization is believed to be an active mechanism in the propagation of lightning flashes (Cravath and Loeb 1935; Meek 1939) and in the production of long laboratory sparks (Loeb and Meek 1941; Weissler 1943). The photoelectric effect in gases has been recently further studied in Geiger counters (Jaffé, Craggs, and Balakrishnan 1949) with particular consideration of the absorption coefficients of the radiation. The triggering effect of short wavelength ultraviolet radiation in ultra high frequency discharges has also been reported (Jasinski and Prowse 1952).

There is a definite lack of experimental data on the photoionization of air and the other permanent gases which contrasts with the volume of data from studies of the photoelectric effect in the alkali metal vapors (Hughes and Dubridge 1932). The difference in the state of knowledge in these two allied branches of work is due mainly to the fact that the energy of the photon needed for ionization in the alkali metal vapors is much less than that which will ionize a gas atom in a single stage. Moreover, it was difficult until quite recently to find a material which will serve as a window to transmit those wavelengths less than 1200 Å, the transmission limit of lithium fluoride, with energy sufficient to ionize many gases (Chubb and Friedman 1955).

In the experiments reported here both a spark source of photons and a spark detector of ions are contained in the same chamber. We do not use a window. That radiation from the source entering the gas between the electrodes of a test gap is a likely trigger for a discharge has been previously demonstrated

[1]Manuscript received May 25, 1956.
Contribution from Durham University, Durham, England.
[2]Now at McMaster University, Hamilton, Ontario, Canada.

by Jasinski and Prowse (1951). In particular, among other tests, they placed in the irradiating beam thin films of nitrocellulose, cellulose nitrate, and polystyrene, which considerably reduced the probability of test gap sparks. It is not claimed that the experimental technique which follows gives an accurate method for the measurement of spectral absorption coefficients, since the radiation produced by a spark in the gas is not homogeneous in wavelength. However, a mean coefficient can be measured, characteristic of those wavelengths which ionize the gas through which they pass. Such a coefficient is of value (Dutton, Haydon, and Jones 1952, 1953) in deciding whether or not a discharge streamer is likely to be propagated by the mechanism of photoionization in the gas.

II. DESCRIPTION OF THE APPARATUS

(*a*) *General Circuit Arrangements*

The block diagram of Fig. 1 has, as its centerpiece, two similar, properly terminated delay lines, *A* and *B*, arranged in circular form. These delay lines

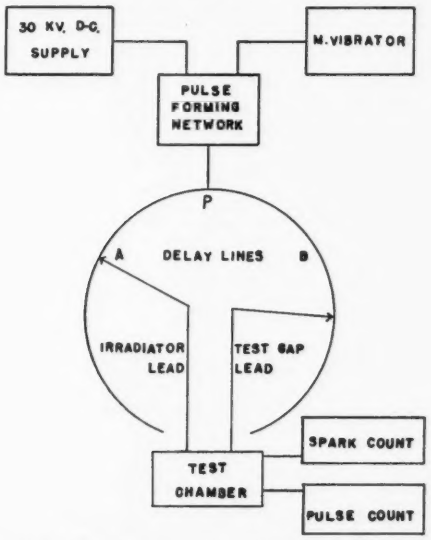

FIG. 1. Schematic view of the arrangement used to generate suitably timed irradiator and test pulses, and to record sparking probability.

receive, at their common point *P*, unidirectional pulses of 0.35 μsec. duration at intervals of two to four seconds, determined by the multivibrator. The peak voltage of these pulses may be set on the 30 kv. d-c. generator. Radial connections are taken from a point on one line to a spark gap with electrode spacing short enough to ensure that it fires for every pulse. This is the source of photons. From the other line similar connections go to a test gap, so adjusted that the pulses will not cause breakdown unless the gap is irradiated.

A delay between the times of arrival of irradiator and test pulses at their respective gaps may be secured by connecting to the delay lines at appropriate radial positions. In this work the irradiator pulse is made to precede the test pulse by about 10^{-8} sec.

Sparking probability is defined as the ratio of the number of pulses causing a spark in the test gap to the number of pulses applied to that gap. This parameter, to be used in assessing the effect of the radiations, is measured by means of two electromechanical counters. One counter is operated only by the current conducted through the test gap, when a spark occurs there. The other counter records pulses applied at the test gap, during which irradiation of the test gas occurs.

(*b*) *The Test Chamber*

In Fig. 2 is illustrated the arrangement of the test and irradiator gaps. The space between the plane-faced brass electrodes of the test gap may be adjusted

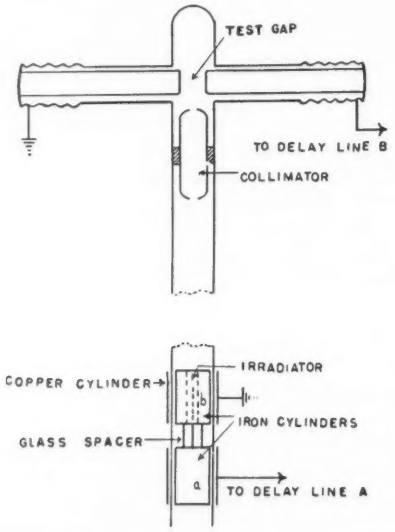

FIG. 2. Irradiator and test gap arrangement in the absorption experiment.

with bellows at the ends of the short crossarms of a T-shaped pyrex glass chamber. A glass collimator, close to the test gap, restricts radiations travelling along the main stem of the T to the mid-gap region. The irradiator consists of two soft iron cylinders joined by an insulating tube. A fine wire, electrically connected to cylinder *a*, projects through the tube into a hole bored centrally through cylinder *b* leaving 1/16 in. clearance. When a pulse is applied to *a* and *b*, via the copper sleeves and glass chamber wall, a spark develops between the fine wire and the inner wall of cylinder *b*. Ultraviolet radiation emerges

from the hole in b and travels towards the test gap. The distance it must travel, x, can be set by using a magnet outside the chamber to move the irradiator.

The chamber can be evacuated by means of a conventional oil-diffusion pump and rotary backing pump system. Mercury vapor, from mercury which is used in the reference manometer to measure the gas pressure, is excluded from the chamber by using differential gauges. Because of the exploratory nature of the experiment, dry commercial cylinder gases were used. In these gases impurities are present which have high absorption coefficients (Jaffé *et al.* 1949) and in some cases are ionized by radiations almost as easily as the gas being examined. However, these impurities are present to about 0.25% of the principal gas and so contribute little to the net results.

III. THEORETICAL CONSIDERATIONS

The magnitude of the absorption coefficient is obtained from values of the sparking probability P for a range of irradiator distances x as follows: Let G photons, sufficiently energetic to ionize the gas and so trigger the spark, be emitted per unit solid angle by the irradiator at S (Fig. 3). The number of

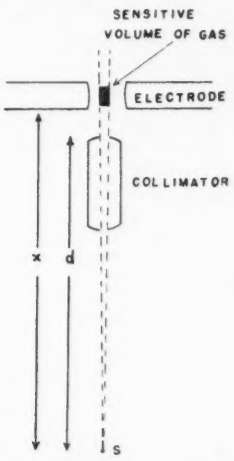

FIG. 3. The beam of radiation is restricted to a small sensitive volume of gas between the electrodes of the test gap.

these photons which travel in a direction such that they will, if unabsorbed, enter the sensitive volume of the test gap through the collimator aperture, of area A, situated at a distance d from the source is GA/d^2. If the mean absorption coefficient of the gas for the photons is μ, then $(GA/d^2)\exp(-\mu x)$ photons arrive in the test gap.

Let the probability that a spark will start per unit time be p and the probability that a spark will start in test time t be P. Then

$$1-P = \exp(-pt) .$$

If p is proportional to the flux of photons in the gap, pt is proportional to $(GA/d^2)\exp(-\mu x)$. Thus

$$\ln_e(1-P) = C_1 GA \exp(-\mu x)/d^2,$$

where C_1 is a constant independent of x and d. Or

$$\ln_e[\ln_e(1-P)] + 2\ln_e d = C_2 - \mu x,$$

where C_2 is another arbitrary constant. The magnitude of μ is given by

$$\mu = dL/dx \text{ where } L = \ln_e[\ln_e(1-P)] + 2\ln_e d.$$

IV. RESULTS AND DISCUSSION

Probability counts were made using 500 to 1000 trial pulses for each of many irradiator distances between 10 and 50 cm. from the test gap. Although radiation from a naked spark source is not monochromatic, graphs of L with x were found to be reasonably linear over appreciable ranges of x. Thus a mean absorption coefficient for ionizing radiation could be assessed from the slope of the graphs. Any curvature of the L–x graphs was such as to suggest a higher value of absorption coefficient at shorter distances. This is to be expected if some wavelengths are more penetrating than others and a filtering effect occurs.

Typical graphs of L with x are shown for dry air, Fig. 4, at two working pressures; Fig. 5 shows graphs for argon with two different test pulse voltages.

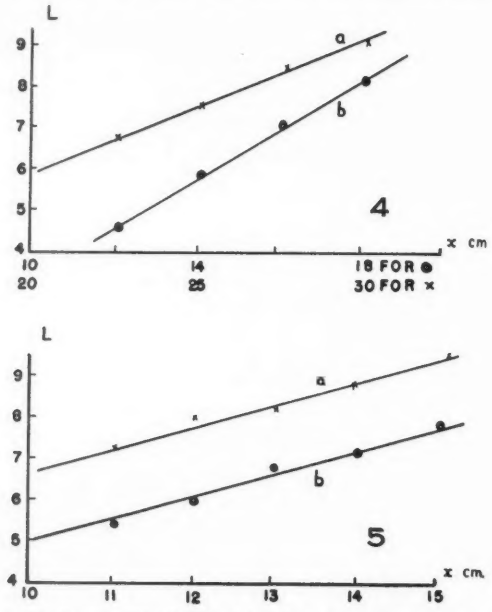

FIG. 4. Graphs of $\ln_e[\ln_e(1-P)]+2\ln_e d$ with x, for air, at two pressures: a, 46 cm. Hg and b, 61 cm. Hg.

FIG. 5. Graphs of L with x, for argon, at two different applied pulse voltages, at atmospheric pressure: a, 16 kv. and b, 20 kv.

It was found that the value of μ was independent of gap length, overvoltage, and irradiator timing. Argon, air, oxygen, and nitrogen were examined. In Table I are representative results for these gases. The last column of this table shows the values of μ at atmospheric pressure, derived by following the reasonable assumption that absorption coefficient is proportional to pressure. Argon was used as the pilot gas in the experiment and so the larger test gap lengths which were tried at first with this gas are indicated. Coefficients are given for at least two radiation ranges and/or pressures for each gas and the effect of the gas in filtering out the more heavily absorbed radiations is clearly seen. Air and oxygen were found to be much more absorbing than argon and nitrogen. The values given by other observers for the absorption coefficients of these four gases are listed with our values in Table II, transformed to the equivalent value at atmospheric pressure to help in comparison. Values for hydrogen are included to show the trend in the results obtained by different methods.

Measurements of the absorption of ionizing radiations in gases have been made in the past using techniques which fall conveniently into three groups. First a large number of these give absorption coefficients for particular wavelengths at low pressures. Table II shows typical earlier values of Schneider (1940) for air, and recent values of Weissler (1952) and his colleagues and of Watanabe *et al.* (1952) for oxygen and nitrogen. Generally the values quoted in this literature for specified absorption bands are high, but they show that absorption coefficients can change very rapidly with wavelength in the region below 1300 Å. Coefficients range from those indicating transparency to several hundred per centimeter. For the more heavily absorbed of these radiations 10^{-3} cm. of dry air at N.T.P. is sufficient to halve the intensity of most wavelengths of radiation between 380 Å and 1600 Å and so such wavelengths will not influence measurements over greater distances at near atmospheric pressures.

TABLE I

VALUES OF ABSORPTION COEFFICIENTS OF SOME GASES AS DETERMINED IN SPARK EXPERIMENTS

Gas	Pressure, cm. Hg	Test gap, cm.	Range, d in cm.	Absorption coefficient μ at 76 cm. Hg
Argon	76	0.75	10–15	0.50
	76	0.75	10–35	0.28
	46	0.60	10–45	0.23
Air	61	0.33	10–18	0.80
	46	0.33	17–30	0.78
Nitrogen	61	0.33	10–35	0.25
Oxygen	61	0.33	10–14	1.24
	46	0.33	10–18	1.18

A second group of useful information on absorption coefficients at low pressures has been gained from experiments of the type pioneered by Hertz (1923) and Mohler (1926), where the group of ionizing radiations is examined,

TABLE II

ABSORPTION COEFFICIENTS OF SOME GASES COMPARED AT ATMOSPHERIC PRESSURE

Worker	Method	Pressure of measurement, cm. Hg	Spectral region where specified, Å	Absorption coefficient of gas, cm.$^{-1}$				
				Argon	Air	Nitrogen	Oxygen	Hydrogen
Schneider 1940	Vacuum spectrometer	0.1	380– 800		140–580			
			800–1000		8–570			
			1000–1600		0–130			
Weissler *et al.* 1952	Vacuum spectrometer	0.5–100×10^{-4}	300– 800			>90		
			800–1300			50–150		
			1300			<10		
		0.5–100×10^{-4}	300– 740				500–1000	
			740–1000				100*	
			1000–1300				<10*	
			1300				<10	
Watanabe *et al.* 1952	Photocell	7–49	Below 1050				2	
			1050–1300				<10*	
		50	1050–1600			<0.01†		
Geballe 1944	Photocell	0.1						418
Maunsell 1955	Kingdon cage	1–8×10^{-3}		>5000				
		1–4×10^{-3}				>5000		
		1–6×10^{-3}						Very low
Greiner 1933	Geiger counter	10						1.36
Christoph 1937	Geiger counter	1.5			53.2			27.36
Raether 1938	Wilson chamber	14–50			1.98		5.02	0.84
Jaffé *et al.* 1949	Geiger counter	2.5–10		0.99				0.91
Jasinski and Prowse 1951	Impulsive spark	76			0.53		2.58	
This paper	Short d-c. spark	46–76		0.23–0.5	0.78–0.8	0.25	1.18–1.24	

*Much higher absorption coefficients are reported in molecular absorption bands in these spectral regions.
†This absorption coefficient is the value in the weak molecular absorption bands thought possible here.

rather than separate wavelengths. A recent report of Maunsell (1955), using a Kingdon cage detector of ions, is of this kind. He reports considerably larger absorption coefficients than those determined for monochromatic radiations of energy greater than the ionizing potential. He also indicates a distinct pressure effect which gives an increase in the observed absorption coefficient for both argon and nitrogen for pressures up to 80 microns.

Lastly we have a number of measurements made of absorption coefficients for ionizing radiation under discharge conditions at higher pressures. The experiments of Greiner (1933), Cravath (1935), Dechène (1936), and Raether (1938) in this group are now among the classics of the subject. More recent experiments of Jaffé, Craggs, and Balakrishnan (1949) in Geiger counter experiments yield information on absorption coefficients in general agreement, where comparison can be made, with Raether's early cloud chamber experiments, the more recent ultra high frequency work of Jasinski and Prowse (1952), and our own presently reported values. They confirm our belief that at near atmospheric pressures in certain tank purity gases ultraviolet radiations arising in one part of the gas can be responsible for photoionization many centimeters away in the same gas, and that this can be of importance in the rapid propagation of electric discharges.

REFERENCES

Appleton, E. 1935*a*. Proc. Roy. Soc. A, **150**: 685.
——— 1935*b*. Proc. I. R. E. **23**: 655.
Christoph, W. 1937. Ann. Physik, **30**: 446.
Chubb, T. A. and Friedman, H. 1955. Rev. Sci. Instr. **26**: 493.
Cravath, A. M. 1935. Phys. Rev. **47**: 254.
Cravath, A. M. and Loeb, L. B. 1935. Physics, **6**: 125.
Dechène, G. 1936. J. phys. radium, **7**: 533.
Dutton, J., Hayden, S. C., and Jones, F. L. 1952. Proc. Roy. Soc. A, **213**: 185.
——— 1953. Proc. Roy. Soc. A, **218**: 206.
Geballe, R. 1944. Phys. Rev. **66**: 316.
Greiner, E. 1933. Z. Physik, **81**: 543.
Hughes, A. L. and Dubridge, L. A. 1932. Photoelectric phenomena. McGraw-Hill Book Company, Inc., New York.
Jaffé, A. A., Craggs, J. D., and Balakrishnan, C. 1949. Proc. Phys. Soc. B, **62**: 39.
Jasinski, W. and Prowse, W. A. 1951. Inst. Elec. Engrs. Monograph 10.
——— 1952. Inst. Elec. Engrs. Monograph 32.
Kip, A. F. 1939. Phys. Rev. **55**: 549.
Loeb, L. B., Hudson, G. G., Kip, A. F., and Bennett, W. H. 1941. Phys. Rev. **60**: 714.
Loeb, L. B. and Meek, J. M. 1941. The mechanism of the electric spark. Stanford University Press, California.
Massey, H. S. W. 1938. Negative ions. Cambridge University Press, London.
Maunsell, C. D. 1955. Phys. Rev. **98**: 1831.
Meek, J. M. 1939. Phys. Rev. **57**: 722.
Mohler, F. L. 1926. Proc. Natl. Acad. Sci. U.S. **12**: 494.
Raether, H. 1938. Z. Physik, **110**: 611.
Sayers, J. 1943. Repts. Progr. Phys. **9**: 52.
Schneider, E. G. 1940. J. Opt. Soc. Amer. **30**: 128.
Trichel, G. W. 1939. Phys. Rev. **55**: 383.
Watanabe, K., Zelikoff, M., and Inn, E. C. 1952. Geophys. Research Papers **No. 21**: 19.
Weissler, G. L. 1943. Phys. Rev. **65**: 95.
Weissler, G. L. and Lee, P. 1952. J. Opt. Soc. Amer. **42**: 200.
Weissler, G. L., Lee, P., and Mohr, E. I. 1952. J. Opt. Soc. Amer. **42**: 84.

AN EMISSION SPECTRUM OF THE DIACETYLENE ION

A STUDY OF SCHÜLER'S "T" SPECTRUM UNDER HIGH RESOLUTION[1]

By J. H. Callomon[2]

ABSTRACT

Schüler and Reinebeck have described a new spectrum which was observed in a discharge through a mixture of an inert gas and the vapor of any of a number of organic compounds. This spectrum was labelled "T". Further experiments by the authors provided evidence that the carrier of the "T" spectrum was the diacetylene molecule. The "T" spectrum has now been reinvestigated using both normal and fully deuterated diacetylenes in a helium discharge and photographed on grating instruments with very high resolving powers. Previous vibrational assignments were extended, and the rotational structure was completely analyzed in four bands. The results, together with other evidence, show that the carrier of the "T" spectrum is the diacetylene ion, $C_4H_2^+$. The vibrational and rotational constants differ but little from those of the diacetylene ground state. The spectrum involves a transition between the first excited state $A^2\Pi_u(i)$ and the ground state $X^2\Pi_g(i)$ of the ion and is analogous in detail to the well-known Fox, Duffendack, and Barker system of CO_2^+.

1. INTRODUCTION

H. Schüler has described a discharge tube in which the effects of organic vapors on the spectrum of the positive column can be studied. The discharge is maintained by a "carrier" gas such as, for instance, helium. With high current densities the emission spectra obtained were, besides that of the carrier gas, almost exclusively those of diatomic fragments, e.g., C_2, CH, and H_2. On decreasing the current, however, these became weaker and were replaced by a number of new spectra obtained from a whole series of organic compounds. These spectra were described by Schüler and Reinebeck (1951, 1952) who labelled them with a series of letters. Many of these spectra are specific to the organic compounds which produced them; however, one of them which occurs in the visible region is common to many of the compounds and was labelled "T". Its origin suggested that it might be due to some common product of decomposition.

The "T" spectrum was obtained by using, amongst others, benzene, naphthalene, phenylacetylene, and acetylene, listed in order of increasing intensity; it appeared most strongly, however, and almost to the exclusion of all other spectra, on using diacetylene. At the same time, diacetylene was shown by means of its first absorption spectrum below 3000 Å to have been formed in a discharge running in acetylene (Reinebeck 1953; Schüler and Reinebeck 1954). On using partially and fully deuterated acetylene, the "T" spectrum showed isotopic shifts which indicated that the molecule responsible for it contains two atoms of hydrogen and that the strongest band involved the zero vibrational levels in both upper and lower states. A vibrational analysis

[1]Manuscript received July 9, 1956.
Contribution from the Division of Pure Physics, National Research Council, Ottawa, Canada. Issued as N.R.C. No. 4089.
[2]National Research Laboratories Postdoctorate Fellow; present address: Department of Chemistry, University College, London, England.

then showed the presence in the lower state of vibrational frequencies which were remarkably close to some of the normal frequencies of diacetylene in its ground state. These facts led Schüler and Reinebeck to ascribe the "T" spectrum to the neutral diacetylene molecule as a transition possibly to the ground state, although the bands could not be observed in absorption. Diacetylene is a colorless liquid.

The experiments just described have been repeated. The vibrational analysis has been extended with the help of fully deuterated diacetylene. The strongest bands were examined with resolving powers of up to 400,000 and a complete rotational analysis of four of them was made. Although no single item of the evidence thus obtained is absolutely conclusive by itself, the evidence taken as a whole leaves no doubt that the nuclear skeleton of the emitter of the spectrum is that of diacetylene as stated by Schüler and Reinebeck. However, it will be shown that the spectrum is due to the ion of diacetylene, $C_4H_2^+$, and the electronic states probably involved will be discussed.

2. EXPERIMENTAL

(*a*) *Preparation of Diacetylene*

The diacetylene was prepared from 2-butyne-1,4-diol in the way described by Keyssner and Eichler (1944), Johnson (1946), and Jones (1952*a*). The product was distilled twice *in vacuo* and its purity checked by its infrared spectrum. It was stored in dry ice, as it polymerized slowly at higher temperatures. The deuterated diacetylene was prepared from ordinary diacetylene by exchange in the liquid phase with heavy water in which a little sodium had been dissolved, in a way similar to that described by Leitch and Morse (1952) for acetylene. The exchange could be followed on a Perkin-Elmer 12C infrared spectrometer by observing the spectra of the successive samples in the regions of the C—H and C—D stretching modes at *ca.* 3300 and 2500 cm^{-1}. The final sample contained 96.5% C_4D_2 and 3.5% C_4HD.

(*b*) *The Discharge Tube*

Schüler's design (1950) was closely followed with some modifications. It consists essentially of a straight tube of pyrex glass with a central section of 35 mm. internal diameter and 40 cm. length which expands into two end sections of larger diameter and makes a total length of 1 meter. The discharge fills the central section only; side tubes lead off through liquid nitrogen traps to two hollow-cathode aluminum electrodes. The carrier gas and organic vapor are premixed and introduced continuously into the discharge at the midpoint of the tube. They divide into two streams flowing up and down the tube and into the side-arms and are pumped off continuously at the electrodes. Current is provided at 3600 v. from the 110 v. a-c. mains by a step-up transformer.

The carrier, which was generally helium, was purified by passing through two charcoal traps cooled in liquid nitrogen. Diacetylene was kept liquid in a trap cooled with ice to 0° C. where its vapor pressure is about 500 mm. The rates of flow of the gases were then controlled by two graduated needle valves which could be calibrated in terms of the pressure in the discharge tube at a

given rate of pumping by means of a mercury manometer. As the current density is increased, the spectra of the C_2 molecule appear with rapidly increasing relative intensity. In order to avoid interference, i.e., by keeping the intensity of the C_2 bands down to less than 1% of that of the "T" spectrum, the current was kept below 5 ma., equivalent to a current density of 0.5 ma./cm.^{2} The total pressure was not critical but was kept between 0.5 and 2 mm. mercury with the ratio of helium to diacetylene between 5: 1 and 20: 1. The diacetylene is completely polymerized in the discharge and hence removed from the stream; thus the part of the discharge emitting the "T" spectrum usually extended from the point of introduction of the gases only partly along the way to the electrodes, being replaced for the remaining way by the spectrum of helium. For a given current and rate of pumping the partial pressure of diacetylene at the point of entry decided only the length of the column emitting the "T" spectrum but not its intensity. The pressure was therefore usually adjusted so that only the central straight section of the discharge tube emitted the "T" spectrum, the change to the helium spectrum occurring in the side-arms. This minimized the formation of polymer which obstructs the tube, as well as conserving material. The diacetylene was used at a rate of about 2 gm. per hour from which its lifetime in the discharge under the above conditions can be calculated to be about a tenth of a second. In a dark room the discharge appeared a bright green, but in daylight it was barely visible.

(*c*) *Optical System*

Before the spectrum could be photographed with high resolution, the available intensity had to be greatly increased, since the exposure time required to bring it out well on a medium Hilger prism instrument, viewing the 40 cm. of discharge end-on, was about 15 minutes. A system of multiply-reflecting mirrors of the type described by White (1942) was accordingly built into the tube at its ends. The radius of curvature of the mirrors was 100 cm. and the available height of image at the exit 12 mm. In using such a system to integrate the intensity of emission of a luminous volume in which reabsorption does not occur (Welsh, Cumming, and Stansbury 1951; Stoicheff 1954), the limit is usually set not by the number of traversals which can be achieved, but by the reflectivity of the mirrors R: for an infinite number of traversals the integrated intensity is $(1-R)^{-1}$ times that after one traversal. In the present case, the region in which maximum intensity was required was between 5000 and 5500 Å. With mirrors coated with silver, 28 traversals could be achieved and gave an increase in intensity estimated at about 14 times. This corresponds to a reflectivity of 95%, for which an infinite number of traversals would give a factor of 20.

A loss of part of this light can occur through the optical system which transfers it from the mirror system in the discharge tube into the spectrograph. This is often a single condensing lens, so placed as to "match" the apertures of the discharge tube and spectrometer. However, when the image at the exit of the discharge tube is comparable in size to the aperture stop of the tube, i.e., the back mirror, considerable loss of light will occur through vignetting or overspill at the aperture stop of the spectrograph, i.e., the

collimator or grating. In the present case this could have amounted to 50% or more. To overcome this, it is necessary not only to match apertures, but also to match the aperture stops, i.e., in this case to focus the back mirror of the discharge tube directly onto the grating of the spectrograph. This has usually been done by placing a second collecting lens either at the exit of the discharge tube or just in front of the entrance slit of the spectrometer (see Hansen 1950). Such a system often presents mechanical difficulties and places severe restrictions on the focal length of the collector lens; hence the following symmetrical arrangement, shown in Fig. 1, was used. The image I_t at the exit

FIG. 1.

of the discharge tube is at the principal focus of the first lens F_t, focal length f_t, rendering light from any point of I_t parallel. The second lens F_g, focal length f_g, refocuses the light to an image I_g at its principal focus at the entrance slit of the spectrometer. At the same time, lens F_t forms an image of the back mirror of the discharge tube H_t at the intermediate point Q and the lens F_g in turn focuses Q on the spectrograph collimator or grating H_g. The requirements are: for the focal lengths

$$f_t/f_g = (NA)_g/(NA)_t = \text{magnification } M$$

where (NA) represents numerical aperture, and for the separation of the lenses

$$q_t = f_t(l_t+f_t)/l_t,$$
$$q_g = f_g(l_g+f_g)/l_g$$

where l_t is the distance of I_t from H_t. Q may serve as a useful aperture stop.

(*d*) *Spectrographs*

Three spectrographs were used. The weaker bands, of which only the heads were resolved, were measured with a high-speed plane grating instrument fitted with a Schmidt-type camera of aperture about $f/4$ (Moser 1955). The grating has 15,000 lines per inch and a reciprocal dispersion of 3.7 Å per mm. at 5000 Å in the third order. With fast plates the strongest bands came out after 10 sec. with an observed resolution of about 1 cm^{-1}. With finer grain plates, 0.5 cm^{-1} could be resolved. Some of the stronger bands were photographed in the second order of a 21-ft. grating in an Eagle mounting. This also has 15,000 lines per inch with the blaze at about 5000 Å in the second order. Enough of the slit could be illuminated to overcome losses due to astigmatism, and exposure times ranged from one-half to three hours with fast Kodak 103a-J plates. The dispersion was 1.27 Å/mm. at 5300 Å in the second order and the resolving power was close to the theoretical value of 180,000 corresponding to 0.10 cm^{-1} at 5300 Å. Finally, the two strongest bands were photographed on a recently completed 35-ft. instrument with a Bausch and Lomb concave grating having 30,000 lines per inch and blazed at 7000 Å in the first order.

At 5000 Å in the second order (dispersion 0.3 Å/mm.) the exposure time required was five hours, which was also the limit set by the formation of polymer in the tube which settled on the walls and reduced its bore sufficiently to obstruct the optical path. The attained resolving power of the grating was about 400,000 (80% theoretical) corresponding to a resolution of 0.05 cm^{-1} at 5000 Å.

(*e*) *Wavelength Determination*

The spectrum of an iron arc in various overlapping orders of the gratings was superimposed on the "T" spectrum to provide wavelength calibration. The final plates used for rotational analysis were each measured four times on a Gaertner comparator in such a way as to minimize periodic errors due to its screw. Wavelength values of the iron spectrum were taken from the M.I.T. Tables (Harrison 1938) and used to construct a correction curve for the deviations from a linear wavelength interpolation in the usual way. The scatter of points on this curve was so great in the case of plates taken on the 35-ft. instrument, however, that it seemed questionable whether, using the M.I.T. values, full advantage could be taken of the performance of a grating of the quality now available in determining wavelengths over a short range with high relative accuracy. Moreover, the scatter could not be reduced sufficiently by preselection of lines which seemed sharp and "good"; neither was it a function of the instrument, for the scatter was reproducible and independent of the degree of photographic exposure. The correction curves used were therefore obtained by fitting the experimental Fe points to a curve calculated theoretically from the grating dispersion formula. In determining rotational constants, it is only the shape of the correction curve that is of importance and small absolute errors in wavelengths are not important. The calculated shape is relatively insensitive to the values of the grating constant and radius of curvature assumed. In the present work, despite very careful examination, no reason could be found for doubting the validity of the method, although it was rejected by Mrozowski (1941, 1942). The good agreement between values of a given rotational constant obtained from different bands in different regions and measured on different instruments lends further support to the method.

The wavelengths measured in air were corrected with the vacuum corrections of Edlén (1953) and converted into vacuum wave numbers.

3. VIBRATIONAL ANALYSIS

(*a*) *Description of the Spectrum*

Figs. 3(*a*) and 3(*b*) show the appearance of the "T" spectrum obtained from normal and fully deuterated diacetylene under low resolution, taken with a medium Hilger prism instrument fitted with glass optics. It consists of an irregular array of broad bands which have been labelled by Schüler and Reinebeck with a series of letters and numbers from *A* to *F*. Their notation is followed here with some additions.

With higher resolving power, each of these broad bands is seen to consist of what is hereafter called a group, containing a large number of separate bands with sharp intense heads and rotational fine structure degraded to longer

wavelengths. As an example, Fig. 3(*c*) shows the appearance of group *A* photographed on the 21-ft. grating spectrograph in the second order. Two features of regularity can be picked out: some of the band heads form pairs of comparable intensity about 2 cm^{-1} apart, and some of these pairs form a regular series with spacings of about 14 cm^{-1} and steadily decreasing intensity resembling a sequence in the spectrum of a diatomic molecule, e.g., *ab*, *cd*, *ef*, *gh*. The complexity of the remaining heads is not unexpected, for corresponding to the various modes of vibration, several sequences with differing spacings and intensities will be superimposed.

The regularity described for group *A* is not found in all the groups. It can be recognized in groups *A*, B_2, C_3, D_4, and *F* of C_4H_2, and groups *A*, C_3, D_4, and *F* of C_4D_2. However, only occasional pairs are recognizable in some of the groups, e.g., B_1, while in others, especially some of C_4D_2, no regular features are apparent at all. Even in the regular groups the spacings of pairs can vary within a group and between groups by factors of two or more. This excludes the possibility of the pairs being *Q* and *R* heads of the same bands, for the rotational analysis shows that the differences in frequency between the origins and heads of bands are constant to within 1/10 cm^{-1}, which is as expected from the very small dependence of rotational constants on vibrational quantum number in diacetylene. That the series of pairs are of vibrational origin, i.e., that they are to be identified as sequences, could be shown by running the discharge tube at a low temperature. Fig. 2 shows microphotometer traces of groups *A* and B_2 taken on different parts of the same plate on the *f*/4 grating instrument at room temperature and with the tube cooled to about −100° C. (Acetylene was used instead of diacetylene as the latter has too low a vapor pressure at the low temperature.) It shows a marked decrease in intensity of

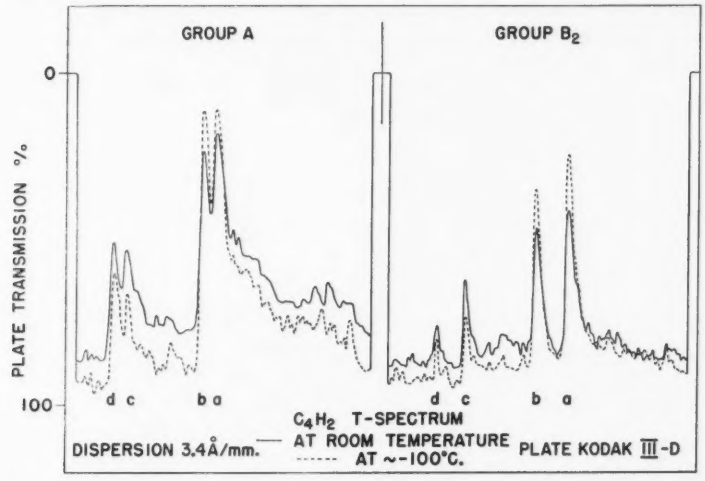

FIG. 2. The effect of temperature on the intensities of groups *A* and B_2 photographed on the *f*/4 grating instrument.

the pairs of heads *c*, *d*, relative to those *a*, *b*, but no significant change within the pairs. The latter observation does not necessarily exclude the possibility that the pairs are the first two members of sequences in one of the low frequency modes of the molecule, which would be expected to be temperature insensitive. However, the question then immediately arises why never more than two members appear, the more so as these two are always of comparable intensity. This argument gives the first indication that the "T" spectrum involves electronic doublet states. If the double heads were due to spin-splitting, however, their separations might be expected to vary but little from band to band, which is contrary to observation.

The various groups form vibrational progressions and again the apparent lack of regularity is due to the existence of more than one vibrational mode. In their analysis, Schüler and Reinebeck (1954) measured the frequency intervals betwen the intensity maxima of the various groups as observed with medium resolving power and pointed out the great similarity to some of the normal frequencies of diacetylene. By measuring the positions of the individual heads composing the groups, their analysis can now be extended; and it appears that, despite the similarity, there are differences which definitely rule out the ground state of diacetylene as being one of the states involved in the transition.

(*b*) *Analysis*

The vacuum wave numbers of all the band heads which have been measured are collected together in the Appendix, Table A1.

Deuterium substitution produces marked isotopic shifts in the spectrum; some of these are listed in Table I together with the positions of some of the principal band heads from normal ("T_{HH}") and fully deuterated ("T_{DD}") diacetylene. The shift is smallest in the strongest group, *A*, which is thus

TABLE I

POSITIONS OF SOME PRINCIPAL BAND HEADS AND ISOTOPIC SHIFTS (CM^{-1})

Group	Band	T_{HH}	T_{DD}	Δ
A	*a*	19724.5	19742.2	17.7
	b	26.7	44.4	17.7
	c	38.8	56.6	17.8
	d	40.8	58.6	17.8
	e	52.8	70.7	17.9
	f	54.7	72.6	17.9
B_1	*d*	18866.1	18918.9	52.8
B_2	*a*	18755.2	18804.8	49.6
	c	68.3	17.8	49.5
	e	81.0	30.5	49.5
C_3	*a*	17548.6	17675.9	127.3
	b	50.1	78.1	128.0
D_4	*a*	16586.2	17211.3	625.1
	b	89.8	213.3	623.5

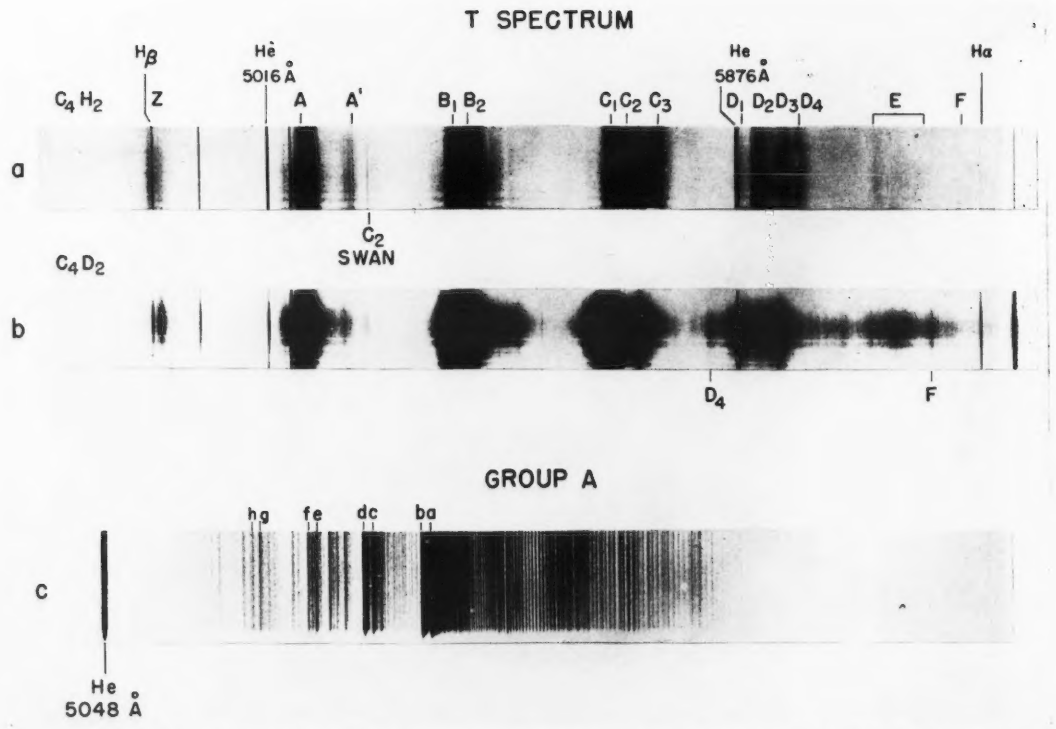

FIG. 3*a* and *b*. Appearance of the "T" spectrum under low resolution taken with a Hilger medium spectrograph with glass optics.

c. Appearance of group *A* (C_4H_2) under higher resolution taken with a 21-ft. grating spectrograph in the second order; resolving power 180,000.

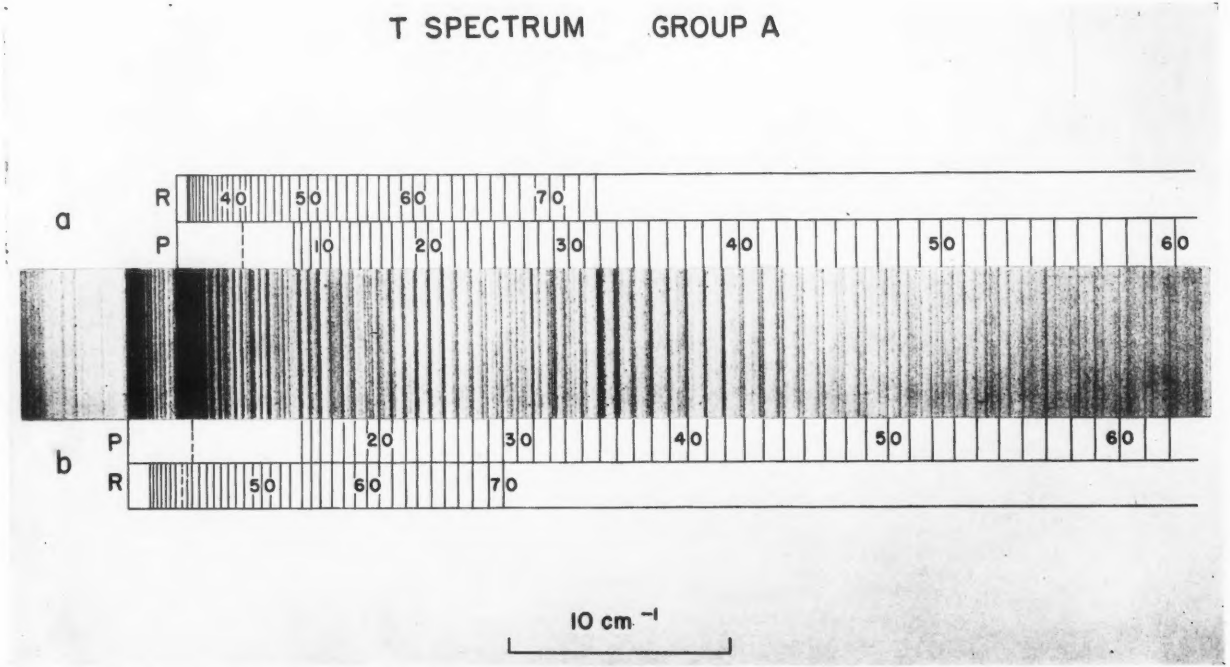

FIG. 4. The strongest bands (group A, (0, 0)) of the "T" spectrum (C_4H_2) photographed in the second order of a 35-ft. grating spectrograph, resolving power 400,000. The rotational lines are labelled according to a running number m for a numbering (X). (For a $^2\Pi$–$^2\Pi$ band $|J| = |m-\frac{1}{2}|$.)

identified as the (0, 0) sequence. The remaining groups, $B, \ldots F$, extending toward longer wavelengths, represent sequences in excited vibrational levels of the lower state of the type $(0, v_i'')$. The dependence of intensity on temperature (see above) indicates that in group A, band a or b represents the actual (0, 0) transition and the rotational analysis (see below) suggests that, of these two, the levels involved in band b are the lower.

The vibrational frequencies of the lower state are then given by the frequency differences between band Ab and the corresponding bands b in the other groups (with the exception of group B_2 in which the rotational analysis shows band a to involve the lower levels, and the irregular groups in which the strongest bands have been taken). They are found to consist, singly or in combinations, of four frequencies only, which are listed in Table II. For

TABLE II

COMPONENT FREQUENCIES OF THE LOWER STATE VIBRATIONAL LEVELS OF THE "T" SPECTRUM

Band	T_{BH}	T_{DD}	C_4H_2, $X^1\Sigma_g^+$			
Ab	0	0				
B_1d	860.6	825.6	874	ν_3	σ_g^+	C—C stretch
B_2a	971.5	939.6	964	$2\nu_7$	$\sigma_g^+(+\delta_g)$	$(=\pi_i^2)$
C_3b	2176.6	2066.3	2184	ν_2	σ_g^+	C≡C stretch
D_4b	3136.9	2531.1	3329	ν_1	σ_g^+	C—H stretch

comparison, the similar frequencies of diacetylene in its ground state as determined from the infrared and Raman spectra by Jones (1952*a*) together with their symmetry type are also listed. The way in which the four frequencies combine to build up the spectrum is shown in Table III, the "calculated"

TABLE III

OBSERVED LOWER STATE VIBRATIONAL LEVELS

Group	Assignment	T_{BH}		T_{DD}	
		Obs.	Calc.	Obs.	Calc.
A	0	0		0	
B_1	ν_3	860.5		825.6	
B_2	$2\nu_7$	971.5		939.6	
C_0	$2\nu_3$	1718.8	(1721)	1635	(1651)
C_1	$\nu_3+2\nu_7$	1847.2	(1832)	1718.1	(1765)
C_2	$4\nu_7$	1958.3	(1943)	1795.9	(1879)
C_3	ν_2	2176.6			
D_1	$2\nu_3+2\nu_7$	2712(SR)	(2693)		
D_2	$\nu_3+4\nu_7$	2819.1	(2804)	2694.3	(2705)
D_2''	$6\nu_7$	2946.5	(2914)	2795.3	(2819)
D_3	$\nu_2+\nu_3$	3068.1	(3037)	2885.7	(2892)
D_5	$\nu_2+2\nu_7$	3171.5	(3148)	3012.2	(3006)
D_4	ν_1	3136.9		2531.1	
F	$2\nu_2$	4352	(4353)	4123	(4133)

values being simple combinations of them (neglecting anharmonicities); group D_1 was not remeasured and Schüler and Reinebeck's value (indicated by (SR)) has been inserted.

Although, strictly speaking, the assignment applies to the strongest bands in the groups only, it accounts in a general way for all the groups with the exception of some very weak features and is seen to be in substantial agreement with that published by Schüler and Reinebeck (1954, Table 2). In addition to the groups $A, \ldots F$, there are some weaker bands in a group Z on the shorter wavelength side of group A which probably represent upper state progressions as suggested by Schüler. His group Y (lying in the (1, 0) sequence of C_2 Swan bands) could not be confirmed.

Another irregular group occurs on the long wavelength side of A and is designated A'. The strongest head is 279 cm^{-1} from head Ab. The corresponding displacement in the isotopic spectrum is 235 cm^{-1}. These values are compatible with the assumption that group A' is the first member of the $\Delta v = 0$ sequence in the mode ν_1, the symmetric carbon–hydrogen stretching mode. If the lower state frequencies of this mode are 3137 and 2531 cm^{-1} for C—H and C—D respectively, the corresponding upper state frequencies would then be 2858 and 2296 cm^{-1} respectively. From these figures the contribution by this mode to the isotopic shift of the (0, 0) band would be 22 cm^{-1}, which is not too different from the observed 18 cm^{-1}.

(*c*) *Discussion*

The frequencies of diacetylene quoted in Table II are seen to be the three possible totally symmetric fundamentals together with the first overtone of the lower of the two symmetric bending modes (π_g) which possesses a totally symmetric component. As is well known (see, for instance, Sponer and Teller 1941, p. 89), transitions between two electronic states in which the molecule has the same symmetry can only give rise to allowed spectral progressions in vibrational modes which are totally symmetric with respect to the molecular symmetry. The similarities shown in Table II between the "T" spectrum and the normal frequencies of diacetylene point strongly therefore to the following conclusions. Firstly, the magnitudes and isotopic shifts of the frequencies indicate that the molecule giving rise to the "T" spectrum has the same atoms joined by similar types of bonds as diacetylene itself. Secondly, the number and types of frequencies observed (just all, but not more than, the totally symmetric fundamentals) indicate that the symmetry of the molecule in both states of the "T" spectrum is the same and is not less than that of diacetylene itself, i.e., that of a linear molecule. The linearity is confirmed by the rotational analysis (see below). There is therefore little doubt that the atomic skeleton of the carrier is that of diacetylene, although, as pointed out above, diacetylene itself in the ground state is not involved. By analogy, the vibrational frequencies in the "T" spectrum are here given the same numbering as those of diacetylene (see Tables II and III).

The "T" spectrum is characterized by relatively short progressions in the lower state, the (0, 0) sequence being the most intense. The Franck–Condon principle indicates that in such a case the transition is accompanied by little change in molecular dimensions.

(*d*) *Vibrational Perturbations*

Two further facts which require comment are that out of the six non-totally symmetric fundamentals of diacetylene, apparently only one, namely ν_7, is

observed in progressions (in double quanta) in the lower state, and that the band groups in the "T" spectrum which are irregular are all the ones which involve $2\nu_7$ or ν_3 or both. This suggests that these levels are mutually perturbed and a consideration of their proximity and similar symmetry indicates the possibility of Fermi resonance. The values of the fundamental frequencies of diacetylene are such (Jones 1952*a*) that only two cases of appreciable first-order Fermi resonance might be expected: between ν_3 (σ_g^+, 874 cm^{-1}) and $2\nu_7$ (π_g^2, $2\times482 = 964$ cm^{-1}); and between ν_3 and $(\nu_8+\nu_9)$ ($\pi_u\times\pi_u$, $630+220 = 850$ cm^{-1}). The latter pair would give by far the closer resonance. However, in the "T" spectrum the level $(\nu_8+\nu_9)$ does not seem to be involved. The mode ν_8 is essentially a hydrogen bending one and hence $(\nu_8+\nu_9)$ would show a marked decrease on deuteration, in contrast to ν_7, which is essentially a carbon skeletal bending mode. In diacetylene itself, a simple force field calculation by the *FG* matrix method (see Ferigle and Weber 1953) shows the expected isotope shift in $(\nu_8+\nu_9)$ to be about 140 cm^{-1} which would effectively remove it from resonance with ν_3; in fact, the observed shift is only about 35 cm^{-1} and the perturbation is no less prominent in the isotopic spectrum.

Higher combinations of the resonating levels may be grouped into so-called polyads: e.g., $\{2\nu_3,\ \nu_3+2\nu_7,\ 4\nu_7\}$ or $\{3\nu_3,\ 2\nu_3+2\nu_7,\ \nu_3+4\nu_7,\ 6\nu_7\}$. As shown by Table III, these are found in the "T" spectrum.

The effects of Fermi resonance will be met again in the rotational analysis (see below).

4. ROTATIONAL ANALYSIS

(*a*) *Preliminary Analysis*

The high resolution plates obtained of the strongest groups allowed a complete rotational analysis to be made of four bands, viz, bands *a* and *b* of group *A* (0, 0 sequence), and bands *a* and *b* of group B_2 (0, $2\nu_7$ sequence); and a partial analysis of bands *a* and *b* of group C_3 (0, ν_2 sequence). Other bands, although sufficiently intense, were not sufficiently free from mutual overlapping to make an analysis possible.

Fig. 4 shows a spectrogram of the bands *Aa* and *Ab* as obtained with the 35-ft. grating. Inspection showed that (i) there are several apparently simple branches to be seen at some distance out from the heads; (ii) these branches do not show any intensity alternation; (iii) the spacings between lines in them are regular, i.e., show no "staggering"; and (iv) no band centers are obvious. One of the partly resolved branches was fitted to a polynomial by taking first and second differences and assuming an arbitrary numbering of the lines. This polynomial was then used to construct a Loomis–Wood diagram on which all the observed lines were plotted (see Herzberg 1950, p. 191). The diagram showed that over 95% of the observed lines fitted into three branches only, two of which extrapolated to head *a* and the third to head *b*. Similarly, the lines of bands *a* and *b* of group B_2 could be shown to form four branches, two connected with each of the heads in such a way that the one was a continuation of the other through the head. It appears therefore that each head is associated with one band consisting of *P* and *R* branches only. The apparently single branch connected with head *Ab* suggests that the *P* and returning *R* branches coincide very closely.

All the lines having been assigned, the branches of both bands *Aa* and *Ab* were fitted to polynomials. Terms of order higher than quadratic were found to be extremely small. With the constants obtained and a triangular slit-function of line half-width corresponding to a resolving power of 400,000, the expected appearance at 20°C. of these two bands in the region of greatest complexity near the heads was calculated and plotted (optical density units) as shown in Fig. 5. Superimposed is a microphotometer trace of the 35-ft.

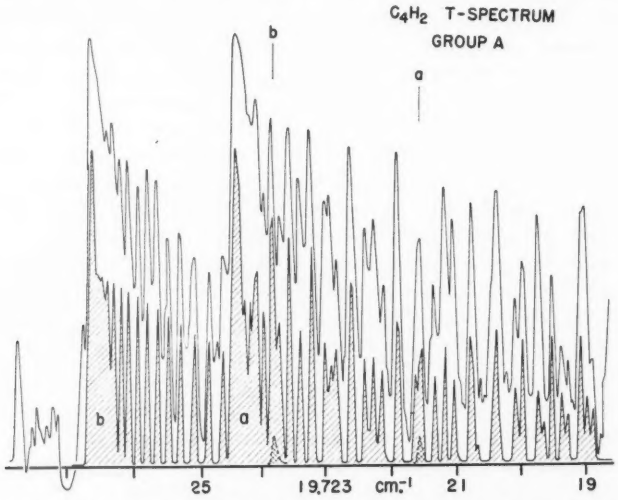

FIG. 5. A microphotometer trace (upper curve) of the spectrum shown in Fig. 4 near the heads, compared with a contour (lower curve) calculated from derived rotational constants (assuming a Π–Π transition) plotted in optical density units.

plate for comparison. The agreement, which is remarkably good considering the level of background due to other overlapping bands on the left, confirms the interpretation of the spectrum.

(*b*) *Electronic State Symmetries*

From the preliminary analysis it appears that the observed bands are due to a molecule that is linear both in the upper and lower states. In a linear molecule the vibronic (vibrational plus electronic) states are characterized by the quantum number of total internal angular momentum K (see Ingold and King 1953, p. 2716), where $K = |\Lambda \pm l|$ and Λ and l are the components of electronic and vibrational angular momentum respectively. In the four bands which have been analyzed, no Q branch has been observed and hence the bands are of "parallel" type, i.e., $\Delta K = 0$. However, the absence of an intensity alternation in the lines of all observed branches indicates that K itself is greater than zero (see Herzberg 1945, pp. 380, 389) and hence the transitions are of vibronic type Π–Π or Δ–Δ, . . . etc. In such transitions Q branches are weak although not altogether absent, their relative intensities increasing

rapidly with K (see the Hönl–London formulae, Herzberg, 1950, p. 208). In Δ–Δ and higher transitions the Q branch would be expected to have an intensity comparable to that of a strong line in the P branch and would have been definitely recognizable in three of the four bands analyzed (see Fig. 5; in Ab it would have been obscured by the head a). Hence at least three of the transitions are of vibronic type Π–Π. The relative intensity of the Q branch to be expected in such cases is indicated by two small doubly-hatched triangles in Fig. 5.

The vibrational analysis has shown that at least one band in each of the pairs Aa, Ab and B_2a, B_2b involves only totally symmetric (including zero) vibrational levels for which the electronic symmetry type must be the same as the vibronic species; and later considerations (see below, Section (*c*)) indicate that both members of a pair should involve the same vibrational symmetries. Hence, the vibronic symmetries associated with all four bands should be the same and equal to the electronic symmetry of the transition, which is therefore Π–Π.

In addition, the electronic states are expected to have the symmetry property g–u, and the transition is either of $\Pi_u \rightarrow \Pi_g$ or $\Pi_g \rightarrow \Pi_u$ type. However, these cannot be distinguished unless transitions to other electronic states of known g, u symmetry are observed.

(*c*) *Electronic State Multiplicities*

In the absence of further evidence, so far it would seem reasonable to proceed with the analysis of the four bands on the assumption that they are due to transitions between two singlet Π-states.

Before the rotational constants B can be determined, it is necessary to fix the positions of the band centers, i.e., to determine the absolute numbering of the lines in the branches. According to the vibrational analysis, the vibrational transitions involved should be of the type (0, 0) and (0, $2\nu_7$); and (ν_A', ν_A'') and (ν_A', $\nu_A''+2\nu_7$) where ν_A' and ν_A'' are two analogous frequency intervals in the upper and lower states respectively. These levels are illustrated in Fig. 6. The four bands should form two pairs, each with a member in

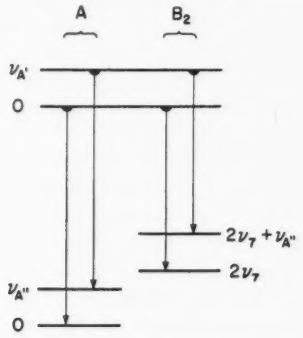

FIG. 6.

group A and group B_2 having common upper-state combination differences and rotational constants. The usual way of finding the correct absolute numbering is to assign an arbitrary numbering to the various bands to determine provisional rotational constants B, and to see how these constants vary with changes of absolute numbering. There is then only one numbering for which the two bands with one state in common yield the same value of B for that state.

Accordingly, with an arbitrary numbering (X) chosen so that the apparent B values obtained were close to B_0 of diacetylene in the ground state, upper state combination differences were formed from the lines of P and R branches and plotted graphically to give B' and D' in the normal way. The upper and lower state B values are sufficiently different that the four bands could be given the same relative numbering by inspection. The following values of B' were found:

band Aa: 0.13732 ± 0.0001 cm^{-1},
band Ab: 0.13601 ± 0.0002 cm^{-1},
band B_2a: 0.13616 ± 0.0001 cm^{-1},
band B_2b: 0.13734 ± 0.0001 cm^{-1}.

It is seen that the numbering (X) is in fact very close to the correct one (see below, Section (d)) and that the pairs of bands with common upper states are Aa and B_2b, and Ab and B_2a. The heads in group B_2 seem to be reversed relative to those in group A.

The most important point to note is the difference between the two upper state B values of about 0.00125 cm^{-1} which is associated with the frequency interval ν_A' (see Fig. 6). A similar difference is found in the values of B''. It was pointed out in the vibrational analysis that were this interval of a vibrational nature, the mode involved would most probably be one of the lower frequency ones. The difference in B expected would be of the order of one or two α's, the vibration–rotation interaction constants. Some estimate of their probable values can be made very roughly from the equations given by Shaffer and Nielsen (1941) for linear X_2Y_2, treating the C—H groups as single masses and using the force constants and bond distances of Jones (1952*b*). The latter author also gives experimentally determined values of α for some of the high frequency modes. For the low-lying modes the upper limit for α appears to be about 0.0002, and for the others 0.0004 cm^{-1}. The observed difference in B's is therefore between three and six times too large if the frequency interval ν_A is vibrational.

This discrepancy presents the most decisive single piece of evidence in favor of the alternative assumption, that the electronic states of the transition are doublet II states belonging to Hund's case (a), the vibrational analysis requiring both states to be regular or inverted. The frequency intervals ν_A' and ν_A'' are then the separations of the origins of the doublet components, nearly equal to the spin orbit interaction constants A' and A''; and the four bands which have been analyzed form two pairs of subbands. The actual values of A' and A'' cannot be obtained directly, as may be seen from Fig. 6, since the separation of the subbands gives only their difference.

Indications in favor of this interpretation were already mentioned in the vibrational analysis and the rotational analysis henceforth will be based upon it. Doublet states imply that the carrier of the spectrum is an ion of diacetylene, presumably $C_4H_2^+$. To test this conclusion two additional experiments were carried out. Firstly, if the spectrum involved singlet states, one of them (Π_u) should be capable of combining strongly with the ground state of diacetylene and the resulting spectrum should occur in emission at the same time as the "T" spectrum. A search was made from 1300 Å to 9000 Å and no other spectrum was found, although a band one hundredth of the intensity of the "T" spectrum would have been observable. Secondly, the carrier gas in the discharge tube was varied. Helium, argon, neon, and hydrogen have ionization potentials considerably above that of diacetylene, which Price and Walsh (1945) found to be 10.79 ev. from observed Rydberg series. The "T" spectrum is emitted strongly with these gases present in 10-fold excess. They were now replaced by benzene, whose ionization potential is less than that of diacetylene, namely 9.19 ev. The spectrum emitted was a weak blue continuum (Schüler and Reinebeck's "W" spectrum, 1952), but there was now no trace of the "T" spectrum until the concentration of diacetylene exceeded that of the benzene itself, i.e., until the diacetylene had become the major constituent of the carrier gases. This suggests that more than 9.2 ev. is required to excite the "T" spectrum, i.e., that the diacetylene has to be ionized.

(d) Rotational Constants

The measured line positions in all four bands are collected in the Appendix, Table A2. As well over three-quarters of them are more or less blended, no distinction is made from unblended lines.

For electronic states belonging strictly to Hund's case (*a*) the rotational term values of each component in a given vibrational level v are given by

$$F_v(J) = B_{v\,eff}J(J+1) - D_v \cdot J^2(J+1)^2 \ldots . \tag{1}$$

There is in addition for each component a term independent of J involving Ω^2 (where $\Omega = \Lambda + \Sigma$, and Σ is the constant component of the resultant spin; whence Ω is equal to 3/2 or 1/2 units for $^2\Pi$ states), which may be taken into the spin splitting. B_{eff} will differ slightly for the doublet components and the larger value will always be found for the upper of the two, independent of whether the doublet is regular ($^2\Pi_{3/2}$ above $^2\Pi_{1/2}$) or inverted. It is therefore possible from B_{eff} values to distinguish only the upper levels ($F_2(J)$) from the lower ($F_1(J)$), but not to distinguish between regular and inverted states.

Equation (1) is identical in form with the familiar equation for singlet states and the rotational constants may be evaluated from the data in exactly the same way. There is one difference: in doublet states J takes half-integral values and the numbering of the P and R branches starts differently at the band center. This is illustrated in Fig. 7 in which it is assumed that $(B'-B'')$ is zero for simplicity. In forming combination differences, $R(J-1)-P(J+1)$, the lines taken expressed in terms of the running number m are thus $R(m-1)-P(m+1)$ for a $^2\Pi$–$^2\Pi$ analysis instead of $R(m)-P(m+1)$ for a $^1\Pi$–$^1\Pi$ analysis.

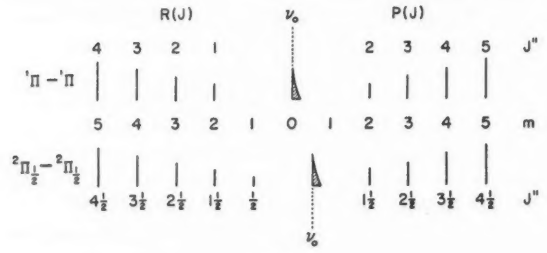

FIG. 7.

An attempt to find the absolute numbering in the branches was made as explained in the previous section. The rotational constants B' and D' were recalculated for a $^2\Pi$–$^2\Pi$ transition and the values of B' obtained for various numberings are shown in Table IV. The estimated errors in the values are

TABLE IV

VARIATION OF B' WITH ROTATIONAL NUMBERING

Numbering	Subband			
	Ab	B_2a	Aa	B_2b
Z	0.15299	0.15292	0.15436	0.15456
Y	0.14620	0.14621	0.14755	0.14767
X	0.13941	0.13951	0.14073	0.14078
W	0.13262	0.13280	0.13391	0.13389
V	0.12584	0.12609	0.12709	0.12700
U	0.11904	0.11939	0.12027	0.12011
Errors	±0.0002	0.0001	0.0001	0.0001

given at the bottom. Because of the relatively poor values for Ab, the decisive pair of subbands are Aa and B_2b. These agree most closely at numbering (W) although their accuracy would not exclude a displacement of two either way. However, (W) will be chosen for the following reasons. For any value of B' in Table IV the value above it in the same column would be the corresponding value of B''. Thus for numbering (X) the B'' values would be those of row Y, and similarly upwards. The mean of the values in row Y is 0.1469, which may be compared with Jones' value (1952*b*) of 0.1464 for B_0 of diacetylene in the ground state. (His absolute numbering, which was slightly in doubt for the same reasons as those here, has been confirmed by the pure rotational Raman spectrum of the gas (Callomon and Stoicheff, unpublished).) The vibrational analysis has shown that the normal frequencies of the lower state are somewhat lower than those of the diacetylene ground state, and it seems unlikely that in a polyatomic molecule a general decrease of the force-constants would be accompanied by a decrease of the moment of inertia, which numbering (X) would imply. By the same argument, the relatively small decrease in the lower state frequencies can be taken to indicate that a large increase in moment of inertia is also unlikely, and the B values corresponding to numbering (W)

TABLE V

ROTATIONAL CONSTANTS, $^2\Pi$–$^2\Pi$ ANALYSIS, NUMBERING (W), CM^{-1}

	Ab	B_2a	Aa	B_2b
B'	0.13262 *±0.0002*	0.13280 *±0.0001*	0.13391 *±0.0001*	0.13389 *±0.0001*
B''	0.13941	0.13951	0.14073	0.14078
$(B'-B'')$	−0.006795 *±0.00001*	−0.006706 *±0.000005*	−0.006818 *±0.000003*	−0.006889 *±0.000005*
D	2.2×10^{-8} *±0.6*	2.1×10^{-8} *±1*	1.9×10^{-8} *±0.8*	(2×10^{-8} assumed)
σ	0.009	0.03	0.014	0.03
ν_0	19,723.99	18,752.43	19,721.72	18,756.39
$(\nu_{head}-\nu_0)$	2.73	2.76	2.76	2.74

WEIGHTED MEANS

	Lower component $F_1(J)$	ΔB_{eff}	Upper component $F_2(J)$
$B'_{0\,eff}$	0.13274 *±0.00015*	0.00116 (±10%)	0.13390 *±0.00007*
$B''_{2\nu_7\,eff}$	0.13945		0.14079
$B''_{0\,eff}$	0.13954	0.00118	0.14072
$(2\alpha_7)_p''$	+0.000089 *±0.000015*		−0.000071 *±0.000008*
$(2\nu_7)_p''$	971.56		965.33

$B_0' = 0.13332 \pm 0.0001$
$B_0'' = 0.14013$
(C_4H_2 $X^1\Sigma_g^+$, $B_0 = 0.14641 \pm 0.00015$)

$T_{00} = 19{,}722.85$ (= 2.4452 ev.)

seem highly reasonable. Analogy with the spectrum of CO_2^+, and the structure of the Rydberg series of diacetylene observed in absorption, both to be discussed below, also favor it.

The remaining constants ν_0 and $(B'-B'')$ were obtained graphically from values of $R(J-1)+P(J)$ in the usual way. The energy level scheme of Fig. 6 is shown in revised form in Fig. 8 and all the constants are collected in Table V.

The standard deviation σ of line positions from those calculated with the constants of Table V are also given in Table V. Rather more lines could be measured in band B_2 than A, and hence the higher standard deviation (0.03) led to little loss in accuracy of the constants. It is unfortunate that in the best-measured subband Ab the returning R branch should almost coincide with the P branch. In the analysis it was assumed that the coincidence was exact, and then the random errors in B and $(B'-B'')$ were only about a quarter of those quoted in Table V with a standard deviation of line position of

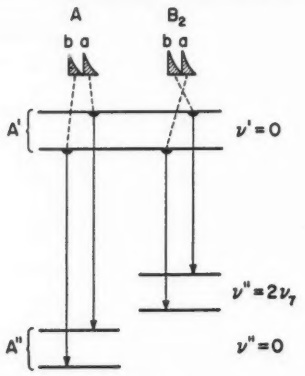

FIG. 8.

0.009 cm^{-1}. However, it would be difficult to distinguish a small divergence such that the line $R(60)$ was just resolved from the overlapping P line, i.e., displaced from it by 0.05 cm^{-1}. The corresponding systematic uncertainty leads to the larger errors actually quoted in the table.

The weighted mean values of B_{ett}' and the values of $(B'-B'')$ give the values of B_{ett}''. The true B values of the doublet states are the means of the B_{ett} values of the components.

The intervals between band heads and band centers are given to show how constant they are. The electronic term difference T_{00} for the transition including zero point energies can be seen from Fig. 8 to be the mean of ν_0 for the two subbands A.

The values of about 2×10^{-8} found for D may be compared with 1.6×10^{-8} calculated for diacetylene with Kratzer's simple formula $4B^3/\omega^2$, where ω is the lowest-lying stretching frequency, and 1.65×10^{-8} for a valence force field with the constants given by Vallance Jones. No difference between D' and D'' could be detected.

Bands A and B_2 are transitions from a common upper state to vibrational levels 0 and $2\nu_7$ in the lower state. Hence the differences between $(B'-B'')$ give effective values of $(B''_{2\nu_7}-B_0'')$, which may be written $(2\alpha_7)_p''$ where the suffix p has been added because $2\nu_7''$ is perturbed by Fermi resonance. Besides being very small, the two values obtained in the two doublet components are of opposite sign suggesting that the intensity of Fermi perturbation differs. This is also reflected in the vibrational frequencies themselves; by subtracting the appropriate values of ν_0, the frequency of the apparently more strongly perturbed $2\nu_7$ in the lower doublet component is seen to be 6.23 cm^{-1} greater than that of the upper.

In addition, one of the plates of group C_3 was sufficiently exposed so that one of the subbands could be partly analyzed. About 30 lines in the P branch gave a value of $(B'-B'')$ of 0.0063 ± 0.0005 cm^{-1}, whence α_2'' is $+0.0005\pm0.0005$ cm^{-1}. Its positive sign confirms the assignment to a stretching mode.

Estimates can now be made of the values of the spin-splitting constants A' and A''. These are related to the effective B values of the doublet components through the equation (see Herzberg 1950, p. 233)

$$B_{eff}=B(1\pm B/A\Lambda+\ldots) \tag{2}$$

where Λ is 1 for Π-states. Hence, if ΔB is the difference between the B_{eff}'s,

$$A=2B^2/\Delta B_{eff}$$

to a first approximation. The values of ΔB_{eff} for the upper and lower states are given in Table V. Individually they depend on the difference between two measured values of B and hence their absolute accuracy is not great; the difference between them, however, depends on the difference between two measured values of $(B'-B'')$ which are known very precisely. The values obtained are:

$$A'=30.6 \text{ cm}^{-1},$$
$$A''=33.3 \text{ cm}^{-1}.$$

These are probably accurate to no better than $\pm 10\%$ but their relative accuracy is much greater. $(A'-A'')$ is -2.7 ± 1 cm^{-1}, compared with the measured value of -2.3 cm^{-1}.

The basic equations (1) and (2) are good approximations only for Hund's coupling case (a). However, it may be readily shown that the more accurate formulae of Hill and Van Vleck give in the present case (large A/B) very closely the same results (to $\backsim 0.01$ cm^{-1} at $J=70$).

There remains the question of Λ-type doubling (see Herzberg 1950, p. 226) which, in the case of Π–Π bands of symmetric linear molecules, leads to the well-known "staggering". In the present case, no staggering is obvious. The lines of low J are heavily overlapped and those of high J weak and obscured by weak subsidiary band heads. It seemed likely that a very small staggering, if present, would be detectable at only two places, in subbands Aa and Ab in the ten or so lines in the P branches above $J(42\frac{1}{2})$ and $J(45\frac{1}{2})$ respectively. First and second differences were taken; any staggering of the lines would be reflected directly in the latter, which would otherwise be constant. A small regular staggering was found in each case. In subband Ab the average displacement of the 14 lines $P(45\frac{1}{2})$ to $P(58\frac{1}{2})$ was ± 0.009 cm^{-1} with a standard deviation of 0.006 cm^{-1} (compared with the line half-width of 0.05 cm^{-1} and standard deviation of measurement over the whole band of 0.009 cm^{-1}); and for subband Aa the average displacement for the lines $P(42\frac{1}{2})$ to $P(52\frac{1}{2})$ was ∓ 0.027 with a scatter of ± 0.023 cm^{-1}. The smaller value for subband Ab would indicate that it represents the $^2\Pi_{3/2}$–$^2\Pi_{3/2}$ transition (see Van Vleck 1929), i.e., that the two $^2\Pi$ states are inverted.

To summarize, the rotational structure shows that the "T" spectrum is a transition between two $^2\Pi$ states of a linear molecule both belonging to Hund's case (a), the most probable moments of inertia differing by only 4.3 and 8.9% from that of the diacetylene ground state. There is some evidence that both states are inverted.

5. THE "T" SPECTRUM AND THE ELECTRON CONFIGURATION OF DIACETYLENE

(*a*) *Electronic Configuration and Molecular Orbitals of Diacetylene*

The "T" spectrum will be more completely understood if its electronic states can be identified with ones predicted in type and separation from the electron configuration of the molecule. For spectroscopic purposes the electron configurations of polyatomic molecules, especially of the unsaturated organic type, are represented most usefully and successfully in terms of delocalized one-electron wave functions, or molecular orbitals, derived in a first approximation from linear combinations of atomic orbitals. The well-known correlation rules determine the types of states which result when two atoms approach to form a diatomic molecule, and the same principles may be applied in building up larger molecules from smaller ones. Thus, the molecular orbitals of diacetylene may be linked to those of acetylene by considering what happens when two C_2H radicals approach each other on-axis to form a C_4H_2 molecule.

The orbitals of acetylene have been much studied (e.g., Ingold and King 1953, p. 2712) and their configuration may be written in the usual notation, neglecting inner closed atomic shells:

$$(1s_H, 2sp_C, \sigma)^2\,(1s_H, 2sp_C, \sigma)^2_{C-H}\,(2sp, \sigma_g)^2_{C\equiv C}\,(2p, \pi_u)^4_{C\equiv C},\ {}^1\Sigma_g^+.$$

A hydrogen atom may now be removed to give a C_2H radical leaving a $2sp$ orbital temporarily unoccupied. Two such radicals are now combined $HC_2 \ldots C_2H$ to create the chain of four carbon atoms through bonding orbitals $(2sp, \sigma_g)^2_{C-C}$. In the absence of interactions, the eight π-electrons would all be equivalent; however, the chemical evidence of conjugation and the physical evidence of bond lengths and force constants indicate that strong interaction does occur. The π-electrons are further delocalized and occupy two groups of four equivalent four-center orbitals, as outlined by Price and Walsh (1945, p. 386; Walsh 1948, p. 79). These are formed according to the two ways of joining two acetylene π_u orbitals:

$$\begin{array}{cc} ++\ .\ ++ & \\ --\ .\ -- & \text{I} \\ \pi_u & \end{array} \qquad \begin{array}{cc} ++\ .\ -- & \\ --\ .\ ++ & \text{II} \\ \pi_g & \end{array}$$

They can be seen from the diagram to be again of symmetries π_u and π_g with bonding and antibonding character now across the central C—C link and accordingly differing energies. This representation has been used as a basis for quantitative calculations by Serre (1954).

A corresponding slight interaction between the C≡C σ orbitals may also be taken formally into account, although the energy difference between the resulting σ_g and σ_u orbitals is probably small. The over-all valence electron configuration of the diacetylene ground state is then:

$$(1s, 2sp, \sigma)^2(1s, 2sp, \sigma)^2_{C-H}\,(2sp, \sigma_g)^2_{C\equiv C}\,(2sp, \sigma_u)^2_{C\equiv C}\,(2sp, \sigma_g)^2_{C-C}$$
$$(2p, \pi_u)^4.\,(2p, \pi_g)^4, \qquad {}^1\Sigma_g^+.$$

From this it is possible to make predictions about the states of the ions which result when an outer electron is removed from one or another of the orbitals.

(*b*) *The Ions of Diacetylene*

The ground state of the ion is obtained by removing an electron from the highest occupied orbital of the neutral molecule, i.e., a π_g electron. The first excited state of the ion is then obtained by removing a π_u electron from the neutral molecule. Other excited states of the ion may be obtained by removal of σ electrons, but these would be expected to lie at higher energies and need not be considered further here.

The first two states of the ion therefore have the π electron configurations $(\pi_u)^4(\pi_g)^3$ and $(\pi_u)^3(\pi_g)^4$ respectively. The electronic states corresponding to these *are unique* and are $^2\Pi_g(i)$ and $^2\Pi_u(i)$, (i) indicating that they are inverted (see Mulliken 1932, p. 10); *the "T" spectrum immediately suggests itself as the observed allowed optical transition between them* (see Fig. 9).

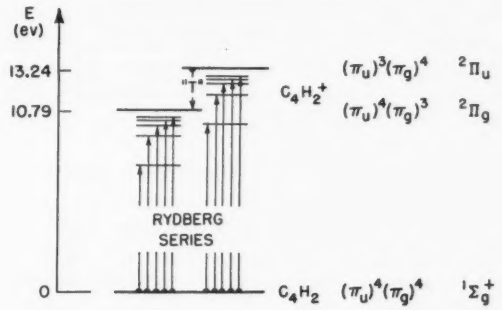

FIG. 9.

Such a transition would be expected to have a very high intensity. A calculation on the basis outlined by Herzberg (1950, p. 384), making the same assumptions, gives a value of the oscillator strength f of about 0.5, although this is necessarily a very rough estimate. Nevertheless, it places such a transition amongst the most intense. Consideration of the conditions in the discharge tube, in which the total concentration of neutral diacetylene is only about 0.1 mm., shows that the intrinsic intensity of the "T" spectrum must be very high, of the order of that of an allowed atomic transition.

Further evidence is available from the Rydberg series of diacetylene described by Price and Walsh (1945), and a comparison with those of acetylene. For the latter, Price (1935) found two Rydberg series which gave an ionization potential of 92,013 cm^{-1} or 11.41 ev. From the separation of Q and R heads in one of the Rydberg series, he concluded that there is an increase in moment of inertia of about 6% in the upper Rydberg states compared to the ground state. The first Rydberg series of diacetylene are in every way similar to those of acetylene, although Q and R heads could not be resolved. Two series go to a common limit and fit the equations:

$$\nu = 87{,}024 - R/(n-0.52)^2, \qquad n = 3, 4, 5 \ldots,$$
$$\nu = 87{,}060 - R/(n-0.95)^2, \qquad n = 3, 4, 5 \ldots.$$

The mean ionization potential is 87,042 cm^{-1} or 10.79 ev. If it is assumed that the removal of a π electron in diacetylene lengthens the C≡C bonds by the same amount as in acetylene, the moment of inertia would increase by about 3%, in keeping with the observed vibrational structure of the Rydberg series, which is very similar to that in the case of acetylene but somewhat less extensive. It consists mainly of a progression in ν_2' with spacings (measured off Price and Walsh's print) of 2150±50 cm^{-1}. The Rydberg series therefore indicate a picture of the ion of diacetylene very similar to that of the lower state of the "T" spectrum as deduced in the preceding sections with the rotational numbering there adopted; the value for ν_2 was 2174 cm^{-1} and the moment of inertia was 4.3% greater than that of the diacetylene ground state.

The first ionization potential of acetylene $(\pi_u)^3$ is 11.41 v., and that of diacetylene $(\pi_g)^3$ 10.79 v., a lowering due to conjugation of 0.62 v. If it were now assumed that the second ionization potential of diacetylene $(\pi_u)^3$ had been raised by an equal amount above that of acetylene, a rough estimate (which is a lower limit) could be made of the energy difference between the two states of the ion and the frequency of the allowed transition between them. The value is 1.24 v., or 10,000 cm^{-1}; that for the "T" spectrum is 2.45 v., or 19,723 cm^{-1}.[3]

Finally, an estimate can be made of the separation of the doublet components of the states of the ion due to spin-orbit interaction. The odd electron moves in molecular orbitals which are to a first approximation normalized linear combinations of atomic carbon orbitals and hence a spin-orbit interaction between the electron and a molecular orbital would be expected to be related to a properly weighted mean of the values for the pure atomic orbitals themselves.

Mulliken (1932, p. 34; 1934, p. 559) has given the simple relations between the observed over-all multiplet widths $\Delta\nu$ of atomic and molecular states, the spin-splitting constants A, and the one-electron spin-orbit interaction constants a which are the determining parameters. In the present case, the molecular orbitals are built up from four carbon atoms which are non-equivalent in their contributions; they have, however, been modified by the removal of one electron and this may be allowed for by considering each carbon atom as a sort of hybrid atom with one quarter ionic character. Consequently, the value of a to be taken in calculating the doublet separation in a $\pi^3.{}^2\Pi$ state might be expected to lie between those of C and C^+ roughly as a mean weighted in the ratio 3:1. Values of a are given in Table VI below (from

TABLE VI

SPIN-ORBIT INTERACTION CONSTANTS (cm^{-1})

State	$\Delta\nu$	A	a
C^+ $2p$, ^3P	$3A/2$	+42.7	42.7
C $2p^2$, ^3P	$3A$	+14.5	29.0

[3]More extensive molecular orbital calculations by Serre (1956) lead to a value of 2.70 v.

Moore 1949). The 3:1 weighted mean is 32.4 cm^{-1} and hence the expected doublet separation A is -32.4 cm^{-1}. The values deduced for the states of the "T" spectrum were -30.6 and -33.3 cm^{-1}.

To summarize, consideration of electron configurations and the evidence from Rydberg series predicts the existence of two states of the diacetylene ion whose symmetry types, energy separation, spin-splitting, and allowed transition moment agree with those of the "T" spectrum sufficiently well to leave little doubt as to its identification.

6. COMPARISON WITH ANALOGOUS SPECTRA

The electron configuration and molecular orbitals of carbon dioxide were first studied by Mulliken (1935). The number and types of orbitals occupied by electrons in the ground state are similar to those of diacetylene, and removal of an electron from successive orbital shells gives states of the ion also completely analogous. Transitions between these states are allowed and the spectra were analyzed by Bueso-Sanllehi (1941) and Mrozowski (1941, 1942) to the same extent as the "T" spectrum above. The characteristics of one of these spectra and the "T" spectrum are analogous in detail.

According to Mulliken, the outer shell electron configuration of CO_2 may be written

$$(2s)_O^2\ (2s)_O^2\ (2p\sigma, 2sp, \sigma_g)_{OCO}^2\ (2p\sigma, 2sp, \sigma_u)_{OCO}^2\ (2p, \pi_u)_{OCO}^4\ (2p, \pi_g)_{OO}^4,\ {}^1\Sigma_g^+ .$$

The last three shells are formally, in order of decreasing energy, non-bonding, O—C—O π-bonding, and O—C—O antibonding, respectively. Removal of an electron from each in turn gives three unique states of the ion:

$$\sigma_u^{-1} = (\sigma_u),\ {}^2\Sigma_u^+,$$
$$\pi_u^{-1} = (\pi_u)^3,\ {}^2\Pi_u(i),$$
$$\pi_g^{-1} = (\pi_g)^3,\ {}^2\Pi_g(i).$$

The transition ${}^2\Pi_u \rightarrow {}^2\Pi_g$ is known in emission as the Fox, Duffendack, and Barker system (T_{00} 28,500.5 cm^{-1}, $\lambda = 3506$ Å), analyzed by Mrozowski; and the transition ${}^2\Sigma_u^+ \rightarrow {}^2\Pi_g$ is the well-known persistent $\lambda\lambda$ 2883–2896 doublet, (T_{00} 34,597.9 cm^{-1}), analyzed by Bueso-Sanllehi. They are well shown in Pearse and Gaydon's plate (2) (1941, 1950), and look much like the "T" spectrum. As in the latter, there are progressions in the symmetrical stretching mode ν_1, which appears to be perturbed (as in the ground state of CO_2) by double quanta of the bending mode ν_2. The degree of perturbation here also differs markedly in the doublet components, giving rise to irregular groups of bands. By using high temperatures in the discharge, upper-state progressions could also be observed. The values for ν_1 were about 1265 cm^{-1} for the ${}^2\Pi_g$ and 1126 cm^{-1} for the ${}^2\Pi_u$ states compared with 1329 cm^{-1} for CO_2 (corrected for Fermi resonance); only the zero levels of the ${}^2\Sigma_u^+$ state were observable in the emission spectrum, but from the vibrational structure of Rydberg series, the value of ν_1 is close to 1120 cm^{-1}. Thus, the removal of a non-bonding

π_g electron reduced ν_1 by 4.8%; a bonding π_u electron by 15.3%; and a formally antibonding σ_u electron by 15.7%.[4]

The moments of inertia were similarly affected. The B_0 values of the $^2\Pi_g$, $^2\Pi_u$, and $^2\Sigma_u^+$ states were 0.3806, 0.3493, and 0.3784 cm^{-1}, compared with 0.3903 for the CO_2 ground state. These are decreases of 2.5%, 10.5%, and 3.0% respectively. Both II states belong to Hund's case (*a*) and are inverted. The doublet separations are again roughly as expected from the atomic spin-orbit interaction constants.

There are a number of spectra of diatomic molecular ions in which an electron is moved from a bonding to an antibonding orbital. Such transitions have been designated *E–N* transitions by Mulliken (1939). The prototype is the transition in H_2^+ from $(1s, \sigma_g)$, $^2\Sigma_g^+(N)$ to $(1s, \sigma_u)$, $^2\Sigma_u^+(E)$. Others are

$$O_2^+ \quad (\pi_u)^3(\pi_g)^2, A^2\Pi_u(E) \text{ to } (\pi_u)^4(\pi_g), X^2\Pi_g(N)$$

$$? \quad Cl_2^+ \quad (\pi_u)^3(\pi_g)^4, A^2\Pi_u \text{ to } (\pi_u)^4(\pi_g)^3, X^2\Pi_g$$

The Cl_2^+ case is entirely analogous to that of $C_4H_2^+$ and CO_2^+. Only one state results from each electron configuration. This type of electron transfer spectra might equally well be regarded as "one-electron-vacancy" transfer spectra. Under the proper conditions, many more molecules might be expected to give such spectra, e.g., F_2^+, CS_2^+, $C_2N_2^+$ (cyanogen), polyacetylene ions. Discharge tubes of the Schüler type suggest themselves as good sources.

7. APPENDIX

(*a*) *Tables of Measured Frequencies*

See Tables A1 and A2 at the end of the paper.

(*b*) *The Near Ultraviolet Absorption System of Diacetylene*

In the attempts mentioned previously to identify one of the states of the "T" spectrum with a known state of diacetylene, the absorption spectrum of the gas was photographed in the region 2500–3000 Å in the second order of the 35-ft. grating with a resolving power again of about 400,000, corresponding to a line half-width of about 0.1 cm^{-1}. A 50 cm. cell was used filled with gas to a pressure of about 150 mm. at which the rotational line half-width due to Doppler and pressure broadening, calculated with an optical collision diameter of 1.5 times that of acetylene (see Smith 1952), is also 0.1 cm^{-1}.

The spectrum consists of a very large number of very sharp band heads irregularly spaced, as described by Woo and Chu (1937), who used a large prism instrument. Most are degraded to shorter wavelengths, but some are so sharp that no shading could be seen. None of them occur in regular pairs like *Q* and *R* heads. At no point in the spectrum could rotational structure be observed; the spectrum is completely predissociated. The diffuseness increases towards shorter wavelengths until even the heads cease to be sharp

[4]Removing an antibonding π electron from diacetylene leaves the carbon–carbon bond force constants virtually unchanged (see Table II) and affects mainly the C—H bonds; thus ν_2 and ν_3 decrease by 0.3 and 1.5% respectively, whereas ν_1 decreases by 5.8%.

(below 2600 Å, Woo and Chu's "low pressure bands") and merge into each other. This is reflected in the ease with which diacetylene is photolyzed.

ACKNOWLEDGMENTS

It gives me great pleasure to acknowledge my debt and express my gratitude to Dr. G. Herzberg, who suggested this problem to me, for much valuable advice and constant encouragement during the progress of the work; and to Drs. A. E. Douglas and D. A. Ramsay for many interesting discussions and much help so readily given. I should also like to thank them and Professor C. K. Ingold for carefully reading and improving the manuscript. The above account was written during the tenure of an Imperial Chemical Industries Research Fellowship at University College, London.

REFERENCES

BUESO-SANLLEHI, F. 1941. Phys. Rev. **60**: 556.
EDLÉN, B. 1953. J. Opt. Soc. Amer. **43**: 339.
FERIGLE, S. M. and WEBER, A. 1953. J. Chem. Phys. **21**: 722.
HANSEN, G. 1950. Optik, **6**: 337.
HARRISON, G. 1938. M.I.T. wavelength tables. John Wiley & Sons, Inc., New York.
HERZBERG, G. 1945. Molecular spectra and molecular structure. II. Infrared and Raman spectra of polyatomic molecules. D. Van Nostrand Company, Inc., New York.
——— 1950. Molecular spectra and molecular structure. I. Spectra of diatomic molecules. 2nd ed. D. Van Nostrand Company, Inc., New York.
INGOLD, C. K. and KING, G. W. 1953. J. Chem. Soc. 2702.
JOHNSON, A. W. 1946. J. Chem. Soc. 1009.
JONES, A. V. 1952*a*. Proc. Roy. Soc. A, **211**: 285.
——— 1952*b*. J. Chem. Phys. **20**: 860.
KEYSSNER, E. and EICHLER, E. 1944. Chem. Zentr. (i), **115**: 163.
LEITCH, L. C. and MORSE, A. T. 1952. Can. J. Chem. **30**: 924.
MOORE, C. E. 1949. Atomic energy levels. Natl. Bur. Standards (U.S.) Circ. 467.
MOSER, C. 1955. J. Opt. Soc. Amer. **44**: 660.
MROZOWSKI, S. 1941. Phys. Rev. **60**: 730.
——— 1942. Phys. Rev. **62**: 270.
MULLIKEN, R. S. 1932. Revs. Mod. Phys. **4**: 1.
——— 1934. Phys. Rev. **46**: 549.
——— 1935. J. Chem. Phys. **3**: 720.
——— 1939. J. Chem. Phys. **7**: 20.
PEARSE, R. W. B. and GAYDON, A. G. 1941, 1950. The identification of molecular spectra. 1st and 2nd ed. Chapman & Hall, Ltd., London.
PRICE, W. C. 1935. Phys. Rev. **47**: 444.
PRICE, W. C. and WALSH, A. D. 1945. Trans. Faraday Soc. **41**: 381.
REINEBECK, L. 1953. J. phys. radium, **15**: 398.
SCHÜLER, H. 1950. Spectrochim. Acta, **4**: 85.
SCHÜLER, H. and REINEBECK, L. 1951. Z. Naturforsch. **6a**: 160, 270.
——— 1952. Z. Naturforsch. **7a**: 285.
——— 1954. Z. Naturforsch. **9a**: 350.
SERRE, J. 1954. J. chim. phys. **51**: 568.
——— 1956. J. chim. phys. In press.
SHAFFER, W. H. and NIELSEN, A. H. 1941. J. Chem. Phys. **9**: 847.
SMITH, W. V. 1952. Ann. N.Y. Acad. Sci. **55**: 891.
SPONER, H. and TELLER, E. 1941. Revs. Mod. Phys. **13**: 75.
STOICHEFF, B. P. 1954. Can. J. Phys. **32**: 330.
VAN VLECK, J. H. 1929. Phys. Rev. **33**: 467.
WALSH, A. D. 1948. Quart. Revs. **2**: 73.
WELSH, H. L., CUMMING, C., and STANSBURY, E. J. 1951. J. Opt. Soc. Amer. **41**: 712.
WHITE, J. U. 1942. J. Opt. Soc. Amer. **32**: 285.
WOO, S. C. and CHU, T. C. 1937. J. Chem. Phys. **5**: 786.

NOTE: Tables A1 and A2 follow.

TABLE A1

COLLECTED VALUES OF MEASURED BAND HEAD POSITIONS

At the head of each group are given the vibrational assignment of the sequence; whether or not the bands in the group show regularity in their spacings; the wavelength in air of the principal head of the sequence in the T_{HH} spectrum; and a rough visual estimate of its intensity as a whole, relative to other groups, on a scale of 100.

Values listed are vacuum wave numbers, measured with grating instruments; a few measured with a prism instrument are marked (p). Some of the leading bands are labelled with small letters, and some spacings in the regular groups indicated. Groups marked (n) are additional to those introduced by Schüler and Reinebeck.

T_{HH}			T_{DD}		
cm^{-1}		I	cm^{-1}		I
Group Z ?(ν_3 or $2\nu_7$, 0)					
Irregular; strongest bands b 4856.00 and a 4869.20 Å; intensity 5					
20,604.5		2	20,560	(p)	2
00.1		4	537		7
595.4		3	521		10
92.3		4	512		2
87.3	b	10	462		1
76.8		8			
71.5		4			
66.5		8			
49.0		3			
46.7		5			
31.6	a	10			
16.4		7			
Group A (0, 0)					
Regular; strongest band Ab 5067.858 Å; intensity 100					
19,866.33		00	19,868.5		00
53.97		0	55.1		0
41.49		1	41.8		1
29.40		0	788.3		1
08.27		0	86.3	h	1
780.01		0	84.7	1.8	1
78.53		0	84.5	g	2
76.45		1	77.1	13.7	1
70.65		1	74.3		2
68.29	h	1	72.6	f	4
1.78			1.9		
66.51	g	2	70.7	e	3
58.56		0	64.6		4
13.58			14.0		
58.12		1	60.5		3
57.22		1	58.6	d	7
2.0					
54.71	f	3	56.6	c	7
53.63	1.94	1	44.4	b	10
2.2					
52.77	e	4	42.2	a	10
49.42		3	35.6		3
13.89			33.5		3
45.61		2	08.9		3
45.18		2	07.9		3
41.14		3	04.8		2
40.82	d	7	03.8		2
2.06			694.3		3
38.76	c 14.11	6	93.1		3
36.87		4	89.3		2
26.71	b	10	87.9		2
2.21			81.0		1
24.50	a	10	79.7		1
17.53		1			
15.56		1			
07.97		1			
05.75		1			
02.22		0			
692.65		00			
88.36		0			
84.18		00			
77.78		00			
60.44		0			
58.67		0			

TABLE A1 (*continued*)

T_{HH}			T_{DD}		
cm^{-1}		I	cm^{-1}		I
Group A' (n) ?(v_1', v_1'')					
Irregular; strongest head a 5142.04 Å; intensity 8					
19,471.2		8	19,517.6		5
60.4		5	07.1	a	10
47.5	a	10			
Group B_1 (0, v_2'')					
Irregular; strongest band B_1d 5299.042 Å; intensity 30					
18,907.10		00	18,990.2		0
04.97		00	69.7		1
02.55		0	53.1		3
899.99		0	50.0	f	2
90.70		2	46.8	e 14.0	3
88.17		0	36.0	d	5
86.63		00		12.4	
82.69		2	34.4	c	5
81.26		1		17.2	
78.38		1	27.5	15.6	3
76.77		5	18.8	ab	10
76.11		3	898.0		3
74.04		2	95.9		3
71.86		0			
70.31		2			
66.07	d	10			
62.19	c	10			
58.50	b	7			
53.19	a	4			
35.47		3			
27.12		1			
25.67		4			
23.56		1			
18.80		2			
Group B_2 (0, $2v_1''$)					
Regular; principal band B_2a 5330.369 Å; intensity 50					
18,800.79		3	19,877.2		7
793.52	g	1	67.2		5
90.40		0	61.7		3
85.20	f 12.18	3	53.4		8
81.90	4.16	4	30.5	e	3
81.04	e	5	25.8		4
				12.7	
79.21		2	23.0		4
77.83	12.74	3	17.8	c	6
				13.0	
72.27	d	7	04.8	a	10
	3.97		794.5		8
68.30	c	8	89.5		3
63.53		4	87.3		5
	13.09		81.9		3
59.15	b	10	75.4		7
	3.94		01.2		1
55.21	a	10			
25.53		1			
16.36		1			
696.97		00			
92.35		0			
86.63		00			
84.21		0			
83.52		1			
80.40		0			
72.23		0			
69.00		0			
Group C_0 (n) (0, $2v_2''$)					
Irregular; strongest band a 5551.57 Å; intensity 4					
18,021.0		vw	18,109	(p)	
13.8		vw			
07.9	a	vw			

TABLE A1 (*continued*)

T_{HH}			T_{DD}		
cm^{-1}		I	cm^{-1}		I
Group C_1 (0, $\nu_3''+2\nu_7''$)					
Irregular; strongest band *b* 5591.46 Å; intensity 25					
17,899.4		2	18,026.3	*a*	
90.9		4			
88.4		4			
86.5		4			
79.5	*b*	10			
78.8		8			
66.7	*a*	9			
57.0		2			
Group C_2 (0, $4\nu_7''$)					
Irregular; strongest band *a* 5626.42 Å; intensity 20					
17,828.5		3	17,961.2	*b*	6
25.9		3	48.5	*a*	10
793.9		2			
80.0	*b*	8			
76.2		6			
68.4	*a*	10			
67.2		2			
Group C_3 (0, ν_3'')					
Regular; principal band *b* 5696.39 Å; intensity 25					
17,593.0		0	17,721.7		2
88.2		1	11.6	*f*	3
83.6	*f*	2	09.7	*e* (1.9)	3
81.8	*e* (1.8)	2	693.9	*d*	4
80.0	16.1	3	91.9	*c* (2.0)	4
72.1		2	78.1	*b*	10
67.5	*d*	6	75.9	*a* (2.2)	9
65.3	*c* (2.2) 17.4	5	25.2		3
50.1	*b*	10	23.8		3
48.6	*a* (1.5)	10	09.6		2
			07.4		2
Group D_2 (0, $\nu_3''+4\nu_7''$)					
Irregular; strongest band *b* 5912.88 Å; intensity 12					
16,916.4		5	17,144.3		0
07.6	*b*	10	38.9		1
05.0	*a*	10	30.6		2
			089.5		3
			84.0		4
			67.2		7
			50.1	*a*	10
Group D_2'' (n) (0, $6\nu_7''$)					
Irregular; strongest band *b* 5957.74 Å; intensity 10					
16,784.2	*d*	5	16,993.2		6
82.7	*c* (1.5)	4	85.8		8
80.2	*b*	10	48.5	*a*	10
78.4	*a* (1.8)	9			

TABLE A1 (*concluded*)

T_{HH}			T_{DD}		
cm^{-1}		I	cm^{-1}		I
Group D_3 $(0, \nu_2'' + \nu_3'')$					
Irregular; strongest head *a* 6001.24 Å; intensity 15					
16,701.9		7	16,889.3		3
697.2		4	75.8		5
93.2		5	60.6		6
88.7		4	58.7	*a*	10
84.1		2	32.6		3
81.6		2	16.1		4
75.0		4			
71.3		5			
58.6	*a*	10			
55.5		4			
49.8		4			
36.4		3			
Group D_4 $(0, \nu_1'')$					
Regular; principal head *b* 6026.12 Å; intensity 15					
16,620.4	*f*	2	17,246.3	*f*	2
14.8	*e*	3	44.8	*e*	1
05.2	*d*	6	30.1	*d*	6
01.4	*c*	8	28.3	*c*	5
589.8	*b*	10	13.3	*b*	10
86.2	*a*	10	11.3	*a*	10
Group D_5 (n) $(0, \nu_2'' + 2\nu_1'')$					
Irregular; strongest head 6038.73 Å; intensity 8					
16,555.2			16,792.6		6
Obscured by group D_4, many weaker heads			71.9		3
			40.8		7
			38.9		8
			32.2	*a*	10
			15.4		8
			687.3		2
			62.3		3
Group F $(0, 2\nu_2'')$					
Regular; principal band *ca.* 6502.2 Å; intensity 1					
15,375	(p)		15,621	(p)	

TABLE A2

FREQUENCIES OF MEASURED ROTATIONAL LINES; $^2\Pi$–$^2\Pi$ ANALYSIS, NUMBERING (W); CM^{-1}

	Lower doublet components $F_1(J)$				Upper doublet components $F_2(J)$			
	Band Ab (0, 0)		Band B_2a (0, $2v''$)		Band Aa (0, 0)		Band B_2b (0, $2v''$)	
J''	R	P	R	P	R	P	R	P
½	—	—	—	—	—	—	—	—
1½	—	—	—	—	—	—	—	—
2½	—	—	—	—	—	—	—	—
3½	—	—	—	—	—	—	—	—
4½	—	—	—	—	—	—	—	—
5½	19,725.465	—	—	—	—	—	—	—
6½	655	19,721.944	—	—	—	—	—	—
7½	814	589	—	—	—	19,719.255	—	—
8½	960	200	—	—	19,723.747	18.906	—	—
9½	26.089	20.787	—	—	876	502	—	—
10½	222	418	—	18,748.840	999	106	—	18,752.712
11½	322	19.981	—	406	24.111	17.659	—	236
12½	424	534	—	—	216	—	—	51.884
13½	508	078	—	47.513	—	16.768	—	383
14½	—	18.618	—	006	—	305	—	50.960
15½	—	160	—	46.590	—	15.826	—	483
16½	—	17.659	—	111	—	330	—	49.966
17½	—	149	—	45.587	—	14.840	—	512
18½	26.705	16.642	18,755.205	060	24.496	313	18,759.151	48.980
19½	705	107	205	44.564	496	13.798	151	406
20½	—	15.558	—	026	—	236	—	47.849
21½	—	14.992	—	43.477	—	12.656	—	323
22½	—	432	—	42.907	—	088	—	46.726
23½	—	13.898	—	304	—	11.506	—	111
24½	26.508	236	—	41.729	—	10.914	—	45.469
25½	424	12.656	—	146	24.216	285	—	44.905
26½	322	007	—	40.516	111	09.664	58.730	266
27½	222	11.377	—	39.866	23.999	014	622	43.612
28½	089	10.724	54.650	227	876	08.369	502	42.967
29½	25.960	061	490	38.578	747	07.691	351	304
30½	814	09.370	331	37.899	589	014	210	41.579
31½	655	08.684	195	228	429	06.317	020	40.874
32½	465	07.971	001	36.510	269	05.608	57.852	185
33½	293	248	53.840	35.785	075	04.878	657	39.462
34½	080	06.520	638	081	22.863	137	443	38.720
35½	24.859	05.753	453	34.323	653	03.410	212	37.952
36½	643	007	220	33.563	435	02.636	56.982	165
37½	—	04.243	52.965	32.805	183	01.834	737	36.407
38½	111	03.410	712	004	21.944	022	480	35.582
39½	23.876	02.636	466	31.218	647	00.237	196	34.786
40½	589	01.834	236	30.446	392	699.429	55.885	33.939
41½	269	022	51.886	29.612	062	98.588	614	129
42½	22.998	00.166	611	28.776	20.787	97.757	—	32.272
43½	653	699.302	296	27.925	504	96.875	54.970	31.413
44½	315	98.437	50.960	051	097	007	589	30.530
45½	21.944	97.558	644	26.191	19.766	95.118	195	29.612
46½	589	96.658	259	25.284	391	94.216	53.840	28.719
47½	200	95.749	49.891	24.406	016	93.267	497	27.847
48½	20.787	94.818	512	23.492	18.618	92.391	—	26.837
49½	418	93.882	111	22.539	160	91.436	—	25.908
50½	19.981	92.929	48.658	21.626	17.786	90.496	—	24.952
51½	534	91.977	264	20.633	324	89.515	—	23.993
52½	078	90.991	—	19.692	16.910	88.530	—	002
53½	18.618	006	—	18.682	436	87.530	—	21.997
54½	160	88.999	—	17.689	15.961	86.515	—	20.963
55½	17.659	87.986	46.395	16.722	442	85.488	—	19.943
56½	149	86.953	45.857	15.698	14.992	84.478	—	18.881
57½	16.642	85.902	302	14.660	432	83.406	—	17.847
58½	107	84.840	44.905	13.574	13.898	82.335	—	16.863
59½	15.558	83.767	266	12.528	—	81.239	—	15.698
60½	14.992	82.680	43.780	11.418	12.812	80.188	—	14.586
61½	432	81.566	213	10.359	216	79.063	—	13.537
62½	13.898	80.452	42.622	09.249	11.656	77.960	—	12.311
63½	236	79.329	087	08.147	—	76.798	—	11.205
64½	12.656	78.183	—	06.995	10.450	75.671	—	10.024
65½	007	77.047	40.874	05.829	09.804	74.545	—	08.756
66½	—	75.919	—	04.752	158	73.340	—	07.689
67½	—	74.715	—	03.502	08.512	72.139	—	06.530
68½	—	73.477	38.945	02.332	07.841	70.951	—	05.362
69½	—	72.286	269	01.105	—	—	—	04.150
70½	—	71.077	37.601	699.891	—	—	—	02.843
71½	—	69.881	36.833	98.638	—	—	—	01.609
72½	—	68.539	156	97.436	—	66.022	—	00.328
73½	—	67.233	35.383	96.175	—	—	—	699.065
74½	—	66.022	—	94.908	—	—	—	97.785
75½	—	64.739	33.939	93.546	—	—	—	96.451
76½	—	63.453	—	92.354	—	—	—	95.139
77½	—	62.163	—	91.048	—	—	—	—
78½	—	60.814	—	89.737	—	—	—	—
79½	—	—	—	88.353	—	—	—	—
80½	—	—	—	88.985	—	—	—	—

A NEW CANADIAN PRIMARY RADIUM STANDARD[1]

By C. Garrett and K. W. Geiger

The National Research Council of Canada has recently acquired a new primary radium standard. This standard is one of the twenty which were prepared by O. Hönigschmid (1945) from radium salt he had purified for an atomic weight determination; carefully weighed amounts of this salt were sealed into glass tubes to form the standards.

A set of secondary standards, compared by their gamma radiation with the national standard, is also in custody of the National Research Council to carry out measurements on samples of radium submitted for certification. National radium standards contain an amount of radium the weight of which is probably known to an accuracy of $\pm 0.2\%$, whereas for routine measurements of radium samples an accuracy of between ± 0.5 and 1% is achieved in this laboratory.

The first Canadian radium standard was not a weighed standard but was certified as to content by comparison with two weighed standards by the International Radium Standards Commission in 1933. It has also been compared with other national radium standards (Michel and Whyte 1955); however it differs considerably in physical dimensions from the other standards so that large corrections must be made for differences of gamma-ray absorption within the standards. The results of the intercomparisons give a value to this standard which is slightly higher than the certified one. For these reasons, it was felt advisable to replace the former standard with a weighed standard, similar in size and shape to other national standards, and in 1955 one of the Hönigschmid standards was acquired. Particulars of both standards are given in Table I.

TABLE I

Particulars of the standards

Identification No.		XIII	5425
Content of $RaCl_2$	(mgm.)	31.83_6 (1934)*	31.73 (1934)†
Content of Ra element	(mgm.)	24.23_4 (1934)	24.15_3 (1934)
Length of glass tube	(mm.)	10.5	40
Internal diameter	(mm.)	1.5	3.0
Wall thickness	(mm.)	0.25	0.27
Volume occupied by salt		94%	6%
Approximate density of salt (gm./cm.^{3})		2.2	2.2

*As certified by the International Radium Standards Commission, corrected for 1934.
†As weighed by O. Hönigschmid.

[1]Issued as N.R.C. No. 4068.

Comparisons of the former and the new standard have been made using the National Research Council standard radium measuring apparatus which contains a one-atmosphere, air-filled, parallel-plate ionization chamber (Michel 1955). A scintillation counter has also been used. Details on the method of measurement and corrections will be given in a forthcoming publication. After application of the appropriate corrections for absorption within the standards, the following mean ratio for the contents has been obtained:

$$\frac{\text{former standard}}{\text{new standard}} = \frac{\text{No. XIII}}{\text{No. 5425}} = 1.0039 \pm 0.0005.$$

By using Hönigschmid's weight for No. 5425 (Table I) the derived content of No. XIII is

$$31.73 \times 1.0039 = 31.85_4 \text{ mgm. of } RaCl_2 \text{ as of 1934,}$$

which corresponds to 24.24_8 mgm. of radium element. This is 0.06% higher than the certified value of 24.23_4 mgm. of radium element. For the accuracy required for routine measurements this difference is completely negligible and therefore the use of the new standard will not alter the results of measurements on radium sources submitted for certification.

Earlier the new standard had been compared with a number of other national standards. In 1955 it was included in a series of intercomparison measurements of some of the remaining Hönigschmid standards, the international primary, and the former Vienna standard, which were undertaken by Prof. P. Kipfer and Mme. I. Joliot-Curie in Brussels. The new Canadian standard was also compared with the Austrian, British, German, and U.S. standards. Although most of the results are only preliminary, they indicate that the derived contents deviate from the certified weight in both directions by at most 0.2%. No final conclusions can be drawn from these measurements before the final figures are available.

HÖNIGSCHMID, O. 1945. Anz. Akad. Wiss. Wien, Math.-naturw. Kl. **82**: 30.
MICHEL, W. S. 1955. Radium certification in Canada. National Research Council of Canada, Ottawa, Publ. No. 3675. June.
MICHEL, W. S. and WHYTE, G. N. 1955. Can. J. Phys. **33**: 521.

RECEIVED JULY 13, 1956.
DIVISION OF APPLIED PHYSICS,
NATIONAL RESEARCH COUNCIL,
OTTAWA, ONTARIO.

PERIODIC FLUCTUATIONS IN OXIDE-CATHODE DIODES*

By P. A. Redhead

Periodic fluctuations of very low frequency have been observed in the current through an oxide-cathode diode; the cause of this has not yet been established. These periodic effects may be important in any measurements at very low frequencies using oxide-cathode tubes, and may explain some of the anomalous results obtained in the measurement of flicker noise at very low frequencies.

Measurements were made of low-frequency fluctuations in thermionic diodes using the circuit shown schematically in Fig. 1. In most of the measure-

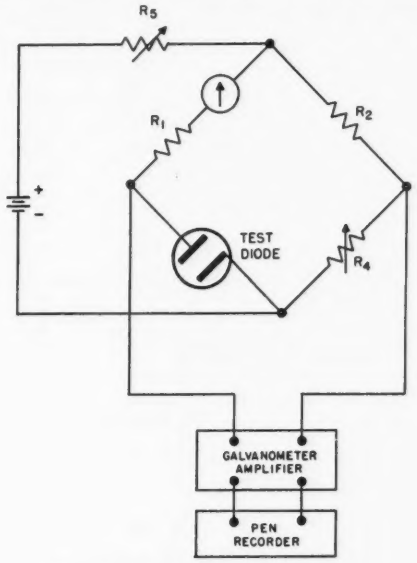

Fig. 1. Schematic circuit diagram.

ments $R_1 = R_2 = 10{,}000$ ohms. The output of the bridge was fed to a galvanometer amplifier having a response time of 0.15 sec. and a high input impedance; the output of the galvanometer amplifier was recorded on a pen-recorder of 0.6 sec. response time. Full scale deflection of the pen-recorder at maximum gain corresponded to a bridge output of 25 μv.

Periodic voltage fluctuations in the bridge output were observed on some occasions; the period of these fluctuations ranged from 5 to 120 sec. Examples of these periodic records are shown in Fig. 2. These periodic fluctuations would start, stop, or change frequency in a completely random fashion; however they have been observed to continue with a nearly constant period

*Issued as N.R.C. No. 4069.

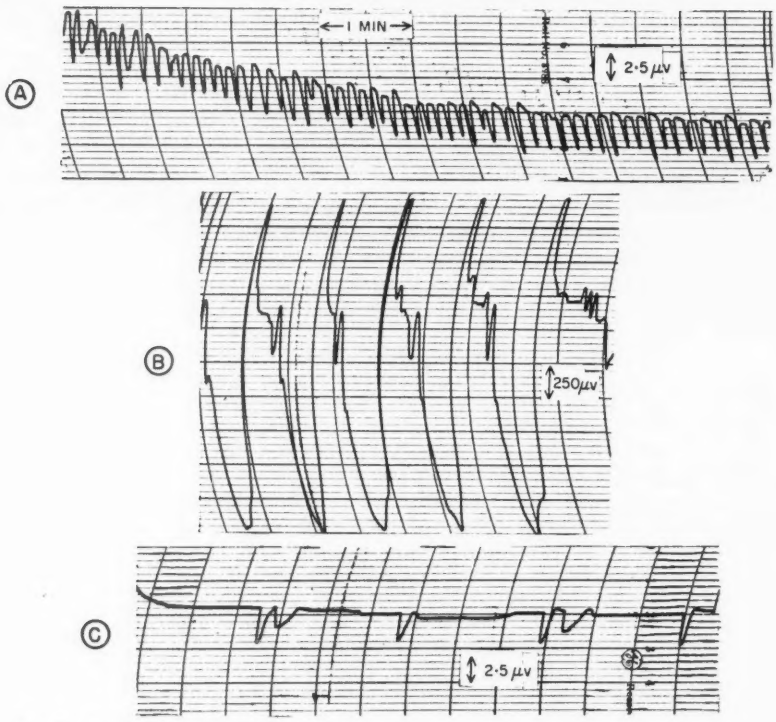

FIG. 2. Examples of periodic fluctuations:
(A) Tube Type 5751, No. 2, Section 1. Anode current 2 ma. Full scale deflection 25 μv.
(B) Tube Type 5751, No. 1, Section 1. Anode current 1 ma. Full scale deflection 25 μv.
(C) Tube Type 5751, No. 3, Section 2. Anode current 2 ma. Full scale deflection 2500 μv.
The time scale is identical in all three examples.

for as long as 30 min. Owing to the erratic nature of the phenomena it has not been possible, so far, to determine the dependence of the fluctuation period on cathode temperature and anode current with any certainty. In general, the periodic effect is observed only after the tube has been allowed to stabilize for some hours at a fixed cathode temperature and current.

The periodic effect has been observed in two tube types (5751 and 5965); these tubes are twin-triodes which were diode-connected for these measurements. All tubes tested (a total of six) have shown this periodic effect. The cathode coating in these tubes is BaO–SrO and the cathode core contains approximately 0.2% Si. The diodes were operated under space-charge limited conditions and with anode voltages less than two volts.

A degree of covariance has been observed between the amplitude of a pulse and the period following the pulse in those records exhibiting the most stable oscillations. The correlation coefficient in all cases exceeds $+0.9$ for samples of approximately 20 pulses.

Since similar periodic voltage fluctuations have been observed in electrolytic

cells, simultaneous measurements of the battery voltage were made to check that the battery was not the source of the periodic effects. Measurements indicated that a change in battery voltage of about 300 μv. was necessary to cause a change in bridge output corresponding to the amplitude of the observed periodic pulses, at a cathode temperature of 1050°K. and an anode current of 2 ma. Using the same galvanometer and pen-recorder no fluctuations could be observed in the battery voltage larger than 1 μv., and these fluctuations were purely random. All the components of the bridge were wire-wound and extreme care was taken to shield the bridge from all external fluctuations. When the diode was replaced by a resistor approximately equal in value to the d-c. resistance of the diode, the fluctuations observed in the bridge output were purely random.

Having established that the periodic fluctuations are caused by the tube and not the external circuit, it is of interest to determine the magnitude of the changes in some of the relevant parameters necessary to cause the observed fluctuations. The following table lists the calculated variation in the various parameters necessary to produce a 1 μv. output from the bridge when the resistance in series with the diode (R_1) is large compared to the d-c. resistance of the diode.

Parameter	Change producing 1 μv. output	Assumed conditions
Anode work function	1 μv.	
Cathode work function	50 μv.	Full space-charge limitation
Cathode resistance	10^{-3} ohms	I_a = 1 ma.
Cathode temperature	3×10^{-4}°K.	T_c = 1000°K.
Heater voltage	3.6 μv.	6-volt heater

Measurement of the fluctuations in the heater voltage showed that these were less than one microvolt and purely random. Thus fluctuation in cathode temperature caused by battery fluctuations cannot explain the observed periodic effect. The periodic effect cannot be caused by ionized gas within the tube since the anode potential was always less than the lowest ionization potential.

Burgess (1955) has recently published an analysis of temperature-sensitive elements and shows that oscillations can occur at very low frequencies under certain conditions. These oscillations have been observed in thermistors and crystal diodes. A similar mechanism in the oxide cathode may explain the periodic fluctuations observed in thermionic diodes if a sufficiently large capacitance exists across the oxide layer. Measurements on oxide cathodes indicate that this shunt capacitance may be quite large (Nergaard 1952).

Measurements are being continued to establish the mechanism responsible for these periodic fluctuations.

Burgess, R. E. 1955. J. Electronics, **1**: 297.
Nergaard, L. S. 1952. RCA Rev. **13**: 464.

Received May 15, 1956.
Radio and Electrical Engineering Division,
National Research Council,
Ottawa, Canada.

SOME UPPER LIMITS OF ISOTOPIC ABUNDANCE—I: A, Mn, and Cd

By Larkin Kerwin

During the progress of recent work with our inflection mass spectrometer, it has been possible to establish the upper limits of abundance for a number of isotopes. Some of the species reported here do not appear to have been subject to previous search; others have previously been established as non-existent, but with a higher upper limit of abundance. The present status of the isotopic abundance of the elements argon, manganese, and cadmium is therefore as follows:

Isotope	Abundance, %	Reference
	Argon	
A 34	<0.01	This note
A 35	<0.01	This note
A 36	0.337	Nier (1950)
A 37	<0.005	Nier (1936)
A 38	0.063	Nier (1950)
A 39	<0.01	Nier (1936), this note
A 40	99.600	Nier (1950)
A 41	<0.01	Nier (1936), this note
A 42	<0.003	Nier (1938)
A 43	<0.01	This note
	Manganese	
Mn 51	<0.01	This note
Mn 52	<0.01	This note
Mn 53	<0.0004	White *et al.* (1956)
Mn 54	<0.0003	White *et al.* (1956)
Mn 55	100.0	This note
Mn 56	<0.01	This note
Mn 57	<0.006	Samson and Bleakney (1936)
Mn 58	<0.01	This note
Mn 59	<0.01	This note
Mn 60	<0.01	This note
	Cadmium	
Cd 103	<0.01	This note
Cd 104	<0.01	This note
Cd 105	<0.01	This note
Cd 106	1.215	Leland and Nier (1948)
Cd 107	<0.01	This note
Cd 108	0.875	Leland and Nier (1948)
Cd 109	<0.01	This note
Cd 110	12.39	Leland and Nier (1948)
Cd 111	12.75	Leland and Nier (1948)
Cd 112	24.07	Leland and Nier (1948)
Cd 113	12.26	Leland and Nier (1948)
Cd 114	28.86	Leland and Nier (1948)
Cd 115	<0.01	This note
Cd 116	7.58	Leland and Nier (1948)
Cd 117	<0.01	This note
Cd 118	<0.007	Nier (1936)

It is a pleasure to acknowledge the support of the Defence Research Board (Grant No. DRB-9510-13) and of the Office de Recherches of the Province of Quebec during the progress of this work.

LELAND, W. T. and NIER, A. O. 1948. Phys. Rev. **73**: 1206.
NIER, A. O. 1936. Phys. Rev. **50**: 1041.
——— 1938. Phys. Rev. **53**: 282.
——— 1950. Phys. Rev. **77**: 789.
SAMSON, M. B. and BLEAKNEY, W. 1936. Phys. Rev. **50**: 732.
WHITE, F. A., COLLINS, T. L., and ROURKE, F. M. 1956. Phys. Rev. **101**: 1786.

RECEIVED JULY 23, 1956.
UNIVERSITÉ LAVAL,
QUÉBEC, CANADA.

A NOTE ON THE ZENITH ANGLE DEPENDENCE OF COSMIC RAY PROTONS AT SEA LEVEL[1]

BY K. W. OGILVIE[2]

In previous papers (Ogilvie 1955 *a*, *b*), it has been shown that the 'heavy particle selector' may be used as a reliable proton detector both at sea level and at high altitudes. The present note will describe its use to study the angular dependence of protons in the momentum range 700 to 1100 Mev./*c*.

DESCRIPTION OF APPARATUS

The apparatus was generally similar to that employed in the previous investigations, except that the sensitive areas of the Geiger counter trays were reduced from 16 in. square to 16 in. by 10 in., while the area of the Cerenkov tank remained the same. An additional Geiger counter tray was incorporated in the apparatus, above the top tray, to form a fourfold telescope, during some of the observations. Thus the separations of the extreme trays could be either $21\frac{1}{2}$ in., three trays, or $42\frac{1}{2}$ in., four trays. The whole apparatus could be tilted about a horizontal axis passing through its center of gravity, and parallel to the side of length 10 in., and could be set vertically and at 10 degree intervals between 50° E. and 50° W. Changing from East to West was done by rotating the whole telescope in azimuth. It was set up below a light wooden roof in the cosmic ray observatory at Ottawa, altitude 320 ft. above sea level. The anti-coincidence, proton, and the triple or quadruple, meson, counting rates were recorded. The telescope contained 3.8 cm. of lead and 20 cm. of water absorber. Proton counting rates were corrected, for barometric pressure variations, using the previously determined pressure coefficient (Ogilvie 1955*b*).

RESULTS

The results obtained for the triple and quadruple counting rates are detailed in Table I.

[1]Issued as N.R.C. No. 4083.
[2]Was National Research Laboratories Postdoctorate Fellow. Now with the University of Sydney, Sydney, N.S.W., Australia.

TABLE I

MESON COMPONENT

θ, zenith angle, degrees	Triples, East, counts per hour	Triples, West, counts per hour	Quadruples, West, counts per hour
0	8225±20	8080±30	2262±40
10	7863±30	7814±30	2153±60
20	7327±30	7090±25	1955±50
30	6109±50	6015±40	1643±40
40	4688±90	4708±80	1192±30
50	3506±75	3495±60	766±30

The disagreement between the two experimental values for triples at zero degrees is probably due to the azimuthal axis of the apparatus not being exactly vertical. If this is so, the discrepancies between these two values and their mean of about 1% can be explained by an inclination of $\frac{1}{2}°$. No correction will be made for this since the other angles were defined by a quadrant whose

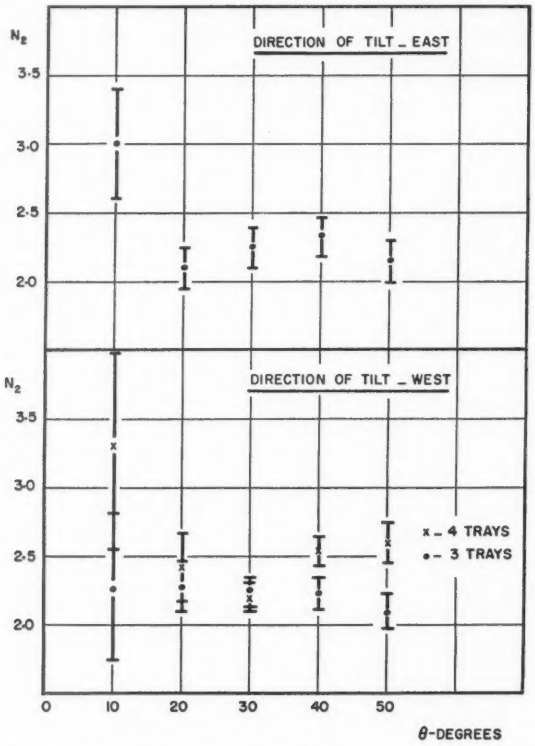

FIG. 1. Angular distribution of counting rate of telescope in easterly and westerly directions, with three and four counter trays, corrected for the telescope angle.

accuracy was $\pm\frac{1}{4}°$. The results are shown in the form of a plot of N, the exponent in an assumed $\cos^N\theta$ law, against θ in Fig. 1. They are corrected for the finite acceptance angle of the telescope, and this correction will now be discussed.

If $I(\theta)$ is the counting rate at angle θ, we have

$$I(\theta) = I(0)\cos^{N_1}\theta$$

and if $I(\theta)/I(0) = r$, then

$$\log r/\log\cos\theta = N_1.$$

Actually $$I(\theta) = I(0)f(\theta, N)\cos^N\theta,$$

where $f(\theta, N)$ is a factor to be obtained, so that

$$\log r/\log\cos\theta = N + \log f(\theta, N)/\log\cos\theta.$$

$f > 1$, $\cos\theta < 1$, so that

$$N_2 = \log r/\log\cos\theta + |\log f(\theta, N)/\log\cos\theta|,$$

where N_2 is the second approximation to the value of N.

Values of $f(\theta, N)$ have been obtained by assuming the telescope to be made up of two uniformly sensitive areas, equal to the effective areas of the trays used, and the results are set out in Table II below, together with the expressions from which the calculations were made. Linear interpolation between the

TABLE II
VALUES OF $f(\theta, N)$

θ, degrees	$N = 2$		$N = 3$		$N = 4$	
	3 trays	4 trays	3 trays	4 trays	3 trays	4 trays
10	1.0021	1.0006	1.0043	1.0021	1.0105	1.0037
20	1.0093	1.0025	1.0191	1.0093	1.0466	1.0162
30	1.0233	1.0062	1.0479	1.0233	1.1177	1.0406
40	1.0492	1.0130	1.1012	1.0492	1.2516	1.0863
50	1.0997	1.0263	1.2047	1.0997	1.5202	1.1754

The results from which these factors were calculated are:

for $N = 2$

$$I(\theta) = \text{const.} \times I(0)\cos^2\theta\left[\frac{3\gamma}{2} + \sin 2\gamma + \frac{\sin 4\gamma}{8} + \frac{L}{x_0}(\cos^2\gamma - 1) + \tan^2\theta\left(\frac{\gamma}{2} - \frac{\sin 4\gamma}{8} - \frac{L}{x_0}\sin^4\gamma\right)\right];$$

for $N = 3$

$$I(\theta) = \text{const.} \times I(0)\cos^3\theta\left[\sin\gamma\left(\cos^4\gamma + \frac{8 + 4\cos^2\gamma}{3}\right) - \frac{L}{x_0}(1 - \cos^5\gamma) + 3\tan^2\theta\left(\sin^3\gamma(\tfrac{2}{3} + \cos^2\gamma) + \frac{L}{x_0}(\sin^2\gamma\cos^3\gamma + \tfrac{2}{3}(\cos^3\gamma - 1))\right)\right];$$

for $N = 4$

$$I(\theta) = \text{const.} \times I(0)\cos^4\theta\left[\frac{1}{6}\left(\cos^5\gamma\sin\gamma + \frac{5}{4}\left(\frac{3}{2}\gamma + \sin 2\gamma + \frac{\sin 4\gamma}{8}\right) - \frac{L}{x_0}(1 - \cos^6\gamma)\right) + \tan^2\theta\left(\cos^3\gamma\sin^3\gamma - \frac{3}{32}(\sin 4\gamma - 4\gamma) - \frac{L}{x_0}(\cos^2\gamma\sin^4\gamma + \tfrac{1}{2}\sin^4\gamma)\right) + \frac{\tan^4\theta}{6}\left(\cos\gamma\sin^5\gamma + \frac{1}{4}\left(\frac{3}{2}\gamma - \sin^3\gamma\cos\gamma - \frac{3}{4}\sin 2\gamma\right) - \frac{L}{x_0}\sin^6\gamma\right)\right];$$

where $\gamma = \tan^{-1}(x_0/L)$, the telescope being tilted in the direction of its x dimension, of magnitude x_0, and the tray separation being L. They are obtained by expanding the counting rate of a telescope as a series in $\tan^2\theta$ and neglecting higher terms.

integral values of N was used in applying the correction to the experimental results, Fig. 1. Better agreement is now obtained between the results for N obtained by the triple and quadruple coincidence experiments in the westerly direction. The total absorber in the telescope is equal to 6.4 cm. of lead, so that, for example, all mesons with momentum above about 180 Mev./c are counted. Using telescopes of small angle Katzman (unpublished) has found that a $\cos^N\theta$ law, with N closely equal to 2, is obeyed for particles able to penetrate 14 cm. of lead. A larger value of N at 10 degrees is found in the latter experiments, agreeing qualitatively with the present work. By assuming that the mesons below 300 Mev./c obey a $\cos^3\theta$ law, while those above obey a $\cos^2\theta$ law (Zar and Shamos 1950), and using the meson spectrum of Owen and Wilson (1955) as extended to lower momenta by Lichtenstein (1954), an estimate can be made of the extent to which the measured N will be raised above 2 in the present apparatus by the inclusion of lower energy mesons. The exponent is raised by 0.05, less than that observed experimentally.

The Proton Counting Rate

The proton, anticoincidence, rates were recorded with three and four Geiger counter trays in the telescope and are set out in Table III.

TABLE III

PROTON COMPONENT

θ, zenith angle, degrees	Triple coincidence		Corrected exponent, triples	Quadruple coincidence, West, counts per hour	N_1	Corrected
	East, counts per hour	West, counts per hour				
0	26.7±0.3	27.2±0.2		7.33±0.2		
10	25.1±0.4	25.5±0.3	4.6±1.0	6.7 ±0.2	5.9 ±1.5	
20	22.6±0.4	23.3±0.3	2.8±0.3	6.1 ±0.2	2.9 ±0.4	3.1 ±0.5
30	17.4±0.3	20.3±0.3	2.9±0.2	4.66±0.2	3.15±0.25	3.33±0.25
40	13.7±0.4	13.9±0.5	2.9±0.2	2.9 ±0.2	3.5 ±0.2	3.72±0.2
50	9.5±0.3	11.1±0.25	2.5±0.1	1.7 ±0.15	3.3 ±0.15	3.6 ±0.15

The sixth column shows the calculated exponent N_1 in the formula $I_\theta = I_\theta \cos^{N_1}\theta$ from the results given, and in the seventh column these are shown corrected for telescope angle.

The corrected values of the exponent obtained from the mean triple coincidence readings are shown in column 4 of Table III. In the 40° and 50° positions especially, these results are subject to an error due to showers, which can cause a coincidence between the Geiger counters without setting off the Cerenkov counter. This effect increases rapidly with angle, while the counting rate due to protons falls, so that at large angles it becomes appreciable. It is reduced by the addition of a fourth tray, and so the exponents in column 4 will not be considered further, deductions being made from those in the seventh column.

DISCUSSION

The zenith angular dependence of cosmic ray protons at an altitude of 3300 meters has been measured by Miller *et al.* (1954) and Charbonnier *et al.*

They have also obtained an expression for the zenith angular intensity variation of the nucleonic component, subject to the following assumptions:

(1) "The primary proton intensity is isotropic." The momentum region under investigation here, 700 to 1100 Mev./c, is similar to that studied by Charbonnier *et al.* so that this assumption will certainly be more nearly true for the primaries of the protons presently observed at greater depth.

(2) "The intensity of secondaries at depth X, due to primaries of zenith angle θ_X independent of azimuth, depends only upon the diagonal distance d, in gm./cm.^{2} as measured along this diagonal direction." This assumption is a very great simplification of the actual situation and must be regarded as justified, on the average, by agreement obtained with experiment.

(3) "The intensity decreases exponentially with depth, with an absorption length of 120 gm./cm.^{2}" This has been shown to be approximately true in the range sea level to 25,000 ft. altitude (~350 gm./cm.^{2}) (Ogilvie 1955*a*).

(4) "The angular spread of secondaries due to radiation in a given direction is represented by a $\cos^n\omega$ law, centered about this direction, with n independent of depth." The present experiments were made to measure N, the exponent for the gross zenith angular distribution, and to check whether the same value of n can be used at sea level and at 3300 meters.

Development of the theory on these assumptions by Miller *et al.* leads to the result:

$$I_X(\theta_X, \phi_X)d\Omega_X =$$

$$K I_0(\theta_0, \phi_0) \int_0^{\frac{1}{2}\pi+\alpha} \cos^n(\xi-\alpha)\left[\int_0^{\pi} \exp\left(-\frac{X}{\sin\lambda \sin\xi}\right) \sin^{n+1}\lambda \, d\lambda\right] d\xi \, d\Omega_X,$$

where θ_X, ϕ_X are the zenith and azimuthal angles respectively, at depth X,

$$\alpha = \tfrac{1}{2}\pi - \theta_X, \text{ and } K = (n+1)/2\pi.$$

Numerical integration of this expression for sea level by the present author (X = 8.58 = depth in units of 120 gm./cm.^{2}), for n = 4, 5, and 6, yields the results shown in Table IV below. These calculations are compared with the proton rates obtained using four Geiger counter trays in Fig. 2. The fit with the theoretical curve for n = 6 is good, indicating that a value of n of 6 is appropriate at sea level. The value obtained by Miller at 3000 meters is 6.5±0.7, which shows that the assumption (4) above is approximately valid,

TABLE IV

θ_X, degrees	$n = 4$ $I_X/I_0\times10^5$	$n = 5$ $I_X/I_0\times10^5$	$n = 6$ $I_X/I_0\times10^5$
0	5.44	6.06	6.59
10	5.19	5.74	6.19
20	4.50	4.87	5.17
30	3.54	3.69	3.77
40	2.49	2.49	2.44
50	1.56	1.46	1.36

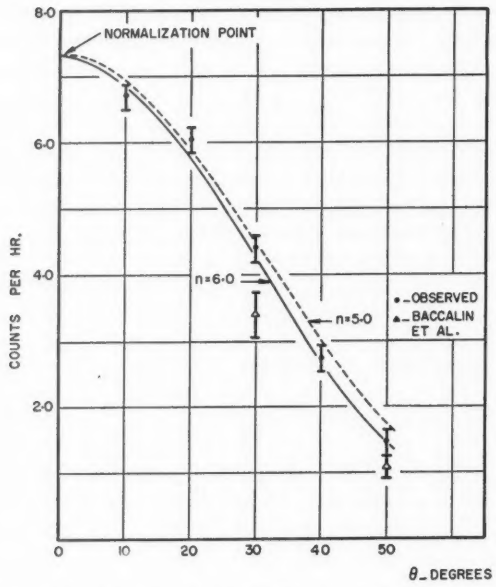

FIG. 2. Theoretical and experimental results for the angular distribution of protons.

and that the foregoing simple theory gives reasonable results when applied to the proton beam in our momentum interval between sea level and 3000 meters. Recently, Baccalin *et al.* (1955) have measured the angular dependence of protons at sea level, using an apparatus similar to the present one. Their results, normalized at 0 degrees, not corrected for solid angle, are shown in Fig. 2. Reasonable agreement is obtained.

ACKNOWLEDGMENT

The author would like to express appreciation to Dr. D. C. Rose for assistance and comments in carrying out the experiments and preparing this manuscript.

BACCALIN, C., BASSI, P., and MANDUCHI, C. 1955. Nuovo cimento, X, **1**: 1126.
CHARBONNIER, F. M., DAVIS, W. R., GARRISON, G. R., HENDERSON, J. E., MILLER, C. E., and SANDSTROM, W. M. The zenith angle dependence of cosmic ray protons—O.N.R. Report. Applied Physics Laboratory, University of Washington, Seattle, Wash.
KATZMAN, J. Unpublished.
LICHTENSTEIN, P. G. 1954. Phys. Rev. **93**: 858.
MILLER, C. E., HENDERSON, J. E., POTTER, D. S., TODD, J., SANDSTROM, W. M., GARRISON, G. R., DAVIS, W. R., and CHARBONNIER, F. M. 1954. Phys. Rev. **93**: 590.
OGILVIE, K. W. 1955*a*. Can. J. Phys. **33**: 555.
——— 1955*b*. Can. J. Phys. **33**: 746.
OWEN, B. G. and WILSON, J. G. 1955. Proc. Phys. Soc. A, **68**: 409.
ZAR, J. L. and SHAMOS, M. H. 1950. Phys. Rev. **79**: 207.

RECEIVED APRIL 4, 1956.
DIVISION OF PURE PHYSICS,
NATIONAL RESEARCH COUNCIL,
OTTAWA, CANADA.

LETTERS TO THE EDITOR

Under this heading brief reports of important discoveries in physics may be published. These reports should not exceed 600 words and, for any issue, should be submitted not later than six weeks previous to the first day of the month of issue. No proof will be sent to the authors.

Gamma–Gamma Angular Correlation in W^{182} [1]

The isotope Ta^{182} decays by beta-minus emission into excited states of W^{182}, which is one of several complex gamma-emitting nuclei of even–even species. The decay scheme of W^{182}, containing some 27 gamma-rays, has been subject to a number of investigations (Cork *et al.* 1951; Fowler *et al.* 1954; Mihelich 1954; Muller *et al.* 1952; Murray *et al.* 1955). These investigations have established that W^{182} contains 11 energy levels, the spins of the first three only having definite assignments; i.e. 0(even) for the ground state and 2(even) and 4(even) for the first and second excited states respectively.

We shall follow the nomenclature of Murray *et al.* (1955) and label the energy levels, from the ground state to the 10th excited state, A to K consecutively. The spin assignments of levels H, F, and D can be investigated because of the following gamma-ray cascades:

(1) the 67.74 → 1222 kev. cascade, i.e. $F \rightarrow D \rightarrow A$;
(2) the 152.4 → 1222 kev. cascade, i.e. $H \rightarrow D \rightarrow A$;
(3) the 67.74 → 1122 kev. cascade, i.e. $F \rightarrow D \rightarrow B$.

Mihelich (1954) has shown from his coincidence work that the 1122 kev. gamma-ray is a transition between levels D and B while the 1222 kev. gamma is a transition between D and A.

These three gamma-ray cascades were investigated with a highly stabilized two-channel coincidence spectrometer. The detectors were NaI crystals with DuMont 6292 photomultipliers. These fed conventional pulse amplifiers and differential discriminators. The coincidence unit is a Harwell type 1036A. A resolving time of 0.1 μsec. was used. The angular correlation functions were obtained by a least squares fit to the data; and the coefficients were corrected for the effect of finite angular resolution. It should be noted that the gamma-rays studied (Table I) are fairly intense (Murray *et al.* 1955).

TABLE I

Gamma-ray energy (kev.)	Gamma-ray intensity
67.74	85
152.41	35
1122	100
1222	95

The correlation function for the 67.74 → 1222 kev. cascade is

$$W(\theta) - 1 = +(0.261 \pm 0.095) P_2(\cos\theta).$$

This corresponds to a spin assignment of $2 \rightarrow 2 \rightarrow 0$. The error in the coefficient $A_2 = +(0.261 \pm 0.095)$ is large, but the error in the anisotropy is much less, being of the order of 12%, i.e. $A = +(0.450 \pm 0.054)$. This agrees well with the theoretical anisotropy, $A = +0.4286$, of the $2 \rightarrow 2 \rightarrow 0$ cascade. Other assignments were tried but were found to be incompatible with experimental results. For instance, assuming the Bohr–Mottelson theory to apply to W^{182} in its simplest form, that is to say without K-forbiddenness (K is the projection of the total angular momentum of the nucleus on the nuclear symmetry axis), then level D will have spin 8 because this model predicts the existence of a 677.6 kev. level which would have spin 6. Evidence for a level at 680 kev. is mentioned by Fowler *et al.* (1954). Level F will then have a spin of 12 and the spin sequence for the 67.4 → 1222 kev. cascade would be $12 \rightarrow 8 \rightarrow 0$. The correlation function for this cascade was a four-term function which did not fit the experimental points. Further, the assignment of spin 8 to level D disagrees with the assignment of spin 2 by Murray *et al.* (1955). Since the spin sequence is not $12 \rightarrow 8 \rightarrow 0$, this means that the spectrum of W^{182} must contain more than one rotational band.

Fowler *et al.* (1954) tentatively assign the spin sequence $4 \rightarrow 1 \rightarrow 0$ to the 67.4 → 1222 kev. cascade. The associated correlation function is

[1]Supported by National Research Council Grant.
This letter is based on work submitted by R.C.W. for the degree Ph.D. at the University of Manitoba, Winnipeg, Manitoba.

$$W(\theta)-1 = -0.125P_2(\cos\theta)$$

which yields an anisotropy of $A = -0.2$. This is in complete disagreement with the measured anisotropy, which was positive and of value 0.450 ± 0.054. Thus it is concluded that the 67.4 → 1222 kev. cascade has the spin assignment $2 \rightarrow 2 \rightarrow 0$. Both levels F and D then have spin 2.

The correlation function for the 152.4 → 1222 kev. cascade is

$$W(\theta)-1 = -(0.059\pm0.025)P_2(\cos\theta).$$

This corresponds to a $3 \rightarrow 2 \rightarrow 0$ assignment; however, the error in $A_2 = -(0.059\pm0.025)$ is extremely large. This is to be expected because of the low intensity of the 152.41 kev. transition, which reduces the ratio of genuines to accidentals to quite a low value, i.e. 4 to 1. The error in the anisotropy is not as high as the error in A_2; however, the anisotropy $A = -(0.086\pm0.018)$ agrees reasonably well with the theoretical value $A = -0.104$. Internal conversion data (Murray *et al.* 1955; Fowler *et al.* 1954) indicate that the 152.4 kev. transition is pure E_1; thus, to an uncertainty of 21% we assign spin 3 to level H. The assignment of spin 2 to level D is much more certain in view of the correlation of cascade (1).

Cascade (3) enables the spin of levels F and D to be checked and the mixing in the 1122 kev. transition to be determined. The correlation for this cascade is

$$W(\theta)-1 = -(0.196\pm0.062)P_2(\cos\theta).$$

The anisotropy $A = -(0.268\pm0.029)$ yields a mixing ratio of $\delta = -3$ with a phase of 180° between the two radiations. Thus the 1122 kev. transition is 90% E_2 and 10% M_1 to within 11% for a $2 \rightarrow 2 \rightarrow 2$ cascade. Thus cascade (3) has the assignments:

$$2(E_1) \rightarrow 2(90\%\ E_2,\ 10\%\ M_1) \rightarrow 2.$$

These spin assignments agree with the predictions of the collective model when K-forbiddenness is taken into account (Alaga *et al.* 1955). Evidently there are many transitions in W^{182} which are K-forbidden. Further, according to this model, W^{182} possesses four rotational bands which explains why levels D, F, and H have spin assignments of 2, 2, and 3 respectively. Level D belongs to the second series with spin I and parity π of $2(+)$. Levels F and H belong to the third series with I and π equal to $2(-)$ and $3(-)$ respectively. The 67.74 kev. transition occurs between the first state of the third series and the first state of the second series. The 152.4 kev. transition occurs between the second state of the third series and the first state of the second series. The high percentage of E_2 in the 1122 kev. transition is due to the K-forbiddenness for M_1 radiation. Thus the collective model of the nucleus agrees with the experimental facts.

ALAGA, G., ALDER, K., BOHR, A., and MOTTELSON, B. R. 1955. Kgl. Danske Videnskab. Selskab, Mat-fys. Medd. **29**: No. 9.
CORK, J. M., CHILDS, W. J., BRANYAN, C. E., RUTLEDGE, W. C., and STODDARD, A. E. 1951. Phys. Rev. **81**: 642.
FOWLER, C. M., KRUSE, H. W., KESHISHIAN, V., KLOTZ, R. J., and MELLOR, G. P. 1954. Phys. Rev. **94**: 1082
MIHELICH, J. W. 1954. Phys. Rev. **95**: 626.
MULLER, D. E., HOYT, H. C., KLEIN, D. J., and DUMOND, J. W. M. 1952. Phys. Rev. **88**: 775.
MURRAY, J. J., BOEHM, F., MARMIER, P., and DUMOND, J. W. M. 1955. Phys. Rev. **97**: 1007.

RECEIVED JULY 6, 1956.
R. C. WILLIAMS
K. I. ROULSTON
DEPARTMENT OF PHYSICS,
UNIVERSITY OF MANITOBA,
WINNIPEG, MANITOBA.

THE PHYSICAL SOCIETY

MEMBERSHIP of the Society is open to all who are interested in Physics.

FELLOWS pay an Entrance fee of £1 1*s*. ($3.00) and an Annual Subscription of £2 2*s*. ($6.00).

STUDENTS: A candidate for Studentship must be between the ages of 18 and 26, and pays an Annual Subscription of 5*s*. ($0.75).

MEETINGS: Fellows and Students may attend all Meetings of the Society including the annual Exhibition of Scientific Instruments and Apparatus.

PUBLICATIONS include the *Proceedings of the Physical Society*, published monthly in two sections, and *Reports on Progress in Physics*, published annually. Volume XVIII, 1955, is now available (price 50*s*. ($7.15)). Members are entitled to receive many of the Publications at a reduced rate.

Further information can be obtained from:

THE PHYSICAL SOCIETY

1, LOWTHER GARDENS, PRINCE CONSORT ROAD

LONDON, S.W.7, ENGLAND

CANADIAN JOURNAL OF PHYSICS

Notes to Contributors

Manuscripts

(i) ***General.*** Manuscripts, in English or French, should be typewritten, double spaced, on paper $8\frac{1}{2} \times 11$ in. **The original and one copy are to be submitted.** Tables and captions for the figures should be placed at the end of the manuscript. Every sheet of the manuscript should be numbered.

Style, arrangement, spelling, and abbreviations should conform to the usage of this journal. Names of all simple compounds, rather than their formulas, should be used in the text. Greek letters or unusual signs should be written plainly or explained by marginal notes. Superscripts and subscripts must be legible and carefully placed.

Manuscripts and illustrations should be carefully checked before they are submitted. Authors will be charged for unnecessary deviations from the usual format and for changes made in the proof that are considered excessive or unnecessary.

(ii) ***Abstract.*** An abstract of not more than about 200 words, indicating the scope of the work and the principal findings, is required, except in Notes.

(iii) ***References.*** References should be listed **alphabetically by authors' names,** unnumbered, and typed after the text. The form of the citations should be that used in issues of this journal published in 1956; in references to papers in periodicals, titles should not be given and only initial page numbers are required. The names of periodicals should be abbreviated in the form given in the most recent *List of Periodicals Abstracted by Chemical Abstracts*. All citations should be checked with the original articles and each one referred to in the text by the authors' names and the year.

(iv) ***Tables.*** Tables should be numbered in roman numerals and each table referred to in the text. Titles should always be given but should be brief; column headings should be brief and descriptive matter in the tables confined to a minimum. Vertical rules should be used only when they are essential. Numerous small tables should be avoided.

Illustrations

(i) ***General.*** All figures (including each figure of the plates) should be numbered consecutively from 1 up, in arabic numerals, and each figure referred to in the text. The author's name, title of the paper, and figure number should be written in the lower left corner of the sheets on which the illustrations appear. Captions should not be written on the illustrations (see Manuscripts (i)).

(ii) ***Line Drawings.*** Drawings should be carefully made with India ink on white drawing paper, blue tracing linen, or co-ordinate paper ruled in blue only; any co-ordinate lines that are to appear in the reproduction should be ruled in black ink. Paper ruled in green, yellow, or red should not be used unless it is desired to have all the co-ordinate lines show. All lines should be of sufficient thickness to reproduce well. Decimal points, periods, and stippled dots should be solid black circles large enough to be reduced if necessary. Letters and numerals should be neatly made, preferably with a stencil (**do NOT use typewriting**) and be of such size that the smallest lettering will be not less than 1 mm. high when reproduced in a cut 3 in. wide.

Many drawings are made too large; originals should not be more than 2 or 3 times the size of the desired reproduction. In large drawings or groups of drawings the ratio of height to width should conform to that of a journal page but the height should be adjusted to make allowance for the caption.

The original drawings and one set of clear copies (e.g. small photographs) are to be submitted.

(iii) ***Photographs.*** Prints should be made on glossy paper, with strong contrasts. They should be trimmed so that essential features only are shown and mounted carefully, with rubber cement, on white cardboard with no space or only a **very** small space (less than 1 mm.) between them. In mounting, full use of the space available should be made (to reduce the number of cuts required) and the ratio of height to width should correspond to that of a journal page ($4\frac{3}{4} \times 7\frac{1}{2}$ in.); however, allowance must be made for the captions. Photographs or groups of photographs should not be more than 2 or 3 times the size of the desired reproduction.

Photographs are to be submitted in duplicate; if they are to be reproduced in groups one set should be mounted, the duplicate set unmounted.

Reprints

A total of 50 reprints of each paper, without covers, are supplied free. Additional reprints, with or without covers, may be purchased.

Charges for reprints are based on the number of printed pages, which may be calculated approximately by multiplying by 0.6 the number of manuscript pages (double-spaced typewritten sheets, $8\frac{1}{2} \times 11$ in.) and including the space occupied by illustrations. An additional charge is made for illustrations that appear as coated inserts. The cost per page is given on the reprint requisition which accompanies the galley.

Any reprints required in addition to those requested on the author's reprint requisition form must be ordered officially as soon as the paper has been accepted for publication.

Contents

Page

The Number Density of Meteor Trails Observable by the Forward-scattering of Radio Waves—*Robert E. Pugh* - - - - - - - 997

The Spatial Distribution of Signal Sources in Meteoric Forward-scattering—*C. O. Hines and R. E. Pugh* - - - - - - - - - 1005

High Resolution Raman Spectroscopy of Gases. VII. Rotational Spectra of *s*-Triazine and *s*-Triazine-d_3—*J. E. Lancaster and B. P. Stoicheff* - - - - - - - - - - - - - - - - - - - 1016

The Photoprotons Emitted from Oxygen-16 Nuclei—*D. L. Livesey* 1022

The Lifetime of Positrons Annihilating in Aluminum—*G. Jones and J. B. Warren* - - - - - - - - - - - - - - - - - 1033

The Absorption of Ultraviolet Ionizing Radiation in Gases—*G. R. Bainbridge and W. A. Prowse* - - - - - - - - - - 1038

An Emission Spectrum of the Diacetylene Ion. A Study of Schüler's "T" Spectrum under High Resolution—*J. H. Callomon* - - 1046

Notes:

A New Canadian Primary Radium Standard—*C. Garrett and K. W. Geiger* - 1075

Periodic Fluctuations in Oxide-cathode Diodes—*P. A. Redhead* 1077

Some Upper Limits of Isotopic Abundance—I: A, Mn, and Cd—*Larkin Kerwin* - - - - - - - - - - - - - - - - - - - 1080

A Note on the Zenith Angle Dependence of Cosmic Ray Protons at Sea Level—*K. W. Ogilvie* - - - - - - - - - - - - - 1081

Letters to the Editor:

Gamma-Gamma Angular Correlation in W^{182}—*R. C. Williams and K. I. Roulston* - - - - - - - - - - - - - - - - - 1087

Printed in Canada *by* University of Toronto Press